

ELECTROCHEMICAL AND SPECTROSCOPIC
STUDIES OF METALLOPROTEINS AND
OXYGEN ACTIVATING
HEMOPROTEINS

By

LUDIVINA AVILA

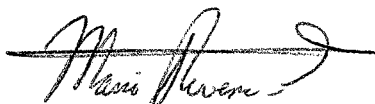
Bachelor of Science
St. Edward's University
Austin, Texas
1993

Master of Science
Texas A & M University-Kingsville
Kingsville, Texas
1998

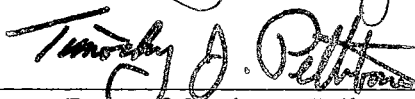
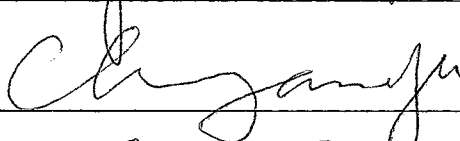
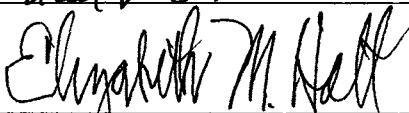
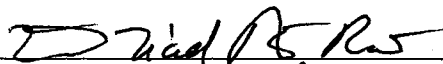
Submitted to the Faculty of the
Graduate College of the
Oklahoma State University
in partial fulfillment of
requirements for
the Degree of
DOCTOR OF PHILOSOPHY
December, 2002

ELECTROCHEMICAL AND SPECTROSCOPIC
STUDIES OF METALLOPROTEINS AND
OXYGEN ACTIVATING
HEMOPROTEINS

Thesis Approved:



Thesis Advisor



Dean of Graduate College

DEDICATION

In memory of my brother,
Homero Avila Jr.
His love of science was and
will always be an inspiration.

ACKNOWLEDGEMENTS

In pursuing my Ph.D., I have benefited greatly from many people. I would like to express my gratitude to all those who, with work, assistance, advice, encouragement and friendship have made an important contribution in my life. I am extremely grateful to Dr. Mario Rivera, my advisor, for all his guidance and support throughout my studies. I am grateful to my colleagues and friends especially Juan Carlos Rodriguez, Carla Bartholomew, Joe Studer, Adriana Altuve, Christopher Damaso and Dattatri Nagesha for their expertise in different areas from molecular biology to life.

I would like to thank Oklahoma State University's Graduate College and Department of Chemistry for their financial support throughout my studies at OSU and my committee members, Dr. Neil Purdie, Dr. Elizabeth Holt, Dr. Ziad El Rassi, and Dr. Chan Ann Yu for their advice and expertise. I am also indebted to Dr. Horacio Motola for his wisdom and unselfish advice which has influenced my life in many ways.

Finally, on a personal note, I am deeply grateful to the Lord, my father, and my family- my parents, Homero and Tita Avila, my sister Titina Bazan and her family, my brothers Homero Jr. and P.R. Avila and finally my best friend Thor. I would have not been able to finish without their unconditional love, patience, support and continuous encouragement despite all that we went through as a family these past several years. Thanks again.

TABLE OF CONTENTS

Chapter	Page
I. INTRODUCTION	
Introduction	1
i). Iron-sulfur proteins	1
ii). Heme Proteins	5
iii). Oxygen Binding Heme Proteins	9
Electroanalytical Methods for Biological Materials	15
i). Cyclic Voltammetry	15
ii). Spectroelectrochemistry	16
Purpose	18
References	22
II. AN ELECTROCHEMICAL STUDY OF THE FACTORS RESPONSIBLE FOR MODULATING THE REDUCTION POTENTIAL OF PUTIDAREDOXIN	
Introduction	28
Experimental Procedures	31
i). Design and Synthesis of the Gene	31
ii). Expression and Purification of Pdx	35
iii). Cyclic Voltammetry.....	37
iv). Spectroelectrochemistry of Pdx	38
v.) Preparation of Modifiers.....	41
Results and Discussion.....	41
i). Gene Synthesis and Bacterial Expression	41
ii). Cyclic Voltammetry	44
iii). Spectroelectrochemistry	48
Conclusion	54

References	57
III. A STUDY OF AXIAL LIGAND MUTANTS OF MITOCHONDRIAL CYTOCHROME b ₅ AND THEIR OXYGEN ACTIVATION MECHANISMS: THE OXIDATION OF HEME TO VERDOHEME AND BILIVERDIN	
Introduction	65
Experimental Procedures	70
i). Site Directed Mutagenesis	70
ii). Expression and Purification of Mutants (Recombinant Protein).....	71
iii). Cuvette utilized for Experimentation ..	72
iv). Coupled Oxidation Assays ..	74
v). Resonance Raman Spectroscopy ..	75
vi). Autooxidation of the Oxyferrous Complexes.....	75
vii). HPLC Analysis of the Product of the Coupled Oxidation Reaction	76
viii). Evaluating the Reactivity of Ferrous Protein.....	77
Results and Discussion.....	78
i). Characterization of H63V and H39V Mutants.....	78
ii). Coupled Oxidation of the Heme in H63V and H39V Mutants.....	80
iii). Catalase Does Not Inhibit the Coupled Oxidation of the H39V.....	82
iv). HPLC Results	89
v). Relative Stability of the Oxyferrous Complex of the H63V and H39V Mutants.....	91
vi). The Distal Helix Flexibility and Heme Oxygenase Activity.....	93
vii). Catalase Inhibits the Coupled Oxidation of the H63V mutant.....	97
Conclusions	110
References	112
IV. A COMPARISON OF ANAEROBIC SPECTROELECTROCHEMICAL CELLS FOR DETERMINING THE REDUCTION POTENTIAL OF ENZYMES	
Introduction.....	120
Theory.....	122
i). Potentiometric titration with sodium dithionite.....	122

ii). Potentiometric titration with a potentiostat and an electron transfer mediator, MV.....	125
Experimental.....	126
i). Enzyme preparation.....	126
ii). Potentiometric titration with sodium dithionite.....	126
iii). Potentiometric titration with a potentiostat and an electron transfer mediator, MV.....	129
iv). Determination of the Formal Reduction Potential.....	132
Results and Discussion	135
Conclusions.....	139
References	142

LIST OF FIGURES

Figure	Page
Chapter I	
1. Structure of the Major Classes of Fe-S clusters.....	3
2. Structure of iron-protoporphirin IX (Heme)	6
3. Schematic presentation of heme proteins upon reacting with O ₂ and reducing equivalents.....	11
4. Heme Oxygenation Pathway.....	14
5. Schematic representation of a polylysine modified ITO electrode	17
6. Schematic representation of the mediated electrochemical approach to activate proteins	19
Chapter II	
1. Amino acid and corresponding DNA sequences of Pdx. The codon signaling for the initiator methionine, codons frequently used by <i>Escherichia coli</i> , and the restriction endonuclease sites were engineered as discussed in the Experimental Section. Arrows indicate the length of the synthetic single stranded oligonucleotides utilized for the assembly of the gene.....	33
2. Schematic representation of the strategy followed to synthesize the gene coding for Pdx. The restriction endonuclease sites <i>Eco</i> RI and <i>Bam</i> HI were utilized to directionally clone the assembled gene	34
3. Potentiometric cell utilized for the spectroelectrochemistry of Pdx. The cell is constructed out of a glass cuvette (1.0 cm path-length) equipped with a reference	

- electrode (Ag/AgCl), indicating electrode (Pt wire), and magnetic stirrer. The cell is also equipped with an attachment for nitrogen inlet for purging.....40
4. Electronic spectra of (a) oxidized and (b) reduced recombinant Pdx43
 5. Ribbon diagram depicting the NMR structure of Pdx [45]. The coordinates (1PUT) were obtained from the Brookhaven Protein Data Bank. The residues Trp-106, Asp-34, and Asp-38 (*clockwise*) and the Fe₂S₂ center are shown in *stick rendering*. The two Asp residues and the carboxy-terminal Trp have been implicated in electrostatic binding with residues Arg-79, Arg-109, and Arg-112 in cytochrome P450_{cam}46
 6. Typical background-subtracted cyclic voltammograms (–) obtained at an indium-doped tin oxide electrode from a solution containing Pdx (0.01 mM) and polylysine (0.20 mM) in 100.0 mM MOPS, pH 7.0. The scale of the voltammograms is shown vs the Ag/AgCl electrode but the values in the text are given vs standard hydrogen electrode. Sweep rate = 5 mV/s. (•) Simulated cyclic voltammograms: $k_s = 1.3 \times 10^{-3} \text{ cm}^2/\text{s}$, $D_0 = 9.8 \times 10^{-7} \text{ cm}^2/\text{s}$, $\Delta E_p = 64 \text{ mV}$ 47
 7. Typical background-subtracted cyclic voltammograms obtained at: **a** gold electrode modified with β -mercaptosulfonate, **b** gold electrode modified with 5-mercaptopentanoate from a solution containing Pdx (0.10 mM) and polylysine (0.20 mM) in 100.0 mM MOPS, pH 7.0. The scale of the voltammograms is shown vs the Ag/AgCl electrode but the values in the text are given vs the standard hydrogen electrode. Sweep rate = 5 mV/s, (•) Simulated cyclic voltammograms: (a) $k_s = 1.1 \times 10^{-3} \text{ cm}^2/\text{s}$, $D_0 = 2.0 \times 10^{-6} \text{ cm}^2/\text{s}$, $\Delta E_p = 74 \text{ mV}$; (b) $k_s = 1.0 \times 10^{-3} \text{ cm}^2/\text{s}$, $D_0 = 3.0 \times 10^{-6} \text{ cm}^2/\text{s}$, $\Delta E_p = 78 \text{ mV}$ 49
 8. Spectroelectrochemical titration of a solution containing recombinant Pdx (70 μM) and phenosafranine (30 μM) in phosphate buffer ($\mu = 0.10$, pH = 7.0) with sodium dithionite (10.0 mM). Inset: Nernst plot constructed from the dependance of the absorbance at 408 nm on the cell potential. The Nernst slope is 62 mV50
 9. Space-filled view obtained by visualizing the coordinates from the NMR structure of putidaredoxin [45] with the program INSIGHT (II): polypeptide (*gray*), Asp-34 and Asp-38 (*blue*), carboxy-terminus Trp-106 (*magenta*), sulfide from the iron-sulfur cluster (*green*), iron ion farthest away from the molecular surface (*red*), cysteine residues (*yellow*). This view of putidaredoxin shows a channel leading into the interior of the protein, which is expected to provide water accessibility to the iron-sulfur cluster. At the end of this channel it is possible to observe one of the sulfide and one of the iron ions in the Fe₂S₂ cluster, as well as Cys-86. These groups are located on the part of the cluster that is farthest away from the molecular surface. This view also shows the location of the channel with

respect to the negatively charged residues implicated in binding to cytochrome
P450_{cam}53

Chapter III

1. Schematic cross-sectional representation of the cell used to obtain electronic absorption spectra. The cell body is outfitted with a (a) 10 mm path length quartz cuvette connected to glass outlets via a gradient seal (b). A teflon coated magnetic cell stirrer (g) was sealed into the cell. A Rotaflow stopcock serves as an inlet for argon (c) and the small glass port (f) is used for reagent delivery and as an argon outlet. This port can be sealed with a rubber septum. (d and e are Teflon stoppers)73
2. Electronic spectra of (a) H63V and (b) H39V OM cyt b₅79
3. Electronic spectra of H63V (top) and H39V (bottom) OM cyt b₅ in the presence of hydrazine and O₂81
4. Electronic spectra obtained during the coupled oxidation of the H39V mutant in the presence of hydrazine and O₂ with (A) and without 0.4 μM catalase (B). Spectra were taken every 10 minutes for over 2 hours83
5. Electronic spectrum of (a) Biliverdin obtained from the coupled oxidation of the heme in the H39V mutant, (b) authentic biliverdin85
6. (A) The rate of formation for the oxyheme complex of the H39V mutant during the coupled oxidation in the presence and in the absence of catalase. (B) Amount of biliverdin formation for the H39V mutant during the coupled oxidation in the presence and in the absence of catalase.....86
7. Top: Electronic spectra obtained during the autooxidation of the H39V-O₂ complex prepared by the addition of sodium dithionite to an anaerobic solution of H39V, folled by exposure to air. Bottom: Electronic spectra obtained approximately 30 seconds after the oxyferrous complex was formed and immediately adding catalase and hydrazine.....88
8. Regiospecificity obtained from the HPLC analysis of samples containing DME derivatives of biliverdin originating from the product of the coupled oxidation of (a) pyridine verdohemochrome (b) alpha-biliverdin standard, (c) H63V coupled oxidation product, (d) H39V coupled oxidation product.....90
9. Top: Electronic spectra obtained during the autooxidation of the H39V-O₂ complex prepared by the addition of sodium dithionite to an anaerobic solution of H39V. Bottom: The rate constant for the autooxidation of the H39V-O₂ complex was measured by fitting the time-dependent decay of the peak at 577nm to a single exponential function.....92

10. Molecular Model of HO-1. Gly 139 (CPK rendering in pink) and 143 are directly contacting the heme (stick rendering in red).....94
11. (A) Molecular Model of the H39V Mutant of OM Cytochrome bs.....96
12. Electronic spectra obtained during the coupled oxidation of the H39V-G41A mutant in the presence of hydrzine and O₂. Sprectra were taken over a period of 12h.....98
13. Electronic spectra obtained during the coupled oxidation of the H39V-G42A mutant in the presence of hydrzine and O₂. Sprectra were taken over a period of 4h.....99
14. Electronic spectra obtained without (A) and with 0.4 μM catalase (B) during the coupled oxidation of the H63V in the presence of hydrazine and O₂. Spectra were taken at 10 minute intervals for 2.5 hours.....100
15. Fe^{III} - H63V mutant + H₂O₂. initial H63V (--) 35 min after 2 equivalents of H₂O₂(---).....102
16. Electronic spectra of an anaerobic solution of Fe^{III}- H63V treated with one equivalent of sodium dithionite and subsequent additions of two equivalents of an anaerobic solution of H₂O₂ to Fe^{II}- H63V. Electronic absorption spectra were taken every 10 minutes until there was no further change. The final resulting spectrum (a) has the soret band at 407 nm and (a') a featureless visible region. The formation of verdoheme can be seen with (b) a decrease in the intensity of the soret band and (b') the growth of the 667 nm peak. Upon addition of CO to verdoheme, CO-verdoheme peaks are formed (c).....104
17. Resulting electronic spectra of the titration of Fe^{III}- H63V (1) using one equivalent of sodium dithionite and subsequent addition of one equivalent of anaerobic H₂O₂. (1'-4') are the resulting spectra after the addition of sodium dithionite and (2-4) are the spectra after the subsequent addition of H₂O₂. Spectrum (5) is the final spectrum before the addition of air. Inset: (a) the final addition of H₂O₂ corresponding to spectrum 4. (b) Verdoheme accumulation after exposure to air.....106
18. (a) Electronic spectrum of the ferric *meso*-hydroxyheme complex of H63V. (b) Electronic spectra of the ferrous complex obtained by titrating the ferric *meso*-hydroxyheme complex of H63V with one equivalent of sodium dithionite. (c) the carbomonoxy adduct formed after anaerobically bubbling CO. Inset: (1) verdoheme-carbomonoxy complex (2) H63V-verdoheme complex formed upon continued bubbling of air.....109

Chapter IV

1.	SEC cell used for dithionite titrations.....	128
2.	Two different views of the cell used for spectroelectrochemical measurements.....	130
3.	Spectral features used for calculation equation derivations. The absorbance is read at the monitored wavelength.....	133
4.	Sigmoidal graph fitting f_{ox} vs. E	134
5.	Spectroelectrochemical titration using sodium dithionite of (A) HemO, (B) PigA	136
6.	SEC titration using a potentiostat and MV and mediators of (A) HmuO, (B) HemO, (C) PigA.....	138
7.	SEC Titration using a potentiostat and MV and mediators of OM cytochrome b_5 (wild type).....	141

LIST OF SCHEMES

Figure		Page
	Chapter III	
1.	Catalytic cycle of heme oxygenase	66

LIST OF TABLES

Figure	Page
Chapter IV	
1. Table of Mediators.....	124
2. Results of potentiometric titrations for HO.....	137

List of Symbols and Abbreviations

Ala	Alanine
ALA	δ -Aminolevulinic acid
Arg	Arginine
Asp	Aspartic acid
ATP	Adenosine Triphosphate
Cys	Cysteine
Cyt c	Cytochrome c
D_o	Diffusion coefficient of oxidized species
dNTP	Deoxynucleotide triphosphates
D_r	Diffusion coefficient of reduced species
DTT	Dithiothreitol
ΔE_p	Peak to peak separation
ϵ	Extinction coefficient
E^o	Formal reduction potential
EC	Electrochemical
EDTA	Ethylenediamine tetraacetic acid
EPR	Electron paramagnetic resonance
GC	Gas chromatography
Gly	Glycine

Gln	Glutamine
His	Histidine
HO	Heme Oxygenase
HPLC	High pressure liquid chromatography
i_{pa}	Peak anodic current
i_{pc}	Peak cathodic current
IPTG	Isopropyl- β -thiogalactoside
IM	Imidazole
ITO	Indium tin oxide
k_s	Heterogeneous electron transfer rate constant
k_f	Forward homogeneous electron transfer rate constant
k_b	Backward homogeneous electron transfer rate constant
μ	Ionic strength
Met	Methionine
MOPS	3-[N-Morpholino]propane sulfonic acid
MS	Mass spectrometry
MW	Molecular weight
MWCO	Molecular weight cut off
n	Number of electrons transferred
NADH	Nicotinamide adenine dinucleotide
NHE	Normal hydrogen electrode
NMR	Nuclear magnetic resonance
OD	Optical density

OM	Outer mitochondrial
Ox	Oxidized Species
Pdx	Putidaredoxin
RR	Resonance Raman
Red	Reduced Species
rpm	Revolutions per minute
SHE	Standard hydrogen electrode
Ser	Serine
Thr	Threonine
TRIS	Tris-hydroxy methyl aminomethane
Trp	Tryptophan
UV-Vis	Ultraviolet-visible
v	Scan rate
Val	Valine
WT	Wild type

CHAPTER I

INTRODUCTION

Proteins play an important role in all biological processes. Nearly all catalysts in biological systems are proteins called enzymes [1]. Proteins mediate a wide range of functions, including enzymatic catalysis, transport, coordinated motion, mechanical support, immune protection and control of growth and differentiation [1]. Specifically, the catalytic role of enzymes is of particular interest because enzymes catalyze chemical reactions as diverse as hydroxylation, heteroatomic oxygenation and unsaturated epoxidations [2].

Redox metalloproteins are proteins whose main function is to act as electron carriers. Often redox metalloproteins act in conjunction with other metalloproteins to supply electrons needed to carry out the enzymatic work necessary for biological function. Alternatively these proteins can act in the respiratory electron cascade [3]. Redox metalloproteins can be divided into three main groups according to their prosthetic centers: iron sulfur proteins, heme proteins and copper containing proteins. This brief overview will only cover iron sulfur proteins and heme proteins.

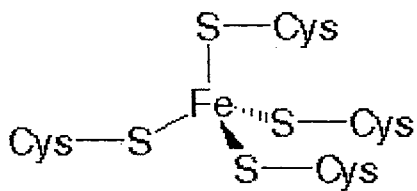
i). Iron-sulfur Proteins

Iron-sulfur proteins constitute a class of redox proteins that are found in animals, bacteria and plants [4]. They are among the oldest known biological catalysts [5, 6]. Iron

sulfur clusters embedded in protein frameworks catalyze a wide variety of critical electron transfer and biosynthetic processes in all living organisms. These processes include simple electron transfer, proton-coupled electron transfer with energy transduction, and biosynthetic electron transfer [5, 6]. As shown in Figure 1, iron-sulfur proteins exist in a variety of forms and are characterized by the number of irons in the prosthetic center: (1Fe) rubredoxin (Rd); (2Fe) ferredoxins (Fd); (4Fe) ferredoxins (Fd). The clusters are bound to the enzyme by side chain thiolates (RS^-) of cysteine ligands, and occasionally contain a metal other than Fe. Iron-sulfur proteins are characterized by the presence of polymetallic systems containing sulfide ions, in which the iron ions have variable oxidation states. The simplest iron-sulfur center is the rubredoxin-type $[\text{Fe}(\text{Cys})_4]$ mononuclear iron center, in which iron is tetrahedrally coordinated with four cysteines, Figure 1A [7, 8]. The polymetallic system, $[\text{Fe}_2\text{S}_2]$, is constituted by two iron ions bridged by two sulfide ions, coordinated by four cysteine ligands in Fe_2S_2 ferredoxins or by two cysteines and two histidines in Rieske proteins, see Figure 1B [7-9]. The oxidized forms of these clusters contain two Fe^{3+} ions, whereas the reduced forms contain one Fe^{3+} and one Fe^{2+} ion.

Putidaredoxin, adrenodoxin, and terpredoxin are soluble Fe_2S_2 iron-sulfur proteins that act as single electron carriers. In mitochondrial monooxygenase systems, adrenodoxin transfers an electron from NADPH: adrenodoxin reductase to membrane-bound P450 [10-13]. In bacteria, putidaredoxin and terpredoxin serve as electron carriers between corresponding NADH dependent ferredoxin reductases and soluble cytochrome P450 [12, 14].

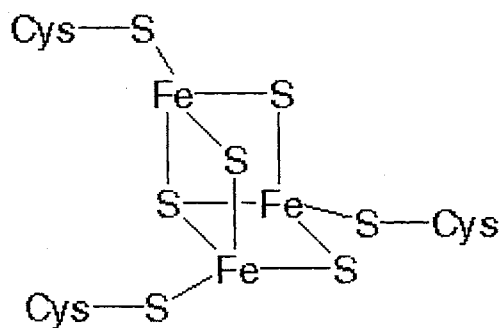
A. [Fe(Cys)₄]



B. [Fe₂S₂]



C. [Fe₃S₄]



D. [Fe₄S₄]

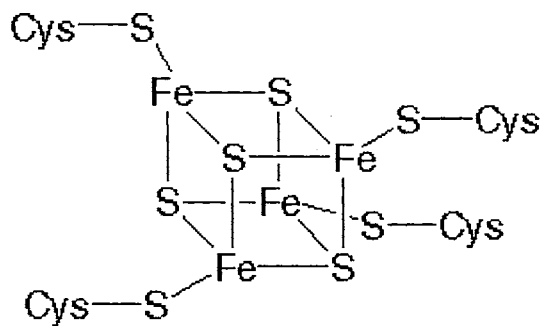


Figure 1. Structures of the major classes of Fe-S clusters. The larger clusters, [F₈S₇]_{ox} and [F₈S₇]_{red} are not shown.

One of the most common polymetallic systems, $[\text{Fe}_4\text{S}_4]$, is characterized by four iron ions and four sulfide ions placed at the vertices of a cubane-type structure, coordinated by four cysteine ligands, Figure 1D [8]. Several high potential iron-sulfur proteins (HiPIPs) have so far been characterized structurally [15-17]. As in other bacterial ferredoxins, the $[\text{Fe}_4\text{S}_4]$ cluster adopts a cubane-like conformation and is ligated to the protein *via* four cysteine sulfur ligands, see Figure 1D[7, 8]. The $[\text{Fe}_4\text{S}_4]$ electron-transfer proteins ($[\text{Fe}_4\text{S}_4]$ ferredoxins) may be further subdivided into low potential (bacterial type) and high potential (HiPIP) ferredoxins [7, 8]. The formal oxidation numbers of the iron ions can be $[2\text{Fe}^{3+}, 2\text{Fe}^{2+}]$ or $[1\text{Fe}^{3+}, 3\text{Fe}^{2+}]$ in low potential ferredoxins. The oxidation numbers of the iron ions in high potential ferredoxins can be $[3\text{Fe}^{3+}, 1\text{Fe}^{2+}]$ or $[2\text{Fe}^{3+}, 2\text{Fe}^{2+}]$ [7]. There are also proteins containing an $[\text{Fe}_3\text{S}_4]$ center, Figure 1C, in which one iron is missing from the $[\text{Fe}_4\text{S}_4]$ core. Three sulfide ions bridge two iron ions each, while the fourth sulfide bridges three iron ions. Their formal oxidation states may vary from $[\text{Fe}_3\text{S}_4]^+$ (all Fe^{3+} form) to $[\text{Fe}_3\text{S}_4]^{2-}$ (all Fe^{2+} form) [7, 8].

The aforementioned iron-sulfur clusters function in a wide range of biological processes; most commonly, they function as simple electron carriers and have been structurally designed for this purpose [7]. Iron sulfur clusters are found at the active sites of numerous enzymes where they commonly facilitate electron transfer and substrate transformations. Processes involving cluster assembly, rearrangement, degradation, redox changes and ligand substitution are important aspects of the chemistry of these systems. Ranges of synthetic analogues of iron-sulfur clusters are known and have played an important role in revealing the characteristic reactivity patterns of this family of proteins [7].

One of the characteristics of iron sulfur proteins is that most have fairly low reduction potentials typically ranging from -700 mV to +300 mV [18, 19]. However, as shown earlier, there is one exception- the high potential iron-sulfur proteins (HiPIPs). These unique Fe₄S₄ ferredoxins function in anaerobic electron transport chains and some have a redox potential higher than any other known iron-sulfur protein (e.g., HiPIP from *Rhodospila globiformis* has a redox potential of ca. 450 mV which is 100 mV higher than any other known iron-sulfur protein) [17].

ii). Heme Proteins

Heme containing proteins are involved in an array of important biological functions, including oxygen binding (hemoglobin and myoglobin), oxygen metabolism (monooxygenases and peroxidases), electron transfer reactions (cytochromes), and signal transduction (guanylate cyclase, nitric oxide synthase) [20]. This diversity in function arises from a combination of differences in the substituents of the various hemoproteins and in the variety of interactions with protein scaffolds that generate different heme environments [20-22]. Due to these reasons, heme proteins have been the focus of a great deal of work since the pioneering work on the structure determination of myoglobin and hemoglobin [20-22]. The redox functions of heme proteins are mainly governed by the precise protein heme interactions that modulate and direct the chemistry of the iron center. The changes in the substituent groups at the periphery of the porphyrin ring give rise to different types of iron-porphyrin derivatives [20, 22]. The most common representative of heme is heme-*b*, also termed iron-protoporphyrin IX. Heme-*b* constitutes the prosthetic group of hemoglobin, myoglobin, catalase, most peroxidases,

the b-type cytochromes such as the bis-histidine ligated cytochrome b_5 and the cytochromes P-450 [23]. The structure of iron-protoporphyrin IX (heme) is shown in Figure 2.

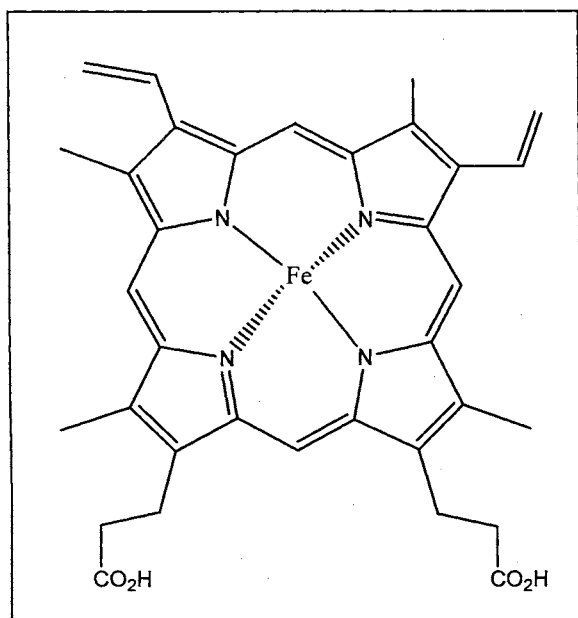


Figure 2. Structure of iron-protoporphyrin IX (Heme)

The prosthetic group in heme proteins is embodied within a cavity composed of amino acid residues in the polypeptide backbone. This cavity, for a given hemoprotein, possesses unique structural elements that to a large extent determine the function and properties of the protein. The central iron ion, is coordinated to the pyrrole nitrogens of the heme macrocycle forming a complex with square planar geometry. In hexacoordinated heme proteins, the inner coordination sphere of the metal center is typically completed by ligands that originate from protein amino acid side chains (endogenous ligands) and by small non protein ligands (exogenous). In spite of the presence of potential ligands such as water in the heme crevice, the sixth coordination

site of a few heme proteins can remain vacant, consequently producing pentacoordinated heme proteins [24].

Heme in electron-transfer proteins typically possesses two strongly coordinated axial ligands bound to iron, and generally these proteins do not bind exogenous ligands. On the contrary, the heme in oxygen transport enzymes has the sixth coordination site (distal site) accessible for coordination by an exogenous sixth ligand. In fact, the accessibility to the sixth coordination site constitutes a fundamental structural difference between proteins that function exclusively as electron-transport proteins and those that may carry out reactions with substrates.

Heme proteins serve as electron donors and electron acceptors in biological electron transfer chains. Their reduction potential directly reflects the relative stabilization of the Fe (II) and Fe (III) states of the bound heme [23]. The modulation of the reduction potential of a particular cytochrome is one of the major functional roles carried out by the polypeptide moiety and is important for regulation of electron flow among physiological redox partners [25]. There are four relatively independent, additive factors which govern the reactivity of hemes: (a) the nature of the axial ligation to the heme-iron, (b) substituent groups on the porphyrin ring, (c) the hydrophobic environment and electrostatic effects and (d) the heme exposure or solvent accessibility [22, 25].

Axial ligands play a major role in controlling redox potential due to their electronic effects on the metal center. The influence exerted by the proximal ligand and its environment has been studied by determining the structures of heme proteins together with the data from site-directed mutagenesis [22, 26-28] In heme-proteins, three residues are used as proximal ligands: histidine in globins and peroxidases; tyrosine in catalase;

and cysteine in chloroperoxidases and cytochrome P450 (mono-oxygenases). Hydrogen bonding to the iron proximal ligand affects the distribution of charge as well as the strength of the ligand metal bond. The proximal histidine in globins, for instance, donates a hydrogen bond to the main chain carbonyl oxygen, whereas in peroxidases it interacts with an aspartate. Furthermore, the interaction with the negatively charged aspartate leads to a stronger hydrogen bond in peroxidases than in the globins resulting in a better electron donor to the metal center. It has been proposed that the anionic character of the proximal histidinate ligand in peroxidases contributes to the capability of peroxidases to stabilize higher oxidation states of the iron during catalysis [22]. Dawson has described these effects in terms of a “push-pull” concept [28]. The push comes from the electron donation by the proximal ligand. The pull, on the other hand, is a consequence of the nature of distal residues, such as the arginine in heme-peroxidases, which have been implicated in polarizing the peroxide O-O bond.

The hydrophobic environments and electrostatic effects of hemes were first studied in 1972 when Kassner proposed that heme-proteins decrease their midpoint potential by increasing the polarity of the heme environment, because this tends to stabilize a more highly charged oxidized state [29]. Since then, theoretical calculations and site-directed mutagenesis have provided more insight into how the relationship between electrostatic versus hydrophobic features in the heme pocket affects redox potential [26, 27].

The degree of heme exposure to solvent is also an important factor governing redox potentials. Solvent accessibility calculations on atomic coordinates of a number of protein structures were used to show that as exposure to water increases, or as the polarity

of the heme environment increases, the midpoint potentials decrease [30]. The effect of water on the redox properties of the heme has been shown in a variety of calculations and experiments [26, 31]. In a recent related study, [27], a mitochondrial cytochrome b_5 mutant, V45I/V61I, was engineered with the aim of restricting water accessibility to the exposed heme edge cytochrome b_5 . It was found that the side chain of Ile at positions 45 and 61 restricted water accessibility to the interior of the heme cavity and protected a large section of the heme edge from the aqueous environment. This resulted in a change in the reduction potential of the mutant compared to the wild type cytochrome b_5 [27].

iii). Oxygen Binding Heme Proteins

In biological systems, the dioxygen molecule is used in a number of ways for instance, it can act as a terminal electron acceptor (a metabolite). When O_2 acts as a terminal electron acceptor it is reduced either to H_2O or H_2O_2 by enzymes known as oxidases. Oxidases have three substrates; molecular oxygen, protons and a reductant [20]. Since these heme proteins have an accessible coordination site, they play an active role in the biological chemistry of dioxygen. The oxygen reactivity of these proteins varies from case to case depending on the nature of the axial ligands and the heme environment. Heme proteins that require molecular oxygen to perform their normal function may be classified in two main categories: (1) Proteins that reversibly bind dioxygen and preserve the integrity of the O_2 molecule and (2) proteins that bind dioxygen and utilize it in reactions with substrates by facilitating oxygen-oxygen bond cleavage of the O_2 molecule. The omnipresent involvement of heme proteins in the preservation and

cleavage of the oxygen-oxygen bond highlights the significance of the role played by the polypeptide moiety in modulating protein function. This type of control of the protein environment over the reactivity is illustrated by considering the fact that, with the exception of the cysteine-ligated cytochrome P450 enzymes, all proteins that react with O_2 possess histidine as a proximal ligand.

The species typically produced in the general reaction of dioxygen with heme proteins are shown in Figure 3. The reversible binding of molecular oxygen and the formation of reactive oxygen species in the heme microenvironment are initiated by the one electron reduction of ferric heme to produce its ferrous counterpart. The binding of O_2 to the ferrous heme follows this step, therefore producing the six-coordinate $Fe^{2+}-O_2$ complex. Further differentiation into the reactions depicted in Figure 3 distinguishes the two types of reactivity, and is under strong influence of the protein heme environment.

In addition to its use as an electron acceptor, O_2 is also used directly in the synthesis and degradation of many of the chemical constituents of the cell. The enzymes that catalyze such reactions are called oxygenases. These enzymes either insert one O-atom of dioxygen into a substrate reducing the other to water in which case they are monooxygenases, or insert both O-atoms into a substrate in which case they are dioxygenases. Oxygenases, possessing heme as the prosthetic group, are enzymes that incorporate oxygen atoms from dioxygen into organic substrates. The oxygenases can be classified into two categories: monooxygenases and dioxygenases. The general reaction that describes the function of the monooxygenases is shown in Figure 3. The monooxygenases go through the $Fe^{2+}-O_2$ complex as a key intermediate of the reaction,

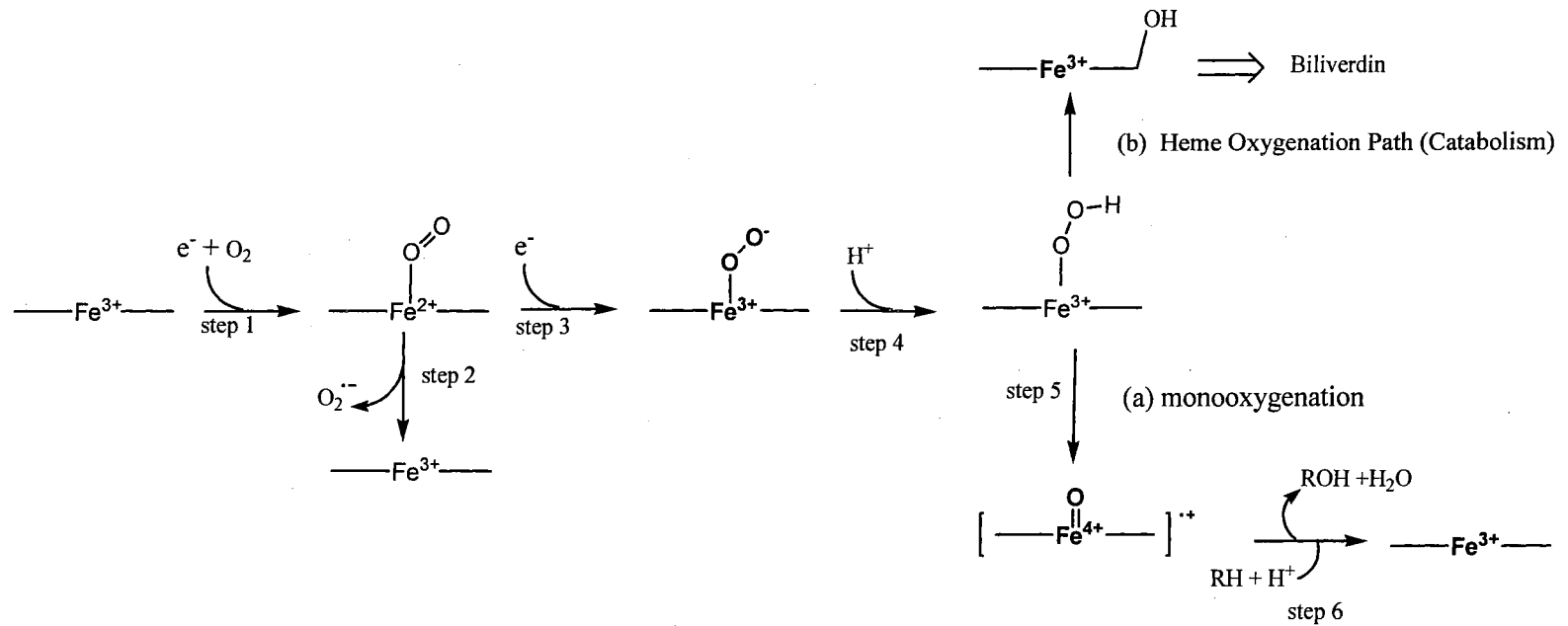


Figure 3. Schematic presentation of heme proteins upon reacting with O_2 and reducing equivalents. Note that after step 5, oxygen activation may be bifurcated to (a) monooxygenation, or (b) heme oxygenation, which is part of the heme catabolism path.

see step 2, figure 3. It requires the input of a second electron for continuation of the catalytic cycle, step 3, figure 3.

The nature of the protein oxo-complex in these proteins is still a matter of debate, but the proven existence of a ferric peroxo complex as catalytic intermediate in several reactions of heme proteins argues in favor of the $\text{Fe}^{3+}\text{O}_2^-$ species [30]. The formation of the ferric peroxo complex may occur as follows: (1) an electron is donated to the heme protein to produce the ferrous species. (2) dioxygen binds to ferrous iron and an electron is transferred from iron to the bound dioxygen yields the ferric-superoxide complex, $\text{Fe}^{\text{III}}\text{-O}_2^{\bullet -}$ intermediate. (3) A second electron is donated to this intermediate, therefore producing the ferric peroxo species, $\text{Fe}^{\text{III}}\text{-O}_2^-$. It is important to note that in the case of heme oxygenases, the catalytic reaction may be initiated by substituting reducing equivalents and dioxygen for the direct addition of peroxide or other peroxides to the ferric protein [30, 32].

Studies of the catalytic mechanisms of heme proteins that employ either oxygen or peroxides as a co-substrate have provided evidence for two types of oxygen reactivity. The most common mode of operation involves the oxidative intermediate ferryl species ($\text{Fe}^{\text{IV}}=\text{O}$) which has been observed spectroscopically in reactions catalyzed by cytochrome P450 and the peroxidases. A less common reactive species is the ferric peroxo anion ($\text{Fe}^{\text{III}}\text{-O}_2^-$) or alternatively, its protonated form, the hydroperoxo species ($\text{Fe}^{\text{III}}\text{-OOH}$) which is presumably the active oxygen species in the reaction catalyzed by the enzyme heme oxygenase [30].

Heme Oxygenase, HO, first characterized by Schmid and co-workers [33], is a microsomal enzyme which catalyzes the first key step in heme catabolism, the oxidative

degradation of heme (iron-protoporphyrin IX) to biliverdin and carbon monoxide [30, 34] (Figure 4). Heme oxygenase by itself contains no prosthetic groups. Thus, it is not a heme protein per se. It binds heme in a 1:1 ratio and constrains it to an environment suitable for a site-specific, O₂-dependent heme self-oxidation [30, 35]. Accordingly, HO is unusual in the context that it uses heme in a dual role of substrate and prosthetic group. It has a histidine residue and a distal H₂O or OH⁻ ligand that coordinate the heme. Even though important aspects of the mechanism of action of HO are not yet clarified, the evidence gathered so far demonstrates that HO acts via a mechanism different from that currently accepted for other oxygen activating heme proteins such as cytochromes P450, peroxidases and catalases [36]. It has already been established that the catalytic turnover of heme oxygenase requires the presence of O₂ and reducing equivalents provided by NADPH-cytochrome P450 reductase. Furthermore, it is also known that the reaction proceeds via the formation of a ferric peroxo intermediate, Fe^{III}-O₂⁻, (figure 3, steps 3, 5 and 6) without producing the ferryl (O=Fe⁴⁺) species (figure 3, step 4) observed in oxygenases and peroxidases [30, 34, 35, 37, 38]

Electroanalytical Methods for Biological Materials

The use of electrochemical methods to study proteins and enzyme electron transfer reactions directly with electrodes is becoming a “mature field” [39]. Twenty years ago, such studies were rarely conducted outside of laboratories with substantial expertise in electrochemistry. Now scientists in diverse fields have taken up cyclic voltammetry and other electrochemical methods such as spectroelectrochemistry to study biological systems.

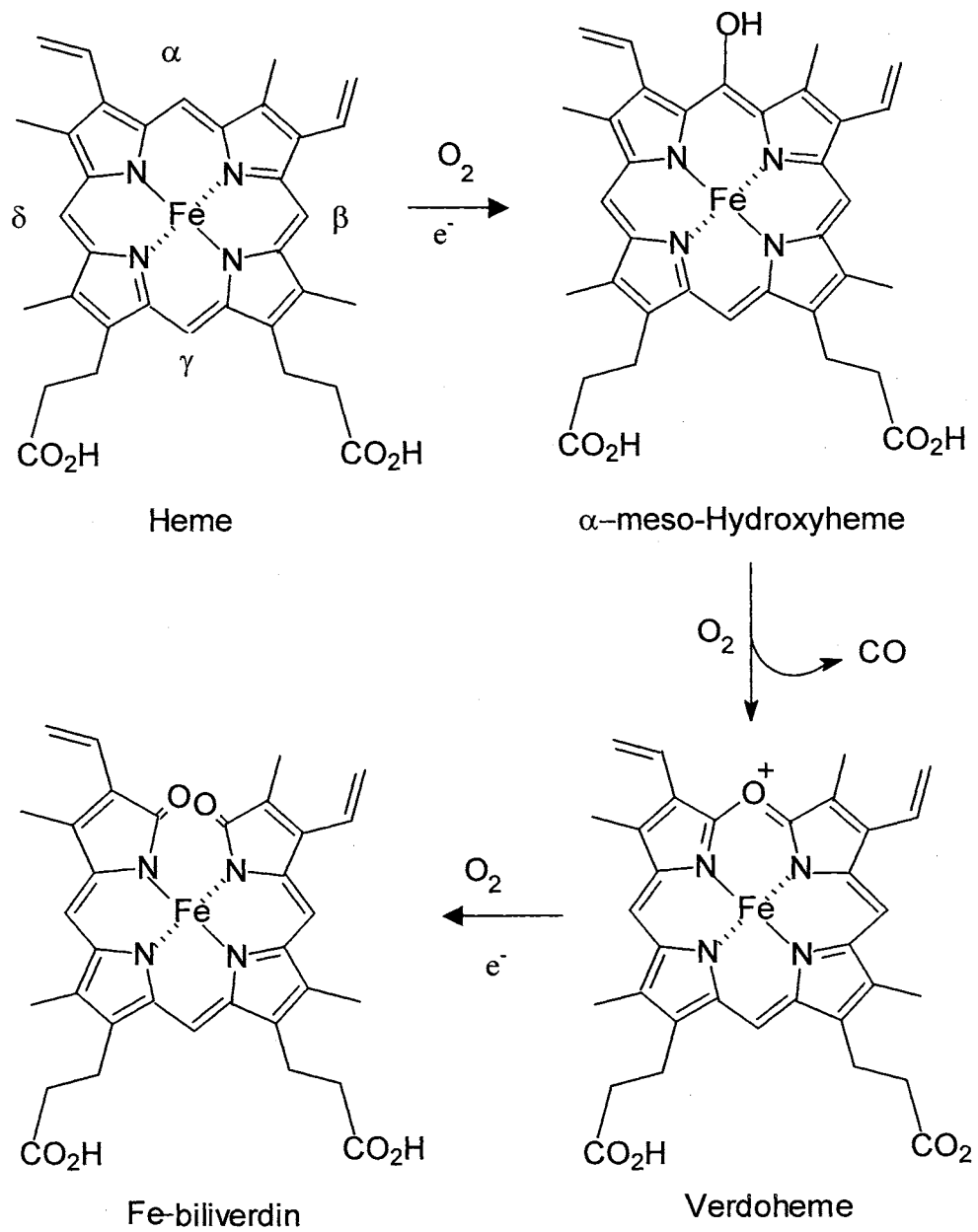


Figure 4. Heme Oxygenation Pathway

i). Cyclic Voltammetry

Cyclic voltammetry is perhaps the most versatile electroanalytical technique for the study of electroactive species. Unfortunately, proteins present a special problem for electrochemistry because their interaction with most common types of electrode surface does not lead to an electrochemical response. Two commonly quoted reasons are (1) that the protein shell acts as an insulator and (2) that the protein denatures upon contact with the electrode and there is strong adsorption of the resulting nonnative and electroinactive material [24]. In many cases these problems have been overcome and voltammetric investigations are being directed at all redox proteins from iron-sulfur proteins to heme proteins [24]. Successes have resulted largely from the use of appropriate electrode material, specific types of surface modification, optimization of interfacial electrostatics, and care in sample preparation. It has long been known that protein-protein interactions are important in biological electron transfer; consequently, efforts have been made to modify the electrode surface and solution interface in such a manner as to mimic physiological environments. For instance, oxide surfaces such as indium tin oxide, polished carbon or glassy carbon, or noble metals such as gold or platinum modified with various organic adsorbances or surfactants, have each proved successful for different systems [19, 40-42]. These surfaces project chemically stable groups that provide the appropriate properties of charge and hydrophobic/hydrophilic balance for interaction with protein molecules, without inducing denaturation [24].

Small iron-sulfur proteins usually possess a significant excess of negatively charged amino acids; therefore, their interaction with an electrode usually requires that the electrode surface or solution interface to contain positively charged groups. One way

of achieving this has been to add certain polycations to the electrolyte, see Figure 5. For instance, Taniguchi and co-workers achieved electrochemistry of chloroplast ferredoxin using an indium oxide electrode and adding a positively charged aminosilane groups [42].

ii). Spectroelectrochemistry

Another technique used for studying proteins electrochemically is spectroelectrochemistry, SEC. SEC combines the techniques of electrochemistry and spectroscopy. In a specially designed electrochemical cell, a redox active compound is oxidized or reduced. The products of the redox transformation or following chemical reactions are monitored in-situ by spectroscopic techniques. Since proteins are usually sluggish in their redox reactions with metallic electrodes, most methods for measuring redox potentials of proteins and enzymes are based upon varying the potential of a protein-mediator solution, while monitoring the change in some property of the protein responsive to its redox state, for instance UV-Visible spectrophotometry, or circular dichroism [44]. A schematic representation of the mediated approach is shown in Figure 6.

Purpose

The goal of any biological study is the understanding of function as an inseparable consequence of molecular structure. The many functions observed in heme-

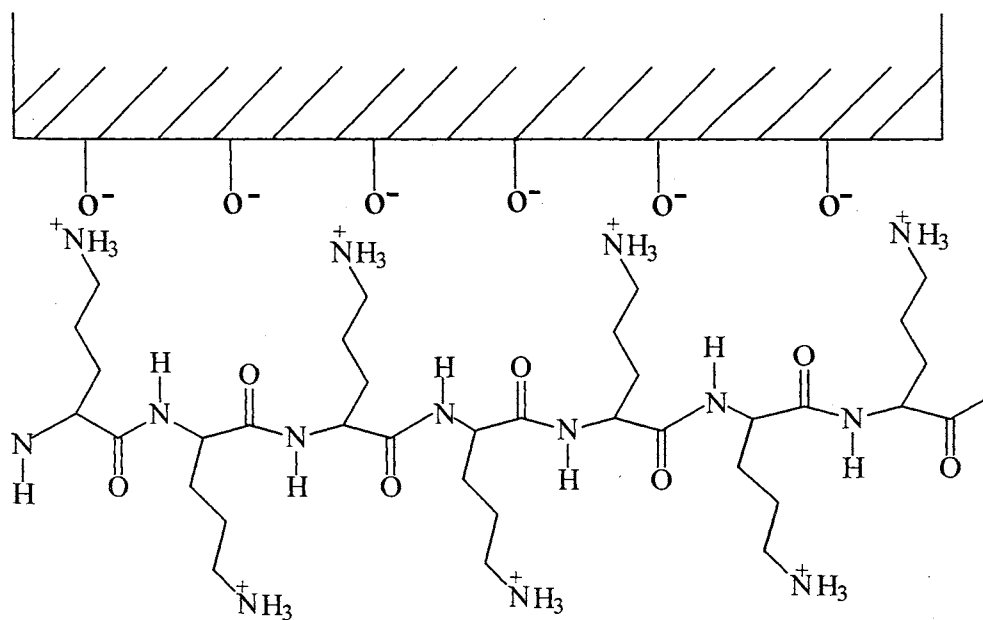


Figure 5. Schematic Representation of a Polylysine modified ITO Electrode (adapted from ref. [43]).

containing proteins are a consequence of the versatility of the heme group whose properties are modulated by its molecular environment. This dissertation will focus mainly on the study of electron transfer proteins 1) an iron sulfur protein, putidaredoxin (Pdx), and 2) several axial ligand variants of mitochondrial cytochrome b₅ engineered to convert a classical electron transfer protein into an oxygen-activating species.

Putidaredoxin (Pdx), an iron sulfur (2Fe/2S) protein, is one of the 3 major proteins involved in the catalytic cycle that results in the stereoselective oxidation of camphor to 5-exo-hydroxycamphor, which is a reaction catalyzed by cytochrome P450cam. The in vivo function of the cytochrome P450cam (CYP101) enzymatic complex is to catalyze the regio- and stereospecific hydroxylation of its substrate, d-camphor [34, 45]. The bacterium *Pseudomonas putida*, from which this enzyme was originally extracted and purified, can survive by using camphor as its sole carbon and energy source [34]. The full catalytic cycle of CYP101 requires an external source of two electrons from NADH, through the combined action of the FAD-containing protein putidaredoxin reductase (PdR). PdR then transfers an electron to (Pdx) [46]. It was proposed that the catalytic cycle could be replaced by the direct reduction of Pdx at an electrode surface, therefore, avoiding the use of expensive chemicals such as NADH. In order to do this, direct and reversible electrochemistry of Pdx was necessary. Chapter II discusses the goals needed to accomplish the direct and reversible electrochemistry of Pdx. First, the synthesis of the gene coding for Pdx using a combination of chemical and enzymatic methods will be discussed, followed by its characterization via electronic spectroscopy and electrochemistry. Finally, the factors responsible for modulating the reduction potential of Pdx will be discussed.

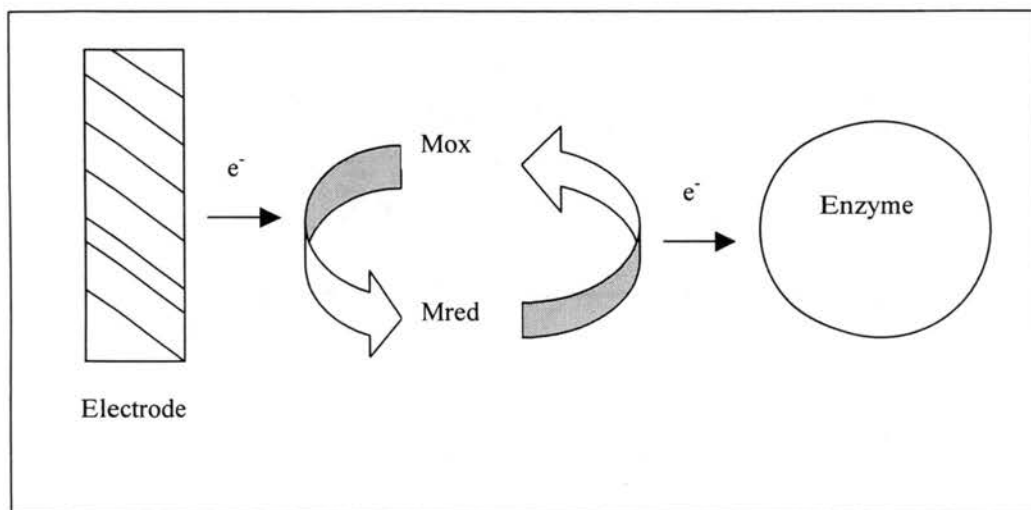


Figure 6. Schematic representation of the mediated electrochemical approach to activate proteins (adapted from ref. [47]).

Heme oxygenase, HO, as mentioned above, carries out the oxidation of heme, it cleaves the heme ring at the α methene bridge to form α -biliverdin and carbon monoxide. These products are currently thought to play important physiological functions. For this reason, it is important to attain a detailed understanding of the mechanism by which heme is converted into CO and biliverdin. Designing novel proteins capable of oxygenating their heme by the process known as coupled oxidation has helped in the study of the structural factors that are accountable for channeling oxygen activation toward heme oxygenation. Chapter III will present how the heme oxygenation reaction carried out by HO and the coupled oxidation reaction carried out by myoglobin and several axial ligand mutants of cyt b_5 proceed by different mechanisms. Strong evidence is presented indicating that while heme oxygenation is brought about by a coordinated peroxide intermediate ($\text{Fe}^{\text{III}}\text{-OOH}$), the coupled oxidation reaction is brought about by non-coordinated hydrogen peroxide. In fact, the coupled oxidation appears to be initiated by a Fenton-type reaction between the ferrous protein and non-coordinated hydrogen peroxide. The latter is produced by the reduction of O_2 by the sacrificial electron donor needed to carry out the coupled oxidation reaction.

The study of electrochemical reactions of redox proteins has been gaining interest throughout the years. These studies can provide information about thermodynamic and kinetic properties of redox proteins, structural properties, such as the orientational requirements for electron transfer between the protein and the electrode, and binding characteristics of proteins at specific types of electrode surfaces [47]. Electrochemical methods have been used to determine the reduction potential of a variety of electron transfer enzymes, however, for enzymes that use oxygen as a substrate, such as heme

oxygenase, it is imperative that the spectroelectrochemical cell is designed to accommodate these types of enzymes. The main difficulty in designing spectroelectrochemical cells of this type is the maintenance of an oxygen-free system over extended periods of time, usually 1-4 hours [48]. Other considerations are the complexity of construction, being able to maintain good stirring, and using minimal volume of enzyme for the experiment. Using the cell models described in Stankovich's, and Kuwana's papers [48, 49], two spectroelectrochemical cells have been designed and optimized for the electrochemical studies of such enzymes. These cells will be tested and compared in Chapter 4 by determining the reduction potentials of several bacterial heme oxygenases.

References

1. Stryer, L. and Editor, *Biochemistry, 4th Revised Edition*. 1996. p. 1100 pp.
2. Guengerich, F.P., *Uncommon P450-catalyzed reactions*, in *Curr Drug Metab.* 2001: Netherlands. p. 93-115.
3. Thony-Meyer, L., *Biogenesis of respiratory cytochromes in bacteria*, in *Microbiology and Molecular Biology Reviews*. 1997. p. 337-376.
4. Berg, J.M. and R.H. Holm, *Structures and reactions of iron-sulfur protein clusters and their synthetic analogs*, in *Met. Ions Biol.* 1982. p. 1-66.
5. Beinert, H., *Iron-sulfur proteins: ancient structures, still full of surprises*, in *JBIC, Journal of Biological Inorganic Chemistry*. 2000. p. 2-15.
6. Noodleman, L., T. Lovell, T. Liu, F. Himo, and R.A. Torres, *Insights into properties and energetics of iron-sulfur proteins from simple clusters to nitrogenase*, in *Current Opinion in Chemical Biology*. 2002. p. 259-273.
7. Cowan, J.A., *Inorganic Biochemistry: An Introduction*. 1993. p. 349 pp.
8. Bertini, I., S. Ciurli, and C. Luchinat, *The electronic structure of FeS centers in proteins and models. A contribution to the understanding of their electron transfer properties*, in *Struct. Bonding (Berlin)*. 1995. p. 1-53.
9. Mason, J.R. and R. Cammack, *The electron-transport proteins of hydroxylating bacterial dioxygenases*, in *Annual Review of Microbiology*. 1992: United States. p. 277-305.

10. Hanukoglu, I., *Steroidogenic enzymes: Structure, function, and role in regulation of steroid hormone biosynthesis*, in *J. Steroid Biochem. Mol. Biol.* 1992. p. 779-804.
11. Coghlan, V.M. and L.E. Vickery, *Electrostatic interactions stabilizing ferredoxin electron transfer complexes. Disruption by "conservative" mutations*, in *Journal of Biological Chemistry*. 1992: United States. p. 8932-5.
12. Peterson, J.A., M.C. Lorence, and B. Amarnah, *Putidaredoxin reductase and putidaredoxin. Cloning, sequence determination, and heterologous expression of the proteins*, in *Journal of Biological Chemistry*. 1990: United States. p. 6066-73.
13. Muller, A., J.J. Muller, Y.A. Muller, H. Uhlmann, R. Bernhardt, and U. Heinemann, *New aspects of electron transfer revealed by the crystal structure of a truncated bovine adrenodoxin, Adx(4-108)*, in *Structure*. 1998: ENGLAND: United Kingdom. p. 269-80.
14. Peterson, J.A., J.Y. Lu, J. Geisselsoder, S. Graham-Lorence, C. Carmona, F. Witney, and M.C. Lorence, *Cytochrome P-450terp. Isolation and purification of the protein and cloning and sequencing of its operon*, in *Journal of Biological Chemistry*. 1992: United States. p. 14193-203.
15. Benning, M.M., T.E. Meyer, I. Rayment, and H.M. Holden, *Molecular Structure of the Oxidized High-Potential Iron-Sulfur Protein Isolated from Ectothiorhodospira vacuolata*, in *Biochemistry*. 1994. p. 2476-83.
16. Breiter, D.R., T.E. Meyer, I. Rayment, and H.M. Holden, *The molecular structure of the high potential iron-sulfur protein isolated from Ectothiorhodospira halophila determined at 2.5 Å resolution*, in *J. Biol. Chem.* 1991. p. 18660-7.

17. Ambler, R.P., T.E. Meyer, and M.D. Kamen, *Amino acid sequence of a high redox potential ferredoxin (HiPIP) from the purple phototrophic bacterium Rhodospira rubra*, in *Arch. Biochem. Biophys.* 1993. p. 215-22.
18. Tollin, G., *Use of flavin photochemistry to probe intraprotein and interprotein electron transfer mechanisms*, in *Journal of Bioenergetics and Biomembranes*. 1995: United States. p. 303-9.
19. Armstrong, F.A. and G.S. Wilson, *Recent developments in faradaic bioelectrochemistry*, in *Electrochimica Acta*. 2000. p. 2623-2645.
20. Chapman, S.K., S. Daff, and A.W. Munro, *Heme: the most versatile redox center in biology?*, in *Structure and Bonding (Berlin)*. 1997. p. 39-70.
21. Ponka, P., *Cell biology of heme*, in *American Journal of the Medical Sciences*. 1999: United States. p. 241-56.
22. Paoli, M., J. Marles-Wright, and A. Smith, *Structure-function relationships in heme-proteins*, in *DNA and Cell Biology*. 2002. p. 271-280.
23. Gibney, B.R. and P.L. Dutton, *De novo design and synthesis of heme proteins*, in *Advances in Inorganic Chemistry*. 2001. p. 409-455.
24. Armstrong, F.A., *Voltammetric investigations of iron-sulfur clusters in proteins*, in *Electroanalytical Methods for Biological Materials*. 2002. p. 143-194.
25. Marchon, J.C., T. Mashiko, and C.A. Reed, *How does nature control cytochrome redox potentials?*, in *Electron Transp. Oxygen Util., [Int. Symp. Interact. Iron Proteins Oxygen Electron Transp.]*. 1982. p. 67-72.

26. Rivera, M., R. Seetharaman, D. Girdhar, M. Wirtz, X. Zhang, X. Wang, and S. White, *The Reduction Potential of Cytochrome b5 Is Modulated by Its Exposed Heme Edge*, in *Biochemistry*. 1998. p. 1485-1494.
27. Wirtz, M., V. Oganessian, X. Zhang, J. Studer, and M. Rivera, *Modulation of redox potential in electron transfer proteins: Effects of complex formation on the active site microenvironment of cytochrome b5*, in *Faraday Discussions*. 2000. p. 221-234.
28. Dawson, J.H., *Probing structure-function relations in heme-containing oxygenases and peroxidases*, in *Science (Washington, D. C., 1883-)*. 1988. p. 433-9.
29. Kassner, R.J., *Effects of nonpolar environments on the redox potentials of heme complexes*, in *Proc. Nat. Acad. Sci. U. S. A.* 1972. p. 2263-7.
30. Sono, M., M.P. Roach, E.D. Coulter, and J.H. Dawson, *Heme-Containing Oxygenases*, in *Chem. Rev. (Washington, D. C.)*. 1996. p. 2841-2887.
31. Warshel, A., A. Papazyan, and I. Muegge, *Microscopic and semimacroscopic redox calculations: what can and cannot be learned from continuum models*, in *JBIC, Journal of Biological Inorganic Chemistry*. 1997. p. 143-152.
32. Wilks, A. and P.R. Ortiz de Montellano, *Rat liver heme oxygenase. High level expression of a truncated soluble form and nature of the meso-hydroxylating species*, in *J. Biol. Chem.* 1993. p. 22357-62.
33. Tenhunen, R., H.S. Marver, and R. Schmid, *Microsomal heme oxygenase. Characterization of the enzyme*, in *J. Biol. Chem.* 1969. p. 6388-94.

34. Ortiz de Montellano, P.R. and Editor, *Cytochrome P450: Structure, Mechanism, and Biochemistry, Second Edition*. 1995. p. 630 pp.(approx.).
35. Yoshida, T. and G. Kikuchi, *Purification and properties of heme oxygenase from rat liver microsomes*, in *J. Biol. Chem.* 1979. p. 4487-91.
36. De Montellano, P.R.O., *The mechanism of heme oxygenase*, in *Current Opinion in Chemical Biology*. 2000. p. 221-227.
37. Yoshida, T. and G. Kikuchi, *Purification and properties of heme oxygenase from pig spleen microsomes*, in *J. Biol. Chem.* 1978. p. 4224-9.
38. Kikuchi, G. and T. Yoshida, *Function and induction of the microsomal heme oxygenase*, in *Mol. Cell. Biochem.* 1983. p. 163-83.
39. Burgess, J.D. and F.M. Hawkrige, *Direct electrochemistry of proteins and enzymes at electrodes*, in *Electroanalytical Methods for Biological Materials*. 2002. p. 109-142.
40. Kasmi, A.E., J.M. Wallace, E.F. Bowden, S.M. Binet, and R.J. Linderman, *Controlling Interfacial Electron-Transfer Kinetics of Cytochrome c with Mixed Self-Assembled Monolayers*, in *Journal of the American Chemical Society*. 1998. p. 225-226.
41. Rusling, J.F., *Enzyme Bioelectrochemistry in Cast Biomembrane-Like Films*, in *Accounts of Chemical Research*. 1998. p. 363-369.
42. Taniguchi, I., K. Watanabe, M. Tominaga, and F.M. Hawkrige, *Direct electron transfer of horse heart myoglobin at an indium oxide electrode*, in *J. Electroanal. Chem.* 1992. p. 331-8.

43. Wirtz, M.-O.S., *Electrochemical activation of proteins at electrode surfaces through electrostatic promotion and discrimination*. 2000. p. 158 pp.
44. Watt, G.D., *An electrochemical method for measuring redox potentials of low potential proteins by microcoulometry at controlled potentials*, in *Analytical Biochemistry*. 1979: United States. p. 399-407.
45. Unno, M., J.F. Christian, T. Sjodin, D.E. Benson, I.D.G. Macdonald, S.G. Sligar, and P.M. Champion, *Complex formation of cytochrome P450cam with putidaredoxin: evidence for protein-specific interactions involving the proximal thiolate ligand*, in *Journal of Biological Chemistry*. 2002. p. 2547-2553.
46. Roitberg, A.E., M.J. Holden, M.P. Mayhew, I.V. Kurnikov, D.N. Beratan, and V.L. Vilker, *Binding and Electron Transfer between Putidaredoxin and Cytochrome P450cam. Theory and Experiments*, in *Journal of the American Chemical Society*. 1998. p. 8927-8932.
47. Dong, S., J. Niu, and T.M. Cotton, *Ultraviolet/visible spectroelectrochemistry of redox proteins*, in *Methods Enzymol*. 1995. p. 701-32.
48. Stankovich, M.T., *An anaerobic spectroelectrochemical cell for studying the spectral and redox properties of flavoproteins*, in *Anal. Biochem*. 1980. p. 295-308.
49. Szentrimay, R., P. Yeh, and T. Kuwana, *Evaluation of mediator-titrants for the indirect coulometric titration of biocomponents*, in *ACS Symp. Ser.* 1977. p. 143-69.

CHAPTER II

AN ELECTROCHEMICAL STUDY OF THE FACTORS RESPONSIBLE FOR MODULATING THE REDUCTION POTENTIAL OF PUTIDAREDOXIN

Introduction

Putidaredoxin (Pdx) is a 106-amino acid electron-transfer protein (MW 11,594), which contains a 2Fe-2S-Cys₄ cluster in its active site [1]. During the process of electron transfer, one iron atom in the cluster undergoes change from the ferrous and ferric oxidation states, whereas the other iron atom remains in the ferric oxidation state [2]. Pdx is one the three major proteins involved in the catalytic cycle that results in the stereoselective oxidation of camphor to 5-exo-hydroxycamphor, a reaction catalyzed by cytochrome P450_{cam} [3, 4]. It has recently been shown that cytochrome P450_{cam} is also capable of catalyzing the reductive dehalogenation of halogenated hydrocarbons [5-7], the hydroxylation of carbon and the epoxidation of double bonds [8, 9], and the sulfoxidation of thioethers [10]. Consequently, there has been an intense effort aimed at harnessing the catalytic ability of cytochrome P450_{cam} for its applications in electrosynthesis and bioremediation processes[11-14].

The catalytic cycle of cytochrome P450_{cam} starts with reduction of the FAD-containing protein putidaredoxin reductase (PdR) by NADH; PdR, in turn, transfers one electron to the oxidized form of Pdx. The reduced form of Pdx forms a complex with ferric cytochrome P450_{cam} and subsequently transfers one electron to the latter within the

complex [3]. Consequently, in the complete catalytic cycle leading to the hydroxylation of camphor, two electrons are transferred from Pdx to cytochrome P450_{cam} in two discrete events [15].

It has been proposed that the catalytic cycle described above can be replaced by the direct reduction of Pdx at an electrode surface, therefore avoiding the use of expensive and fragile chemicals and enzymes such as NADH and PdR [16]. Thus, it is evident that in order to accomplish this goal it is necessary to obtain the direct and reversible electrochemistry of Pdx. Despite the impressive advances in the area of bioelectrochemistry aimed at exploring the direct and reversible electrochemistry of redox-capable proteins and enzymes, the reversible electrochemistry of Pdx was somewhat elusive. For example, Wong and Vilker [16] utilized a gold electrode modified with mercaptoethylamine to study the direct electrochemistry of this electron transfer protein. These authors reported that, although it is possible to obtain the direct electrochemistry of Pdx at the mercaptoethylamine-modified gold electrodes, the cyclic voltammograms were characterized by relatively slow kinetics of heterogeneous electron transfer ($k_s=1.0 \times 10^{-4}$ cm/s), and by rapid deterioration of the electrochemical response [16, 17]. This deterioration was suggested to originate from a conformational change (s-trans to gauche) of the mercaptoethylamine chain on the electrode surface upon scanning the electrode potential in the negative direction [17].

In a different study, a solution consisting of a mixture of Pdx, cytochrome P450_{cam}, and d-camphor was electrolyzed at an antimony-doped tin oxide electrode in the presence of oxygen and d-camphor [14]. The authors indicated that in this system the oxidized form of Pdx is reduced at the semiconductor electrode surface; the reduced form

of Pdx, in turn, transfers the electron to cytochrome P450_{cam} in order to perform the hydroxylation of camphor. It is interesting to note, however, that the hydroxylation of camphor to produce 5-exo-hydroxycamphor required that the concentration of Pdx in the electrolytic cell to be at least 500 times larger than that of cytochrome P450_{cam}. Although the need for such a large excess of Pdx with respect to P450_{cam} is not clear [14], the authors suggested that this may originate from a slow rate of heterogeneous electron transfer (k_s) between the electrode and Pdx. The value of k_s , measured for Pdx at the antimony doped tin oxide electrode was found to be $1.0 \times 10^{-4} \text{ cm s}^{-1}$ [14]. This value is more than one order of magnitude smaller than the values reported for the heterogeneous electron transfer rate constants observed for most electron transfer proteins (approximately $5 \times 10^{-3} \text{ cm s}^{-1}$), including several types of ferredoxins [18-22]. It is therefore important to continue to explore the conditions such as the electrode surface and the electrode modifier that can promote the direct and reversible electrochemistry of Pdx.

The gene synthesis and bacterial expression of the metalloprotein Pdx and its corresponding spectroscopic and electrochemical characterization will be the focus of this chapter. The electrochemical evidence reported here shows that, when the voltammetry of Pdx is promoted at negatively charged electrodes by a polycation such as polylysine, the heterogeneous electron transfer rate constant is one order of magnitude larger than the value reported for this protein previously [16, 17]. It was also determined that the reduction potential of Pdx shifts in the positive direction as a consequence of forming a transient complex with polylysine at the electrode surface. The magnitude of the anodic shift in the reduction potential of Pdx is similar to that reported for this protein when it

forms a complex with cytochrome P450_{cam}. These observations combined indicate that the positive electrostatic field provided by polylysine to the electrode surface steers Pdx toward the electrode surface with an orientation close to optimal for facile heterogeneous electron transfer. Furthermore, it is postulated that the association between polylysine and Pdx lowers the dielectric constant of the solvent-exposed iron sulfur cluster in Pdx, hence resulting in an anodic shift of its reduction potential.

Experimental procedures

Protocols utilized for standard procedures such as plasmid isolation, transformation, ligations, and restriction endonuclease reaction were those published by Sambrook et al. [23]. Protocols that had to be modified are described in detail in the next section. The deoxynucleotide triphosphates (dNTP), and enzymes used for the experiments were purchased from Life Technologies, Grand Island, NY. The Sequenase kit was purchased from Amersham Corp. Cleveland, OH. The pBS+ plasmid was purchased from Stratagene, La Jolla, CA, and the pET11a plasmid and BL21(DE3) *E. Coli* cells were purchased from Novagen, Madison, WI. Polylysine with MW=7500 was purchased from Sigma and used without further purification. Single-stranded oligonucleotides were synthesized by the Recombinant DNA/Protein Facility at Oklahoma State University.

i). Design and synthesis of the gene

The amino acid sequence of Pdx [24] was back translated into a nucleotide sequence using the program Mac Vector; the DNA and amino acid sequences of the synthetic gene are shown in Fig. 1. The DNA sequence was subjected to silent mutations in order to introduce codons preferentially utilized by *E. Coli* [25, 26]. The first and last 15 base pairs shown in Fig. 1 were added to the original DNA sequence in order to add start and stop signals and enzyme restriction sites (*EcoRI*, *BamHI*, *NdeI*) convenient for subsequent cloning and subcloning.

Four single-stranded oligonucleotides were designed to cover the 348 total bases; the first two single-stranded oligonucleotides shown in Figure 1 are 93 bases long and the remaining two are 111 bases long. In order to assemble the gene, oligonucleotides 1 and 2, and oligonucleotides 3 and 4 were self-primed and then extended with Sequenase, as shown schematically in Figure 2a. To this end, 1 μ L of a solution containing single stranded oligonucleotide (1 μ g/ μ L) was taken to a final volume of 20 μ L with 5X Sequenase buffer. The solution containing oligonucleotides 1 and 2 was heated to 70° C for 5 minutes and then cooled to 50° C for 5 minutes; the solution containing oligonucleotides 3 and 4 was heated to 90° C for 5 minutes for annealing and then cooled to 50° C for 5 minutes. The annealed (self-primed) oligonucleotides were extended with sequenase version 2 (65 units) in the presence of a mixture of dNTPs (10mM) by incubating the solutions at 37° C for 30 minutes. The solutions were then heated to 70° C for 10 minutes in order to inactivate the sequenase. Each resulting solution (24 μ L) was digested with *Pml* I (*NEB*) in a final volume of 100 μ L at 37° C for 2.5 hours as shown schematically in Fig.2b. The resultant solutions were purified by phenol-chloroform extraction and precipitated with ethanol. The pellets were resuspended in 10 μ L water

	Eco RI	Nde I	OLIGO 1																			
5'	GGGGAATTC	ATG	TCG	AAG	GTA	GTA	TAC	GTA	TCG	CAC	GAC	GGC	ACC	CGC	CGA	GAG	CTG	GAC	GTA	66		
	CCCCTTAAG	TAC	AGC	TTC	CAT	CAT	ATG	CAT	AGC	GTG	CTG	CCG	TGG	GCG	GCT	CTC	GAC	CTG	CAT			
		M	S	K	V	V	Y	V	S	H	D	G	T	R	R	E	L	D	V			
Eco NI																						
	GCG	GAC	GGC	GTA	AGC	CTG	ATG	CAG	GCG	GCG	GTG	TCG	AAC	GGC	ATC	TAC	GAC	ATC	GTA	GGC	GAC	129
	CGC	CTG	CCG	CAT	TCG	GAC	TAC	GTC	CGC	CGC	CAC	AGC	TTG	CCG	TAG	ATG	CTG	TAG	CAT	CCG	CTG	
	A	D	G	V	S	L	M	Q	A	A	V	S	N	G	I	Y	D	I	V	G	D	
3' ←										OLIGO 2												
	TGC	GGC	GGC	AGC	GCT	AGC	TGC	GCG	ACT	TGC	CAC	GTG	TAC	GTG	AAC	GAG	GCT	TTC	ACC	GAC	AAG	192
	ACG	CCG	CCG	TCG	CGA	TCG	ACG	CGC	TGA	ACG	GTG	CAC	ATG	CAC	TTG	CTC	CGA	AAG	TGG	CTG	TTC	
	C	G	G	S	A	S	C	A	T	C	H	V	Y	V	N	E	A	F	T	D	K	
5'										5'												
Nhe I							Pml I															
5'																						
	GTG	CCG	GGC	GGC	AAC	GAG	CGC	GAG	ATC	GGC	ATG	CTG	GAG	TGC	GTG	ACC	GCT	GAG	CTG	AAG	CCG	255
	CAC	GGC	CGC	CGC	TTG	CTC	GCG	CTC	TAG	CCG	TAC	GAC	CTC	ACG	CAC	TGG	CGA	CTC	GAC	TTC	GGC	
	V	P	A	A	N	E	R	E	I	G	M	L	E	C	V	T	A	E	L	K	P	
3' ←												3' ←										
	AAC	AGC	CGC	CTG	TGC	TGC	CAG	ATC	ATC	ATG	ACC	CCG	GAG	CTG	GAC	GGC	ATC	GTG	GTG	GAC	GTG	318
	TTG	TCG	GCG	GAC	ACG	ACG	GTC	TAG	TAG	TAC	TGG	GGC	CTC	GAC	CTG	CCG	TAG	CAC	CAC	CTG	CAC	
	N	S	R	L	C	C	Q	I	I	M	T	P	E	L	D	G	I	V	V	D	V	
3' Eco 57I										Bsa JI												
5'																						
	CCG	GAC	CGC	CAG	TGG	TAA	TAAGGATCCGGG														348	
	GGC	CTG	GCG	GTC	ACC	ATT	ATTCCTAGGCC															
	P	D	R	Q	W																	
5'																						
Rsr II								Bam HI														
5'																						

Figure 1. Amino acid and corresponding DNA sequences of Pdx. The codon signaling for the initiator methionine, codons frequently used by *Escherichia coli*, and the restriction endonuclease sites were engineered as discussed in the Experimental Section. Arrows indicate the length of the synthetic single stranded oligonucleotides utilized for the assembly of the gene

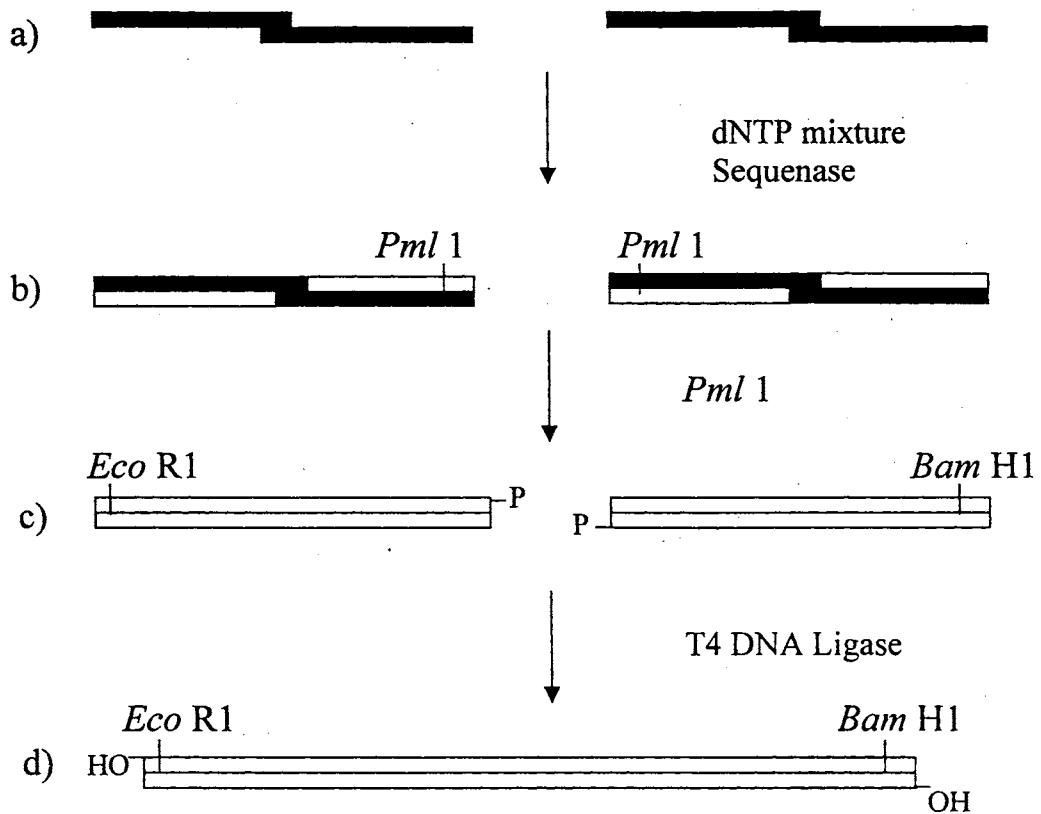


Figure 2. Schematic representation of the strategy followed to synthesize the gene coding for Pdx. The restriction endonuclease sites *Eco RI* and *Bam HI* were utilized to directionally colon the assembled gene

and the two oligonucleotides were ligated together with T4 DNA ligase (5 units/ μ L, *Gibco*) for 12 hours at room temperature as shown schematically in Fig. 2c. This ligation solution was purified by phenol-chloroform extraction and precipitated with ethanol. The pellet was subsequently resuspended in 20 μ L of the appropriate buffer and digested with *Eco* RI and *Bam* HI, as shown schematically in Fig.2d. The resultant solution containing the fully assembled gene was purified by phenol-chloroform extraction, the DNA precipitated with ethanol and then resuspended in 20 μ L water. The assembled gene was cloned into the pBS+ plasmid (*Stratagene*) utilizing the unique *Eco* RI and *Bam* HI restriction sites by ligating for 16 hours at 16° C. The resultant recombinant plasmid (LA1) was used to transform competent *E. coli* strain XL1 Blue for amplification and sequencing of the gene. The DNA was taken to the CORE Facility, Oklahoma State University, for sequencing. Once the correct sequence was obtained, the gene was subcloned in the pET 11a expression vector utilizing the unique restriction sites *Nde* I and *Bam* HI (see Fig. 1). The gene was purified using a Gene Clean II kit and ligated into pET 11a by incubating for 16 hours at 16° C. The resultant recombinant plasmid (LA2) was used to transform competent *E. coli* BL21 (DE3) cells for the subsequent expression of Pdx.

ii). Expression and purification of PDX

A single colony of *E. coli* BL21(DE3) cells harboring the LA2 plasmid was grown overnight at 37° C in 5mL of LB medium containing ampicillin (100mg/l). The overnight culture was used to inoculate 1 L of LB medium and the cells were grown at

37° C to an optical density at 600 nm (OD₆₀₀) of approximately 1.0. When the OD₆₀₀ reached a value of 1.0, the protein synthesis was induced with 1 ml of 1M IPTG (Isopropyl β-D- thiogalactopyranoside). Four hours after the protein synthesis was induced, the cultures were cooled to 4° C and the cells were harvested by centrifugation at 4500 rpm for 10 minutes. The supernatant was decanted and the brown cells frozen at -20°C overnight.

The cells were resuspended in 3 mL of lysis buffer (20 mM MOPS, 8.3 mM NaAc, 5 mM EDTA, 10 mM MgSO₄, 1 mM DTT) for each gram (wet weight) of cells. An additional 0.15g/L of DTT to known volume of lysis buffer was then added. The cells were lysed with a solution containing lysozyme (10 mg/mL), 50 mM PMSF (phenylmethylsulfonyl fluoride) dissolved in ethanol, and deoxycholic acid. For each gram of wet cells, 160 μL lysozyme, 32 μL PMSF, and 4 mg of deoxcholic acid were added while stirring the suspension every 10-15 minutes for about 1 hour at 4 °C. When the lysate became viscous, 20 μL of DNase I (1mg/mL) per g of *E. coli* was added and stirred for another hour or until it was no longer viscous at 4°C. Cell debris was removed by ultracentrifugation at 45,000 rpm at 4°C for 1 hour. The Pdx containing solution was dialyzed using a dialysis membrane with a 6 kD molecular weight cutoff against Buffer A (50 mM MOPS, 1 mM DTT, adjust to pH 7.4 with Tris base). The buffer was changed at least 3 times in a period of 16-24 hours. The desalted protein solution was loaded onto a DE 52 anion exchange column pre-equilibrated with Buffer A and the protein eluted with a linear salt gradient consisting of 0-500 mM KCl dissolved in Buffer A.

Aliquots containing Pdx (brown band) were collected and then concentrated by ultrafiltration using a membrane with a 3 kD molecular weight cutoff. The protein was subsequently purified in a gel filtration column (Pharmacia Sephadex G -50) pre-equilibrated for at least 3 days prior to this final purification step with fresh Buffer A containing 100 mM KCl. The fractions with an absorbance ratio (A_{455}/A_{275}) of 0.5 were collected in order to obtain a homogeneous protein. After each collected fraction, additional DTT (0.15g/L) was added and then concentrated by ultrafiltration using a membrane with a 3 kD molecular weight cutoff. Finally β -mercaptoethanol (β ME), ≤ 10 mM, was added as a protective agent (see note) and the purified Pdx was frozen in liquid nitrogen and stored at -80 °C under argon in approx. 1 mL aliquots. A typical yield for 1 L of culture media was 5 mg of homogeneous Pdx. The protein concentration was calculated using extinction coefficients of $10.4 \text{ mM}^{-1} \text{ cm}^{-1}$ at 455 nm for the oxidized protein and $8.5 \text{ mM}^{-1} \text{ cm}^{-1}$ at 480 for the reduced protein respectively [27].

Note: Pdx slowly loses the prosthetic group during standing at 0 °C in the absence of active β ME. This is seen by a decrease in absorbance measured by UV-vis. β ME retards the apoprotein formation.

iii). Cyclic Voltammetry

Cyclic voltammetry was carried out with a BAS-CV 50W potentiostat (Bioanalytical Systems, West Lafayette, IN) and single-compartment electrochemical cells containing the working, reference, and auxiliary electrodes. A 1.5 mm diameter

gold-disk working electrode, platinum wire auxiliary electrode, and an Ag/AgCl reference electrode equipped with a fiber junction were purchased from Cypress Systems (Lawrence, KS). Before each experiment, the gold-disk working electrode was polished using 15-, 6-, and 1- μm diamond polishing slurries on nylon, then polished with 0.05- μm alumina polishing slurry on cotton wool, and finally thoroughly rinsed with deionized water and sonicated for 3 minutes in deionized water. Surface modification of the electrode was achieved by dipping the polished gold electrode into a 100.0 mM methanolic solution of 5-mercaptopentanoic acid for 20 minutes, followed by rinsing with ethanol and then with water. The modified electrode was immediately transferred into the electrochemical cell containing a deaerated protein solution.

Cyclic voltammograms of Pdx were also obtained utilizing indium-tin oxide working electrodes (ITO). The ITO-coated slides (one-side coated), $R_s \leq 10$ ohms (Delta Technologies, Stillwater, MN) were cleaned by sonication: 20 minutes in 1%alconox solution, followed by 20 minutes in ethanol and then 20 minutes in distilled water. Solutions used for cyclic voltammetry were prepared in 100 mM MOPS buffer pH 7.0 and were typically 70 μM in Pdx and 140 μM in polylysine. The electrochemical cell used for these experiments was made of plexiglass and consisted of three electrodes and a nitrogen inlet for maintaining anaerobicity. A Pt wire was used as the counter electrode, and the reference used was a Ag/AgCl electrode (Cypress Systems, Lawrence, KS).

iv). Spectroelectrochemistry of Pdx

Transmission mode spectroelectrochemical titrations were carried out in a custom-made spectroelectrochemical cell shown in Fig. 3, which was constructed from a glass cuvette (1.0 cm path-length) that contained a platinum foil working electrode, an Ag/AgCl reference electrode and a magnetic stirrer. The set up consisted of a spectrophotometer, power supply, voltmeter, and potentiometric cell. The power supply was used to operate a magnet, which in turn allowed the movement of the magnetic stirrer. The voltmeter was connected to the reference and indicating electrodes to measure the potential. The spectroelectrochemical cell used in this research was modeled from the anaerobic spectroelectrochemical cell reported previously by Stankovich [28]. The spectrochemical titrations were carried out by adding appropriate volumes of a 100 mM solution of sodium dithionite to a solution consisting of Pdx (70 μ M) and the redox mediator phenosafranine (30 μ M), $E^{\circ} = -252$ mV vs NHE [29] in phosphate buffer ($\mu=0.10$, pH =7.0). The potentiometric titration was monitored with absorbance at 408 nm because this wavelength corresponded to a peak in the spectrum of oxidized Pdx, to a minimum in the spectrum of the reduced form of the protein, and to an isosbestic point in the spectrum of phenosafranine. Potentiometric titrations were also performed with solutions containing Pdx and polylysine (70 μ M and 140 μ M, respectively) and the redox mediators anthroquinone-2-sulfonic acid ($E^{\circ} = -225$ mV vs NHE) and anthroquinone-2,6-disulfonic acid ($E^{\circ} = -184$ mV vs NHE) [29], 60 μ M each. The need to use these mediators instead of phenosafranine originated from an anodic shift in the reduction potential Pdx upon forming a complex with polylysine. These potentiometric titrations were monitored by following the absorbance at 570 nm because the redox mediators do not absorb in this spectral region.

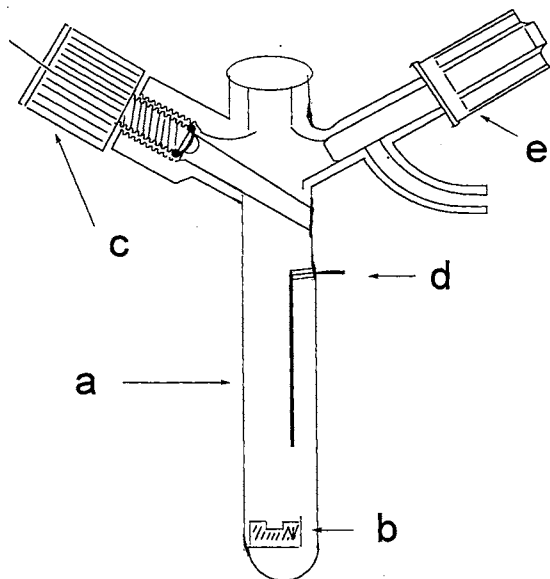


Figure 3. Potentiometric cell utilized for the spectroelectrochemistry of Pdx. The cell is constructed out of a glass cuvette (1.0 cm path-length) (a) equipped with a Ag/AgCl reference electrode (c), a Pt wire as the indicating electrode (d), and a magnetic stirrer (b). The cell is also equipped with a Rotaflow stopcock that serves as an inlet for argon or nitrogen (e)

v). Preparation of modifiers

The modifiers 5-(ethoxycarbonyl)pentylisothiuronium bromide and 5-mercaptopentanoic acid were prepared using the general procedure of Speziale [30] by Richard Bunce, OSU Chemistry Department [31].

Results and Discussion

i). Gene synthesis and bacterial expression

The synthetic gene was assembled from two pairs of self-priming single stranded oligonucleotides, as shown in figure 1 and schematically in figure 2. The first and last 15 base pairs were added to the original sequence in order to add stop codons and restriction sites used for cloning and subcloning. The first two oligonucleotides were each 93 bases long and the other two were 111 bases long. The 3' ends of the double-stranded oligonucleotides were not phosphorylated with T4 polynucleotides kinase and ATP; instead, selective phosphorylation of the desired ends was achieved by restricting the double-stranded DNA with *Pml* I as shown schematically in Fig. 2b. This strategy diminishes the number of undesired side-products obtained upon ligation of the two double-stranded oligonucleotides show schematically in Fig. 2c, consequently increasing the probability of obtaining the total gene coding for Pdx. The completely assembled gene was cloned into pBS + plasmid, sequenced, and then subcloned into expression vector pET 11a utilizing methods described previously [32].

Addition of IPTG to a growing culture of *E. coli* BL21 (DE3) cells harboring the recombinant pET 11a plasmid resulted in the overexpression of Pdx. Four hours after inducing protein expression by addition of IPTG, the cells were harvested and Pdx was purified to homogeneity as described in the Experimental Procedures. Sequential Edman degradation of homogeneous recombinant putidaredoxin indicated that the engineered initiator methionine residue (Fig.1) was not present in the isolated protein. The 43 subsequent residues observed in the amino terminal analysis were found to have a sequence identical to the one predicted from the coding sequence, where a serine residue is the amino-terminal residue.

Homogeneous recombinant putidaredoxin in its oxidized state displays an electronic spectrum (Fig. 4a) identical to that reported for Pdx isolated from *Pseudomonas putida* [33], hence demonstrating that the expression of the synthetic gene reported here produces the holo protein. The electronic spectrum shown in Fig. 4b corresponds to recombinant Pdx reduced with sodium dithionite; this spectrum is identical to that reported for the reduced protein isolated from *Pseudomonas putida*. The pure protein was also analyzed by electrospray mass spectrometry and shown to have a mass of 11,420 Da. This mass compares well with the value of 11419 Da calculated for apo-Pdx, hence indicating that the Fe_2S_2 cluster is lost under the acidic conditions that were utilized for electrospraying the protein. The experimentally measured mass of recombinant putidaredoxin also indicated that the engineered initiator methionine residue is clipped-off, a finding that is in good agreement with the amino-terminal sequence information discussed above.

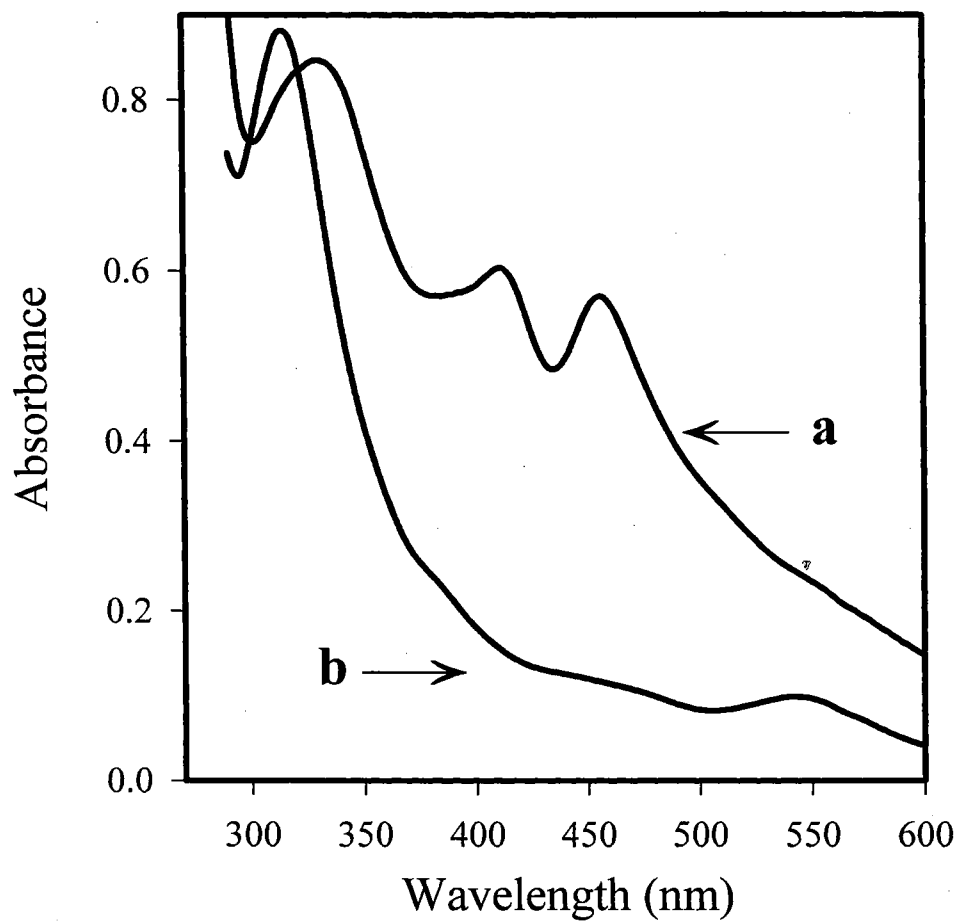


Figure 4. Electronic spectra of recombinant Pdx (approximately 70 μ M in MOPS buffer, pH=7.4) (a) oxidized and (b) reduced with sodium dithionite.

ii). Cyclic voltammetry

In the past two decades, significant advances have been made toward achieving fast and direct electron transfer between electrode-surfaces and redox-capable proteins; this active area of research has been recently reviewed [18, 34-37]. A generalized picture emerging from these studies implies that the direct and reversible electrochemistry of electron-transfer proteins is typically obtained at electrode surfaces possessing a charge complementary to that exhibited by the protein surface near its active site. This is typically accomplished by modifying electrode-surfaces with molecules possessing an ionizable group in order to impart the desired charge to the electrode surface, or alternatively, by the utilization of polyvalent ions in order to mediate the interactions between electrode and protein surfaces. The NMR structural information reported by Pochapsky and coworkers [18, 34-38], combined with the information obtained from the Poisson-Boltzmann electrostatic calculations performed by Roitberg et al. [39] indicate that the surface of Pdx possesses a unique patch of contiguous negative electrostatic potential. This patch is provided by residues Asp-34, Asp-38, and Trp-106 (Fig.5); the latter amino acid is negatively charged because it is the carboxy-terminal residue in the amino acid sequence of putidaredoxin. Given the negative charge on the electrode surface of Pdx, polylysine was added to promote the electrochemistry of Pdx. Polylysine was chosen because it has been successfully utilized to promote the reversible electrochemistry of several other negatively charged proteins [22, 40, 41].

A typical background-subtracted cyclic voltammogram obtained from a solution containing a mixture of Pdx and polylysine (molar ratio 1:2) at an ITO electrode is shown

in Fig. 6. The ratio of the cathodic to anodic peak currents is unity and the peak to peak separation is 64mV. This reversible electrochemical response persists for at least 4 h. The cathodic peak current is proportional to the square root of the scan rate (inset Fig.6), indicating that the electrochemical process is diffusion-controlled. From the slope of the plot relating the cathodic peak current to the square root of the scan rate, the diffusion coefficient of Pdx was determined to be $9.8 \times 10^{-7} \text{ cm}^2/\text{s}$. This value is in good agreement with values of the diffusion coefficients reported for proteins of similar molecular weight [18, 19]. By comparison, and in agreement with the electrostatic charge on the surface of Pdx, the absence of polylysine in the electrochemical cell results in the total absence of Faradaic response.

The value of the heterogeneous electron transfer rate constant (k) was obtained by simulating the experimental cyclic voltammograms (Fig. 6) with the aid of the program Digisim [42] (Bioanalytical Systems), and found to be $1.3 \times 10^{-3} \text{ cm/s}$. This value is more than one order of magnitude larger than the value of k previously obtained for Pdx with a gold electrode modified with mercaptoethylamine [16]. Consequently, promoting the reversible electrochemistry of Pdx at negatively charged electrodes with polylysine not only permits facile heterogeneous electron transfer but also enables the observation of the reversible electrochemistry of Pdx for at least 4 hours at room temperature.

The reduction potential observed for Pdx at an ITO electrode in the presence of polylysine is $-176 \pm 5 \text{ mV}$ vs SHE. This value is 64 mV more positive than that measured for Pdx by potentiometric techniques [43]. In order to investigate the effect that the ITO surface or the presence of polylysine exerts on the reduction potential of Pdx, the direct electrochemistry of this protein was carried out utilizing gold surfaces modified with 2-

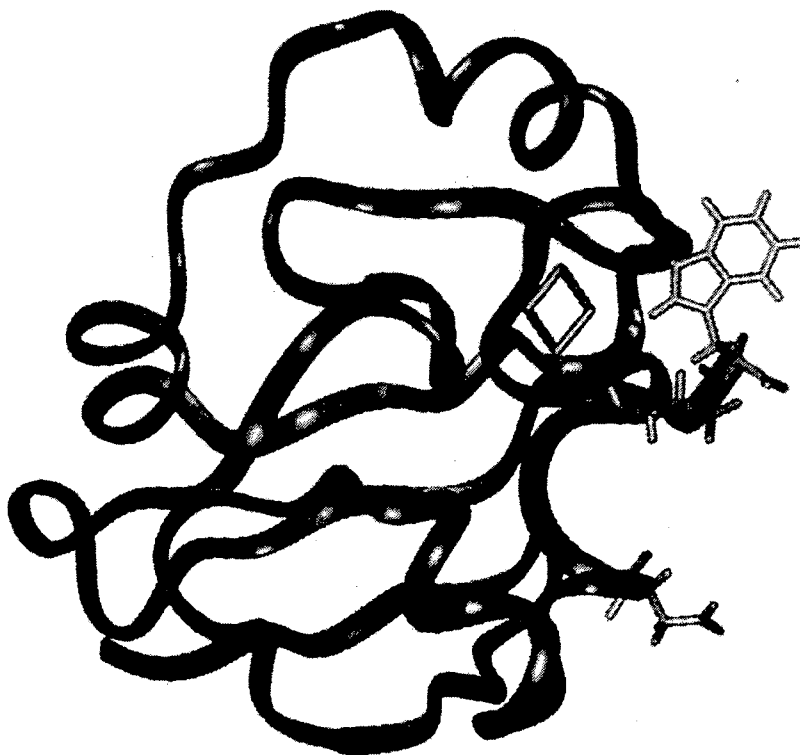


Figure 5. Ribbon diagram depicting the NMR structure of Pdx [45]. The coordinates (1PUT) were obtained from the Brookhaven Protein Data Bank. The residues Trp-106, Asp-34, and Asp-38 (*clockwise*) and the Fe₂S₂ center are shown in *stick rendering*. The two Asp residues and the carboxy-terminal Trp have been implicated in electrostatic binding with residues Arg-79, Arg-109, and Arg-112 in cytochrome P450_{cam}

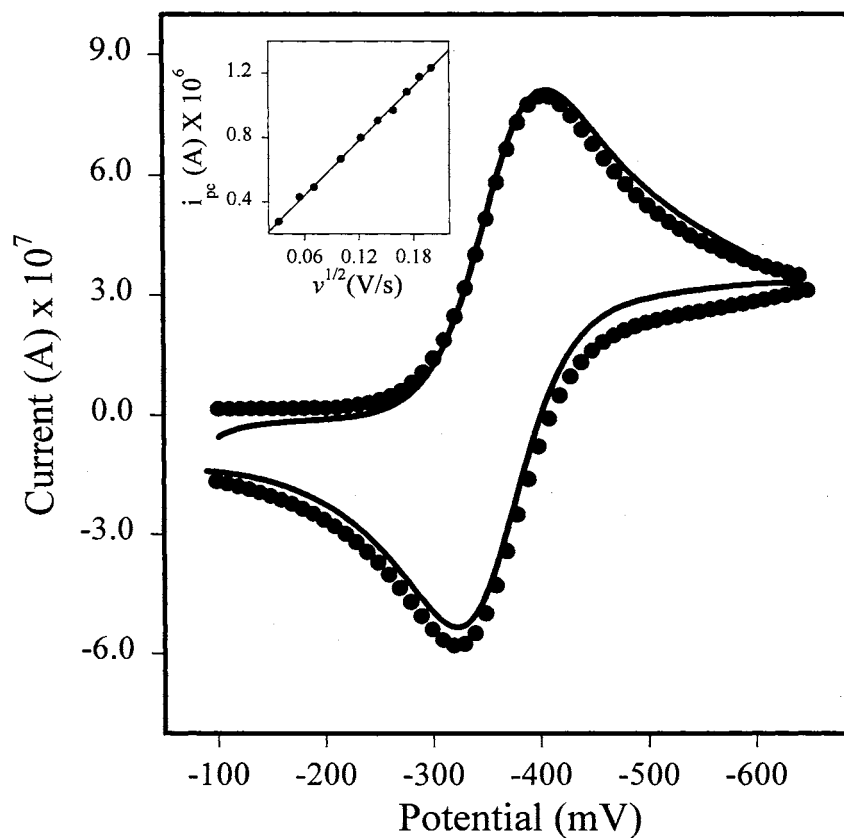


Figure 6. Typical background-subtracted cyclic voltammograms (—) obtained at an indium-doped tin oxide electrode from a solution containing Pdx (0.01 mM) and polylysine (0.20 mM) in 100.0 mM MOPS, pH 7.0. The scale of the voltammograms is shown vs the Ag/AgCl electrode but the values in the text are given vs standard hydrogen electrode. Sweep rate = 5 mV/s. (•) Simulated cyclic voltammograms: $k_s = 1.3 \times 10^{-3}$ cm²/s, $D_o = 9.8 \times 10^{-7}$ cm²/s, $\Delta E_p = 64$ mV

mercaptosulfonate and 5-mercaptopentanoate as the working electrode. The cyclic voltammograms obtained from Pdx at a mercaptoalkanoate-modified electrode in the presence of polylysine (Fig. 7) possess the same attributes as those described for the electrochemistry of Pdx at ITO electrodes. The ratio is typically 1.10, the voltammetry is controlled by linear diffusion, the diffusion coefficient $D = 2.0 \times 10^{-6} \text{ cm}^2/\text{s}$, and the value of the heterogeneous electron transfer rate constant $k = 1.1 \times 10^{-3} \text{ cm/s}$. The reduction potential obtained at these electrodes ($-180 \pm 5 \text{ mV}$ vs SHE) is almost identical to the value obtained at the ITO electrodes. This finding indicates that the 64 mV anodic shift in the reduction potential of Pdx is not unique to the ITO electrode surface.

iii). Spectroelectrochemistry

The reduction potential of recombinant Pdx was measured potentiometrically by spectroelectrochemistry utilizing the experimental conditions outlined in the Experimental Section. A family of spectra obtained during the spectroelectrochemical titration of the protein is shown in Fig. 8, along with the Nernst plot (inset). The value obtained from these measurements, $E^{\circ'} = -237 \pm 3 \text{ mV}$ vs SHE is identical to the reduction potential (-240 mV) reported for Pdx [43, 44]. When the spectroelectrochemical titration of Pdx was carried out in the presence of polylysine, however, the reduction potential of the protein shifted to $-221 \pm 3 \text{ mV}$, thus indicating that the association between putidaredoxin and polylysine caused an anodic shift in the reduction potential of the protein.

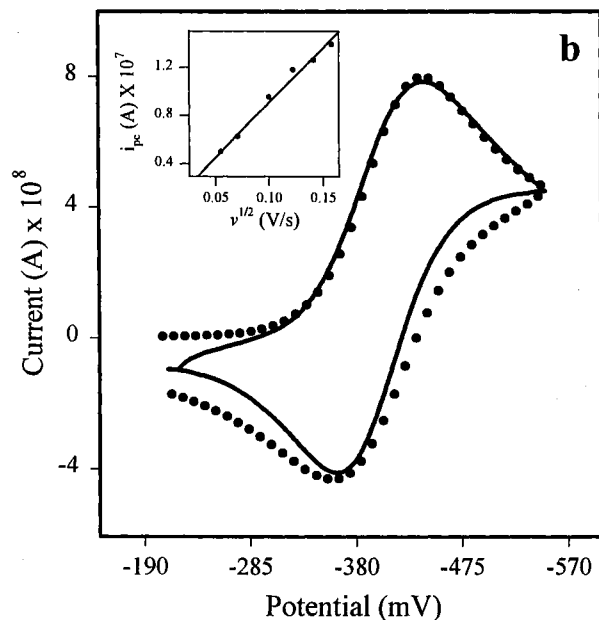
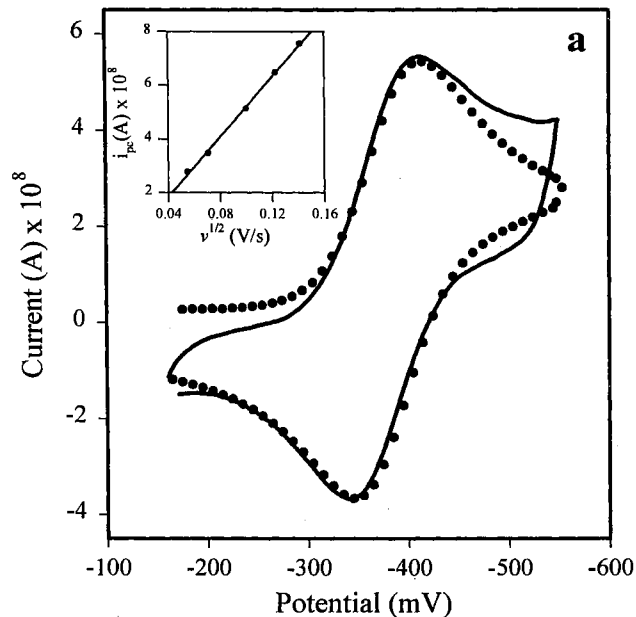


Figure 7a,b. Typical background-subtracted cyclic voltammograms obtained at: **a** gold electrode modified with β -mercaptosulfonate, **b** gold electrode modified with 5-mercaptopentanoate from a solution containing Pdx (0.10 mM) and polylysine (0.20 mM) in 100.0 mM MOPS, pH 7.0. The scale of the voltammograms is shown vs the Ag/AgCl electrode but the values in the text are given vs the standard hydrogen electrode. Sweep rate = 5 mV/s, (•) Simulated cyclic voltammograms: (a) $k_s = 1.1 \times 10^{-3}$ cm/s, $D_0 = 2.0 \times 10^{-6}$ cm²/s, $\Delta E_p = 74$ mV; (b) $k_s = 1.0 \times 10^{-3}$ cm/s, $D_0 = 3.0 \times 10^{-6}$ cm²/s, $\Delta E_p = 78$ mV

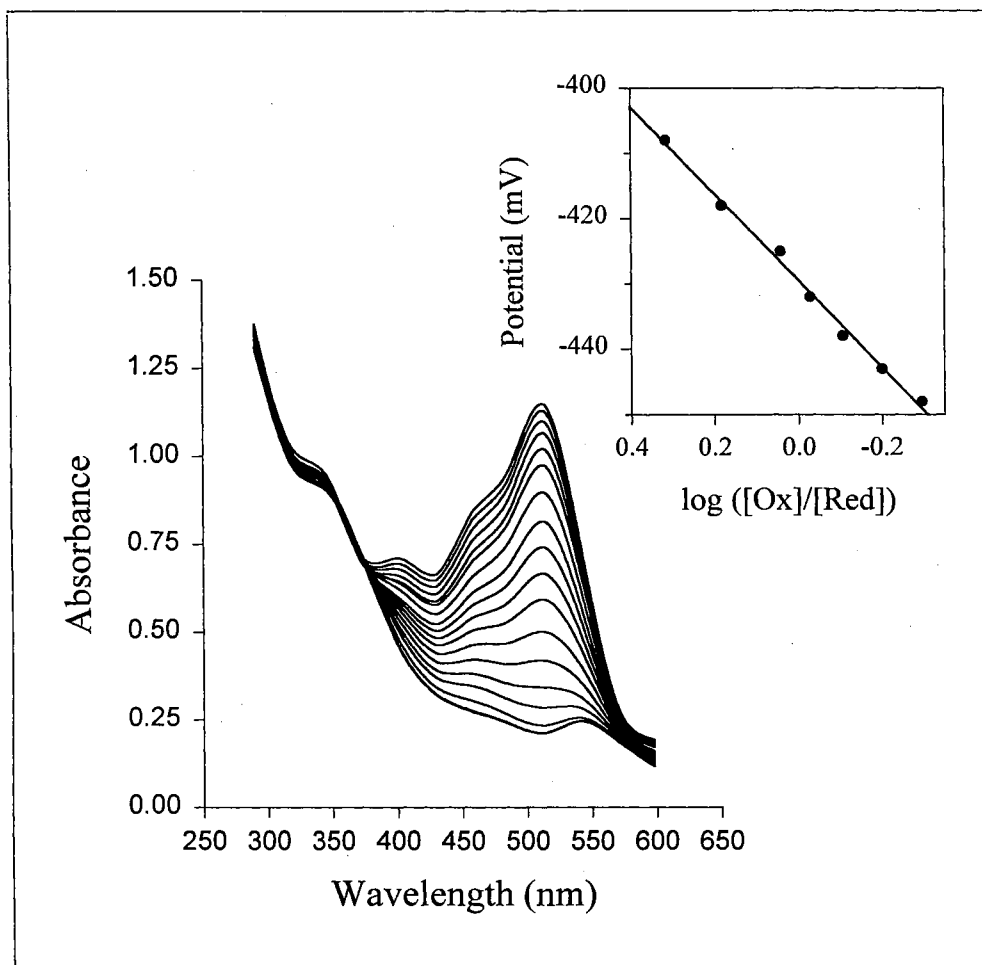


Figure 8. Spectroelectrochemical titration of a solution containing recombinant Pdx (70 μM) and phenosafranine (30 μM) in phosphate buffer ($\mu = 0.10$, $\text{pH} = 7.0$) with sodium dithionite (10.0 mM). Inset: Nernst plot constructed from the dependence of the absorbance at 408 nm on the cell potential. The Nernst slope is 62 mV

The results described above indicate that the formation of an electrostatic complex between polylysine and Pdx result in an anodic shift in the reduction potential of the protein. In this context, it is noteworthy that the reduction potential of Pdx in the Pdx-cytochrome P450 complex is -196 mV [3], a value that is 44 mV more positive than that measured for uncomplexed putidaredoxin. It is also currently accepted that in the Pdx-cytochrome P450 complex the two proteins form electrostatic interactions between positively charged residues in cytochrome P450 (Arg79, Arg109, and Arg112) and negatively charged residues in Pdx (Asp34, Asp38, and the carboxy-terminal Trp106) [39, 45]. These residues and their orientation with respect to the iron sulfur cluster of Pdx are shown in Fig. 5. Furthermore, it is also known that the Pdx-cytochrome P450 complex excludes approximately 700 Å of surface area per protein from the aqueous environment [37], which in Pdx encompasses the area delineated by Asp38, Asp34, and Trp106. It is therefore conceivable that the anodic shift observed in the reduction potential of Pdx upon forming a complex with cytochrome P450, or with polylysine at electrode surfaces, originates from electrostatic neutralization of negatively charged residues surrounding the Fe_2S_2 cluster and elimination of water from the complex interface that encompasses the solvent-accessible iron-sulfur cluster. The reduced value of the dielectric constant around the active-site microenvironment of Pdx is expected to stabilize the single positive charge on the reduced $[\text{Fe}_2\text{S}_2]^+$ cluster with respect to the doubly charged oxidized $[\text{Fe}_2\text{S}_2]^{2+}$ cluster, thus resulting in a concomitant anodic shift in the reduction potential of the protein.

The above postulation is in agreement with previous studies indicating that the surface charge and local dielectric constant around the iron-sulfur cluster of ferredoxins is capable of influencing the reduction potentials of these proteins[43, 46]. For example, on the basis of calculations, Banci et al.[46] predicted that neutralization of a negative charge on the protein surface of ferredoxins near their active site may induce a 20-30 mV anodic shift in their reduction potential. In agreement with this prediction, Aoki et al.[43] observed a 20-mV anodic shift in the reduction potential of the Glu72Gln variant of putidaredoxin. The anodic shift was proposed to originate from neutralization of the negative charge on residue 72, which is located in close proximity to the active site of putidaredoxin.

The idea that the formation of a complex between polylysine and putidaredoxin modulates the E° of the protein by lowering the dielectric constant of the active site microenvironment is supported by examining the three-dimensional structure of putidaredoxin [47]. The structure (Fig. 9) reveals that part of the Fe₂S₂Cys₂ active site in putidaredoxin is accessible to water. Water accessibility to the active site is provided by a channel that permits the exposure of one of the sulfide groups (green), the iron ion (red) farthest away from the molecular surface, and Cys 86 (yellow) to the aqueous environment. This channel is located immediately below the area delineated by the acidic residues implicated in the binding of Pdx to cytochrome P450, namely, Asp34 (blue), Asp38 (blue) and the carboxy terminal group in Trp 106 (magenta). Consequently, it is not unreasonable to postulate that when a transient complex is formed between Pdx and polylysine at the electrode surface, the neutralization of these acidic

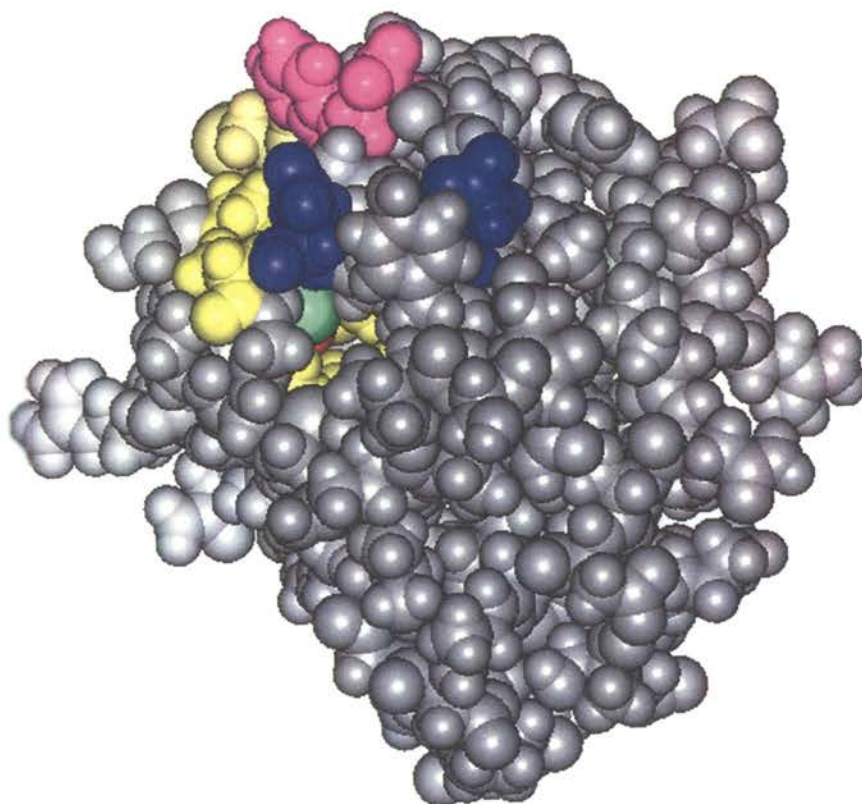


Figure 9. Space-filled view obtained by visualizing the coordinates from the NMR structure of putidaredoxin [45] with the program INSIGHT (II): polypeptide (*gray*), Asp-34 and Asp-38 (*blue*), carboxy-terminus Trp-106 (*magenta*), sulfide from the iron-sulfur cluster (*green*), iron ion farthest away from the molecular surface (*red*), cysteine residues (*yellow*). This view of putidaredoxin shows a channel leading into the interior of the protein, which is expected to provide water accessibility to the iron-sulfur cluster. At the end of this channel it is possible to observe one of the sulfide and one of the iron ions in the Fe_2S_2 cluster, as well as Cys-86. These groups are located on the part of the cluster that is farthest away from the molecular surface. This view also shows the location of the channel with respect to the negatively charged residues implicated in binding to cytochrome P450_{cam}

groups and the dehydration of the complex interface lowers the dielectric constant of the iron-sulfur cluster microenvironment, with a concomitant anodic shift in $E^{\circ'}$.

In order to continue to test this idea, the reduction potential of spinach ferredoxin was obtained voltammetrically using conditions identical to those used for putidaredoxin. Spinach ferredoxin is an electron transfer protein whose active site also consists of a Fe_2S_2 cluster and whose molecular surface also possesses an asymmetric distribution of acidic residues. At physiological pH these residues impart a highly localized negative charge to the area on the protein surface that surrounds the active site. It is important to point out, however, that the Fe_2S_2 cluster in spinach ferredoxin is not readily accessible to the aqueous environment. The formal reduction potential of spinach ferredoxin, obtained at an ITO electrode in the presence of polylysine, is -418 ± 4 mV vs NHE [31], a value that is in good agreement with previous voltammetric studies [19, 20]. It is noteworthy that the values of $E^{\circ'}$ obtained by cyclic voltammetry in the presence of polylysine is almost identical to the value of $E^{\circ'}$ measured by potentiometric titration [48-50], a finding that is consistent with the low water-accessibility of the iron-sulfur cluster observed by visualizing its three-dimensional structure [51]. Finally, given the fact that the direct electrochemistry of putidaredoxin and spinach ferredoxin promoted by the formation of a transient complex with polylysine at the electrode surface, it is possible to conclude that the large modulation observed for the reduction potential of Pdx is not likely to be dominated by double-layer effects originating from polylysine at the electrode surface.

Conclusions

It is well documented that the dielectric constant of the cofactor environment has

a large influence on the reduction potential of redox-active proteins [52, 53]. For example, it is known that the binding of camphor to the cytochrome P450 active site results in dehydration of the distal heme pocket with the concomitant shift of its reduction potential from -300 mV to approximately -170 mV [3]. In cytochrome *c*, a 240mV cathodic shift in reduction potential has been observed for the folded protein with respect to its unfolded counterpart; the cathodic shift has been attributed to exposure of the cofactor to the aqueous environment [54]. In addition to the large modulation of reduction potential that originates from sequestering the redox-cofactor as a consequence of protein folding, a secondary modulation appears to originate from protein-protein associations. This secondary modulation of $E^{\circ'}$ is especially noticeable in those redox-capable proteins whose active sites are transferred from a relatively hydrophilic environment to a more hydrophobic one upon complex formation. For example, it has been reported that the reduction potential of cytochrome *b_s* is shifted approximately 80 mV in the anodic direction upon complexation with polylysine [55]. This large shift is thought to result from lowering the dielectric constant of the heme microenvironment by neutralizing surface-acidic residues in the vicinity of the exposed heme edge and by excluding water from the complex interface. A similar mechanism appears to be responsible for the anodic shift observed in the cyclic voltammetric measurement of the $E^{\circ'}$ of putidaredoxin. Moreover, it is interesting that the shift in the reduction potential of Pdx observed during that electrochemical investigation has a parallel physiological counterpart, namely, the modulation of the $E^{\circ'}$ of Pdx upon complexation with cytochrome P450. Consequently, it is important to recognize that for those electron-transfer proteins possessing relatively exposed redox active sites, the potentiometric

values of E° may not be truly representative of the reduction potential utilized by the protein during normal physiological function.

References

1. Cushman, D.W., R.L. Tsai, and I.C. Gunsalus, *The ferroprotein component of a methylene hydroxylase*, in *Biochem. Biophys. Res. Commun.* 1967. p. 577-83.
2. Spiro, T.G. and Editor, *Biological Applications of Raman Spectroscopy, Vol. 1: Raman Spectra and the Conformations of Biological Macromolecules.* 1987. p. 352 pp.
3. Sligar, S.G. and I.C. Gunsalus, *A thermodynamic model of regulation: Modulation of redox equilibria in camphor monooxygenase*, in *Proc. Natl. Acad. Sci. U. S. A.* 1976. p. 1078-82.
4. Gunsalus, I.C. and G.C. Wagner, *Bacterial P-450cam methylene monooxygenase components: cytochrome m, putidaredoxin, and putidaredoxin reductase*, in *Methods Enzymol.* 1978. p. 166-88.
5. Castro, C.E., R.S. Wade, and N.O. Belser, *Biodehalogenation: reactions of cytochrome P-450 with polyhalomethanes*, in *Biochemistry.* 1985. p. 204-10.
6. Wackett, L.P., M.J. Sadowsky, L.M. Newman, H.-G. Hur, and S. Li, *Metabolism of polyhalogenated compounds by a genetically engineered bacterium*, in *Nature (London).* 1994. p. 627-9.
7. Lam, T. and V.L. Vilker, *Biodehalogenation of bromotrichloromethane and 1,2-dibromo-3-chloropropane by Pseudomonas putida PpG-786*, in *Biotechnol. Bioeng.* 1987. p. 151-9.

8. Fruetel, J.A., J.R. Collins, D.L. Camper, G.H. Loew, and P.R. Ortiz de Montellano, *Calculated and experimental absolute stereochemistry of the styrene and .beta.-methylstyrene epoxides formed by cytochrome P 450cam*, in *J. Am. Chem. Soc.* 1992. p. 6987-93.
9. Grayson, D.A., Y.B. Tewari, M.P. Mayhew, V.L. Vilker, and R.N. Goldberg, *Tetralin as a substrate for camphor (cytochrome P450) 5-monooxygenase*, in *Arch. Biochem. Biophys.* 1996. p. 239-247.
10. Fruetel, J., Y.-T. Chang, J. Collins, G. Loew, and P.R. Ortiz de Montellano, *Thioanisole Sulfoxidation by Cytochrome P450cam (CYP101): Experimental and Calculated Absolute Stereochemistries*, in *J. Am. Chem. Soc.* 1994. p. 11643-8.
11. Kazlauskaitė, J., A.C.G. Westlake, L.-L. Wong, and H.A.O. Hill, *Direct electrochemistry of cytochrome P450cam*, in *Chem. Commun. (Cambridge)*. 1996. p. 2189-2190.
12. Zhang, Z., A.-E.F. Nassar, Z. Lu, J.B. Schenkman, and J.F. Rusling, *Direct electron injection from electrodes to cytochrome P450cam in biomembrane-like films*, in *Journal of the Chemical Society, Faraday Transactions*. 1997. p. 1769-1774.
13. Lvov, Y.M., Z. Lu, J.B. Schenkman, X. Zu, and J.F. Rusling, *Direct Electrochemistry of Myoglobin and Cytochrome p450cam in Alternate Polyion Layer-by-Layer Films with DNA and Poly(styrenesulfonate)*, in *Journal of the American Chemical Society*. 1998. p. 4073-4080.

14. Reipa, V., M.P. Mayhew, and V.L. Vilker, *A direct electrode-driven P450 cycle for biocatalysis*, in *Proceedings of the National Academy of Sciences of the United States of America*. 1997. p. 13554-13558.
15. Tyson, C.A., J.D. Lipscomb, and I.C. Gunsalus, *The role of putidaredoxin and P450 cam in methylene hydroxylation*, in *Journal of Biological Chemistry*. 1972: United States. p. 5777-84.
16. Wong, L.S., V.L. Vilker, W.T. Yap, and V. Reipa, *Characterization of Mercaptoethylamine-Modified Gold Electrode Surface and Analyses of Direct Electron Transfer to Putidaredoxin*, in *Langmuir*. 1995. p. 4818-22.
17. Wong, L.S. and V.L. Vilker, *Direct electrochemistry of putidaredoxin at a modified gold electrode*, in *J. Electroanal. Chem.* 1995. p. 201-3.
18. Taniguchi, I., A. Miyahara, K.-i. Iwakiri, Y. Hirakawa, K. Hayashi, K. Nishiyama, T. Akashi, and T. Hase, *Electrochemical study of biological functions of particular evolutionary conserved amino acid residues using mutated molecules of maize ferredoxin*, in *Chemistry Letters*. 1997. p. 929-930.
19. Taniguchi, I., Y. Hirakawa, K. Kwakiri, M. Tominaga, and K. Nishiyama, *Polypeptide-modified indium oxide electrodes for direct electron transfer of ferredoxin*, in *J. Chem. Soc., Chem. Commun.* 1994. p. 953-4.
20. Taniguchi, I., K. Hayashi, M. Tominaga, R. Muraguchi, and A. Hirose, *Direct electron transfer of ferredoxins at an indium oxide electrode in the presence of poly-L-lysine*, in *Denki Kagaku oyobi Kogyo Butsuri Kagaku*. 1993. p. 774-5.
21. Taniguchi, I., *Probing metalloproteins and bioelectrochemical systems*, in *Electrochemical Society Interface*. 1997. p. 34-37.

22. Seetharaman, R., S.P. White, and M. Rivera, *Electrochemical measurement of second-order electron transfer rate constants for the reaction between cytochrome b5 and cytochrome c*, in *Biochemistry*. 1996. p. 12455-12463.
23. Sambrook, J., Fritsch, E.F., Maniatis, T., *Molecular cloning: a laboratory manual*. 2nd ed. 1987, Cold Spring Harbor, New York: Cold Spring Press.
24. Koga, H., E. Yamaguchi, K. Matsunaga, H. Aramaki, and T. Horiuchi, *Cloning and nucleotide sequences of NADH-putidaredoxin reductase gene (camA) and putidaredoxin gene (camB) involved in cytochrome P-450cam hydroxylase of Pseudomonas putida*, in *J. Biochem. (Tokyo)*. 1989. p. 831-6.
25. Ikemura, T., *Codon usage and tRNA content in unicellular and multicellular organisms*, in *Mol. Biol. Evol.* 1985. p. 13-34.
26. Konigsberg, W. and G.N. Godson, *Evidence for use of rare codons in the dnaG gene and other regulatory genes of Escherichia coli*, in *Proc. Natl. Acad. Sci. U. S. A.* 1983. p. 687-91.
27. Gunsalus, I.C. and G.C. Wagner, *Bacterial P-450cam methylene monooxygenase components: cytochrome m, putidaredoxin, and putidaredoxin reductase*, in *Methods Enzymol.* 1978. p. 166-88.
28. Stankovich, M.T., *An anaerobic spectroelectrochemical cell for studying the spectral and redox properties of flavoproteins*, in *Anal. Biochem.* 1980. p. 295-308.
29. Fultz, M.L. and R.A. Durst, *Mediator compounds for the electrochemical study of biological redox systems: a compilation*, in *Anal. Chim. Acta.* 1982. p. 1-18.

30. Speziale, A., in *Organic Syntheses*, N. Rabjohn, Editor. 1963, Wiley: New York. p. 401.
31. Avila, L., M. Wirtz, R.A. Bunce, and M. Rivera, *An electrochemical study of the factors responsible for modulating the reduction potential of putidaredoxin*, in *JBIC, Journal of Biological Inorganic Chemistry*. 1999. p. 664-674.
32. Rivera, M., C. Barillas-Mury, K.A. Christensen, J.W. Little, M.A. Wells, and F.A. Walker, *Gene synthesis, bacterial expression, and ¹H NMR spectroscopic studies of the rat outer mitochondrial membrane cytochrome b5*, in *Biochemistry*. 1992: United States. p. 12233-40.
33. Holden, M., M. Mayhew, D. Bunk, A. Roitberg, and V. Vilker, *Probing the interactions of putidaredoxin with redox partners in camphor P 450 5-monooxygenase by mutagenesis of surface residues*, in *Journal of Biological Chemistry*. 1997. p. 21720-21725.
34. Bowden, E.F., *Wiring mother nature. Interfacial electrochemistry of proteins*, in *Electrochemical Society Interface*. 1997. p. 40-44.
35. Rusling, J.F., *Biocatalysts Work for Us in Biomimetic Environments*. Electrochemical Society INTERFACE, 1997. 6(4): p. 26.
36. Hawkridge, F.M. and I. Taniguchi, *The direct electron transfer reactions of cytochrome c at electrode surfaces*, in *Comments Inorg. Chem*. 1995. p. 163-87.
37. Armstrong, F.A., H.A.O. Hill, and N.J. Walton, *Direct electrochemistry of redox proteins*, in *Acc. Chem. Res*. 1988. p. 407-13.

38. Pochapsky, T.C., X.M. Ye, G. Ratnaswamy, and T.A. Lyons, *An NMR-Derived Model for the Solution Structure of Oxidized Putidaredoxin, a 2-Fe, 2-S Ferredoxin from Pseudomonas*, in *Biochemistry*. 1994. p. 6424-32.
39. Roitberg, A.E., M.J. Holden, M.P. Mayhew, I.V. Kurnikov, D.N. Beratan, and V.L. Vilker, *Binding and Electron Transfer between Putidaredoxin and Cytochrome P450cam. Theory and Experiments*, in *Journal of the American Chemical Society*. 1998. p. 8927-8932.
40. Rivera, M., M.A. Wells, and F.A. Walker, *Cation-Promoted Cyclic Voltammetry of Recombinant Rat Outer Mitochondrial Membrane Cytochrome b5 at a Gold Electrode Modified with .beta.-Mercaptopropionic Acid*, in *Biochemistry*. 1994. p. 2161-70.
41. Glenn, J.D.H. and E.F. Bowden, *Diffusionless electrochemistry of cytochrome b5 adsorbed on a multilayer film electrode*, in *Chem. Lett.* 1996. p. 399-400.
42. Rudolph, M., D.P. Reddy, and S.W. Feldberg, *A Simulator for Cyclic Voltammetric Responses*, in *Anal. Chem.* 1994. p. 589A-600A.
43. Aoki, M., K. Ishimori, I. Morishima, and Y. Wada, *Roles of valine-98 and glutamic acid-72 of putidaredoxin in the electron-transfer complexes with NADH-putidaredoxin reductase and P450cam*, in *Inorganica Chimica Acta*. 1998. p. 80-88.
44. Gunsalus, I.C., J.R. Meeks, and J.D. Lipscomb, *Cytochrome P 450cam substrate and effector interactions*, in *Ann. N. Y. Acad. Sci.* 1973. p. 107-21.

45. Pochapsky, T.C., T.A. Lyons, S. Kazanis, T. Arakaki, and G. Ratnaswamy, *A structure-based model for cytochrome P450cam-putidaredoxin interactions*, in *Biochimie*. 1996. p. 723-733.
46. Banci, L., I. Bertini, G.G. Savellini, and C. Luchinat, *Individual Reduction Potentials of the Iron Ions in Fe₂S₂ and High-Potential Fe₄S₄ Ferredoxins*, in *Inorg. Chem*. 1996. p. 4248-4253.
47. Pochapsky, T.C., N.U. Jain, M. Kuti, T.A. Lyons, and J. Heymont, *A Refined Model for the Solution Structure of Oxidized Putidaredoxin*, in *Biochemistry*. 1999. p. 4681-4690.
48. Cammack, R., K.K. Rao, C.P. Bargeron, K.G. Hutson, P.W. Andrew, and L.J. Rogers, *Midpoint redox potentials of plant and algal ferredoxins*, in *Biochem. J*. 1977. p. 205-9.
49. Ke, B., W.A. Bulen, E.R. Shaw, and R.H. Breeze, *Determination of oxidation-reduction potentials by spectropolarimetric titration. Application to several iron-sulfur proteins*, in *Arch. Biochem. Biophys*. 1974. p. 301-9.
50. Tagawa, K. and D.I. Arnon, *Oxidation-reduction potentials and stoichiometry of electron transfer in ferredoxins*, in *Biochim. Biophys. Acta*. 1968. p. 602-13.
51. Binda, C., A. Coda, A. Aliverti, G. Zanetti, and A. Mattevi, *Structure of the mutant E92K of [2Fe-2S] ferredoxin I from Spinacia oleracea at 1.7 Å resolution*, in *Acta Crystallographica. Section D: Biological Crystallography*. 1998: Denmark. p. 1353-8.

52. Kassner, R.J., *A theoretical model for the effects of local nonpolar heme environments on the redox potentials in cytochromes*, in *Journal of the American Chemical Society*. 1973: United States. p. 2674-7.
53. Kassner, R.J., *Effects of nonpolar environments on the redox potentials of heme complexes*, in *Proc. Nat. Acad. Sci. U. S. A.* 1972. p. 2263-7.
54. Churg, A.K. and A. Warshel, *Control of the redox potential of cytochrome c and microscopic dielectric effects in proteins*, in *Biochemistry*. 1986: United States. p. 1675-81.
55. Tezcan, F.A., J.R. Winkler, and H.B. Gray, *Effects of Ligation and Folding on Reduction Potentials of Heme Proteins*, in *Journal of the American Chemical Society*. 1998. p. 13383-13388.
56. Rivera, M., R. Seetharaman, D. Girdhar, M. Wirtz, X. Zhang, X. Wang, and S. White, *The Reduction Potential of Cytochrome b5 Is Modulated by Its Exposed Heme Edge*, in *Biochemistry*. 1998. p. 1485-1494.

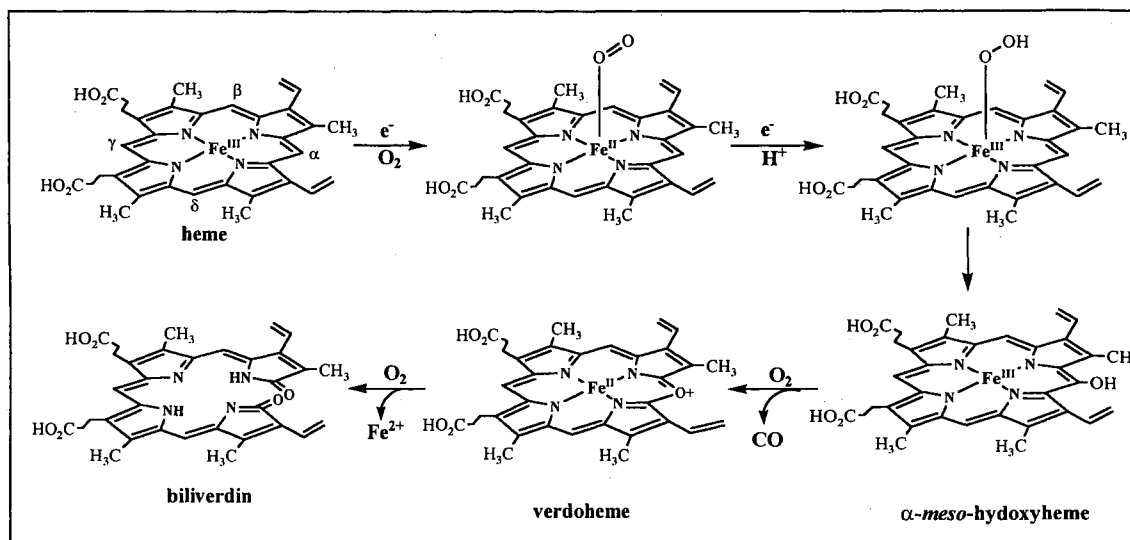
CHAPTER III

A STUDY OF AXIAL LIGAND MUTANTS OF MITOCHONDRIAL CYTOCHROME b_5 AND THEIR OXYGEN ACTIVATION MECHANISMS: THE OXIDATION OF HEME TO VERDOHEME AND BILIVERDIN

Introduction

Heme serves as the prosthetic group in numerous hemoproteins that are integral to life. Heme containing proteins are involved in a remarkably versatile array of important biological functions, including oxygen binding (hemoglobin and myoglobin), oxygen metabolism (monooxygenases and peroxidases), electron transfer reactions (cytochromes), and signal transduction (guanylate cyclase, nitric oxide synthase). Cellular heme levels appear to be tightly controlled by a highly tuned interplay between heme biosynthesis and heme catabolism [1]. In mammals the only physiological path of heme catabolism starts when the enzyme heme oxygenase (HO) binds heme and in a series of electron and dioxygen-dependent steps oxidizes heme to biliverdin, carbon monoxide (CO), and iron [2, 3]. On the basis of spectroscopic [4-6] and X-ray crystallographic [7, 8] studies it has been established that the heme in the heme-HO complex is coordinated by a proximal His residue and by a distal H_2O or OH^- ligand. The X-ray structure revealed that there are no polar side chains (i.e. histidine) in close proximity to form a hydrogen bond to the coordinated water, as is the case of myoglobin [9].

The catalytic cycle of HO (Scheme I) parallels that of cytochrome P450 in that the ferric enzyme is reduced to its ferrous state, followed by the formation of an oxyferrous complex ($\text{Fe}^{\text{II}}\text{-O}_2$), which accepts a second electron from NADPH cytochrome reductase, and is thereby transformed into an activated hydroperoxy ($\text{Fe}^{\text{III}}\text{-OOH}$) oxidizing species



Scheme I. Catalytic cycle of Heme Oxygenase

[10]. This oxidizing species adds a hydroxyl group to the α -meso carbon in order to give α -meso hydroxyheme (Scheme I). The α -meso hydroxyheme undergoes a subsequent O_2 -dependent elimination of the hydroxylated α -meso carbon as CO, with the concomitant formation of verdoheme. Verdoheme is then oxidized to Fe^{III} -biliverdin in a reaction that requires both O_2 and reducing equivalents [11, 12].

Mammalian heme oxygenases are membrane bound enzymes and therefore are relatively difficult to overexpress and purify. Important progress toward the understanding of HO activity has been facilitated by the bacterial expression and characterization of a soluble fragment of mammalian HO [13, 14]. Prior to this breakthrough, the coupled oxidation of myoglobin was used as a model to gain insight into the mechanism of heme oxygenation [15-17]. Coupled oxidation is a process in which a hemoprotein, or an iron porphyrin is incubated with O₂ and a reducing agent such as ascorbic acid or hydrazine, in order to oxidize the heme active site or the iron porphyrin to verdoheme and biliverdin [18]. The coupled oxidation reaction proceeds via the formation of the same intermediates observed during the oxidation of heme by HO, namely, *α-meso*-hydroxyheme and verdoheme (see Scheme I) [19]. It has been recognized that although the coupled oxidation reaction closely resembles the heme oxygenation process carried out by HO, the mechanistic details for both processes may not be identical. It is important to note that while the oxidation of heme by HO produces exclusively *α*-biliverdin, the coupled oxidation of protoheme IX in pyridine solution produces all four isomers of biliverdin, the coupled oxidation of heme in hemoglobin results in the formation of *α*- and *β*-biliverdin,[20] and the coupled oxidation of the heme in myoglobin produces exclusively *α-meso* biliverdin [20]; there is at least one report indicating that the coupled oxidation of myoglobin results in the formation of all four biliverdin isomers and that the ratio of isomers varies from experiment to experiment [21]. More recent studies on the coupled oxidation of the heme in myoglobin have focused on the issue of regioselectivity, thus the coupled oxidation of sperm whale myoglobin mutants in which the distal histidine (His-64) was relocated within the distal

cavity was studied with the aim of understanding the factors that influence the regioselectivity of heme oxygenation [22]. It was observed that relocation of the distal histidine through F43H/H64L produced 40, 16 and 44% of α -, β , and γ -biliverdin, respectively, whereas F43W/H64L produced 33% α -, 61% γ -biliverdin, and approximately 3% of each β - and δ - isomers. These observations led the author to conclude that the polarity of the active site as well as hydrogen bonding of the O₂ molecule within the distal cavity of myoglobin influence the regioselectivity of heme oxygenation [22]. It is noteworthy, however, that the coupled oxidation of myoglobin has been found to be inhibited by the hydrogen peroxide scavenger catalase, therefore suggesting that non-coordinated H₂O₂ is the oxidant that brings about the oxidation of the heme in myoglobin [23]. This finding strongly suggests that the coupled oxidation of myoglobin proceeds via a mechanism that is distinct from that followed by heme oxygenase (shown in Scheme I), even if the same stable intermediates (*meso*-hydroxyheme, and verdoheme) that are isolated during heme oxygenation are also isolated during the coupled oxidation of myoglobin. Consequently, the mechanism of coupled oxidation has to be better understood before firm conclusions regarding heme oxygenation can be drawn from studying the coupled oxidation of myoglobin.

In recent years it has been shown that certain heme containing electron transfer proteins can be made to acquire coupled oxidation activity simply by mutating one of the axial ligands for a weakly- or non-coordinating residue [24-27], thus a mutant of outer mitochondrial membrane (OM) cytochrome b₅, in which one of the axial histidine ligands (His-63) has been replaced by Met, is capable of oxidizing heme to verdoheme when

incubated with O₂ and hydrazine [24, 25]. A similar finding was made when the His axial ligand of cytochrome b₅₆₂ was replaced by methionine [27]. It was suggested that the coupled oxidation of the heme in the OM cytochrome b₅ and cytochrome b₅₆₂ mutants stops at verdoheme as a consequence of the formation of a hexacoordinate verdoheme complex, which is axially coordinated by His-39 and Met-63 in OM cytochrome b₅ [24], and by Met-7 and Met-102 in cytochrome b₅₆₂ [27]. We prepared two additional axial ligand mutants of OM cytochrome b₅, H63V and H39V with the aim of eliminating the coordination of verdoheme by a putative sixth ligand, thus preventing the possibility that the coupled oxidation process is arrested at the verdoheme stage due to the formation of a hexacoordinate verdoheme complex [26]. Through these investigations we demonstrated that the coupled oxidation of the heme in the H63V mutant is still stopped at verdoheme. In contrast, the coupled oxidation of the H39V mutant results in the initial accumulation of an oxyheme complex that is gradually oxidized to produce biliverdin [26]. These observations, therefore, suggest that the coupled oxidation of the H39V mutant might occur via a mechanism different from that followed by H63V and that exploring the mechanism by which the two axial ligand mutants oxidize their hemes might yield some insight into the potential mechanistic differences between heme oxygenation and coupled oxidation. As will be demonstrated below, we found that the coupled oxidation of the heme in H63V is brought about by non-coordinated hydrogen peroxide, thus the function of the sacrificial electron donor (hydrazine) is not limited to the reduction of the ferric protein but is also necessary to reduce non-coordinated O₂ to non-coordinated H₂O₂. Furthermore, the coupled oxidation process is carried out by a reaction between the ferrous protein and hydrogen peroxide that results in the formation of *meso*-

hydroxyheme. In contrast, the coupled oxidation of the H39V mutant is not inhibited by catalase and is carried out via the reduction of coordinated O₂ (Fe^{II}-O₂) to form a ferric hydroperoxide (Fe^{III}-OOH), which is the oxidizing species in the process of heme oxygenation carried out by HO.

Experimental Procedures

i). *Site-Directed Mutagenesis*

The recombinant plasmid MRL1 [28] and the transformer site-directed mutagenesis kit (Clontech) were used to construct the rat OM cyt *b*₅ H63V and H39V mutants following a protocol outlined previously [29]. The sequences corresponding to the mutagenic primers designed to introduce the H63V and H39V, and that corresponding to the selection primer (AflIII to BglII) are 5'-CCGAATCTTTCGAAGATGTTGGCGTGTCTCCGGATGCGCG -3', 5'-CCGAATCTTTCGAAGATGTTGGCGTGTCTCCGGATGCGCG -3', 5'-GGGGATAACGCA GGAAAGAAGATCTGAGCAAAAGGCC -3', respectively. The underlined codons represent mismatches introduced to generate the mutations. The single-stranded oligonucleotides were synthesized by the Recombinant DNA/Protein Facility at Oklahoma State University. The recombinant plasmids were transformed into *Escherichia coli* BL21(DE3) cells for subsequent protein expression. The H63V mutant was prepared in our laboratory by Juan Carlos Rodriguez [26].

The recombinant pET 11a plasmid H39V and the QuickChange site-directed mutagenesis kit (Stratagene) were used to construct the H39V/G41A and H39V/G42A double mutants. The sequences corresponding to the mutagenic primers designed to introduce the G41A mutation are 5'- CCTGTCTGAAGTGCCGGCG GGCGAAGAAGTTCTGC-3' and 5'-CAGAACTTCTTCGCCCGCCGGCACTTCAG ACAGG-3'. The H39V/G42A mutant was prepared in our laboratory by Christopher Damaso. The recombinant constructs were transformed into *E. coli* XL1- blue competent cells for amplification and subsequent sequencing. Once the sequence was established, the recombinant plasmids were transformed into *E. coli* BL21 (DE3) cells for protein expression.

ii). *Expression and Purification of Mutants (Recombinant Proteins)*

Expression, lysis, and purification of the variants was carried out following a procedure similar to that described by Rodriguez, *et al.*[30]. In brief, 1.0 L of LB media was inoculated with 5mL of an *E. coli* BL21(DE3) culture grown overnight. When the OD₆₀₀ reached a value of 0.80-1.0, biosynthesis of the polypeptide was induced by adding IPTG (isopropyl-B-thiogalactoside) to a final concentration of 1.0 mM. After induction of protein synthesis, 17 mg of aminolevulinic acid and 100 mg of FeSO₄ •7H₂O were added to each liter of cell culture. The cells were harvested by centrifugation 2.5 h after induction of protein synthesis. The absence of pink color in the harvested *E. coli* cells indicated that the H63V and H39V mutants do not incorporate heme during their bacterial expression. After lysing, cell debris was separated by ultracentrifugation, the

supernatant made 3 mM in $K_3Fe(CN)_6$ and 1 mM in imidazole, and then dialyzed at 4.0 °C against 50 mM Tris buffer, pH 7.8 containing 10 mM EDTA and 1.0 mM imidazole. The dialyzed solution was then loaded onto an anion-exchange resin (DE52, Whatman) column previously equilibrated with the same buffer and eluted with a linear salt gradient (0.0 to 0.50 M NaCl) made in buffer containing 1.0 mM imidazole.

The pooled fractions were then reconstituted with heme. Hemin (10mg) (Porphyrin Products, Utah) was dissolved in 300 uL $CHCl_3$ and 100 uL pyridine. The $CHCl_3$ was then evaporated under a stream of argon, redissolved in 0.1 M NaOH, and the pH was slowly adjusted to 7.5 with 0.1 M HCl. The pooled fractions containing protein were titrated with 0.5 mL increments of the heme solution while monitoring the intensity of the Soret band at 412 nm. For apoprotein obtained from four liters of culture, a total of 1.5 mL, added over a period of 12 hours was typically necessary before the intensity of the Soret band remained constant. The protein was then dialyzed against 20 mM Tris buffer, pH 7.4 containing 100 mM NaCl and 1.0 mM EDTA until the imidazole was removed, concentrated by ultrafiltration, and further purified by size-exclusion chromatography.

iii). Cuvette Utilized for Experimentation

The cell used for the electronic absorption spectroscopy experiments is shown in Figure 1. It was constructed out of a standard 3mL, 1cm path length quartz cuvette (a) connected to glass outlets via a gradient (quartz to glass) seal (b). It has a Rotaflow ® stopcock (c) that serves as an inlet for argon (c), needed to establish a positive pressure of

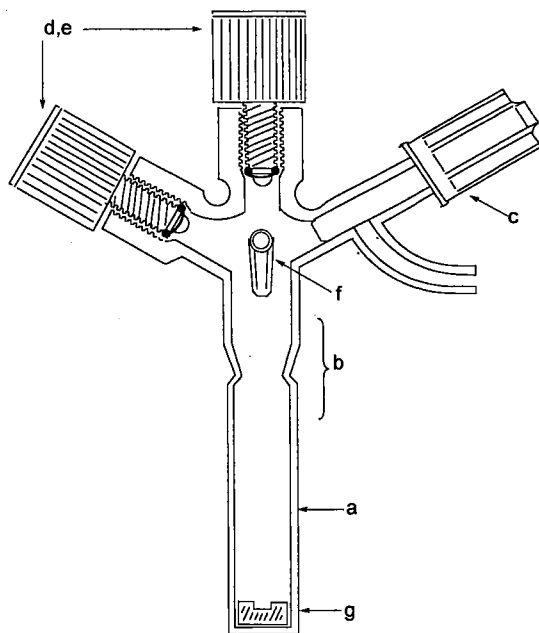


Figure 1. Schematic cross-sectional representation of the cuvette used to obtain electronic absorption spectra. The cell body is outfitted with a (a) 10 mm path length quartz cuvette connected to glass outlets via a gradient seal (b). A teflon coated magnetic cell stirrer (g) was sealed into the cell. A Rotaflow stopcock serves as an inlet for argon (c) and the small glass port (f) is used for reagent delivery and as an argon outlet. This port can be sealed with a rubber septum. (d and e are teflon stoppers)

argon throughout the experiments. A small port (f) was placed into the glass to degass the solutions with argon. This port was also used to introduce the protein samples and reagents with the aid of Hamilton gas tight syringes. The port can then be fitted using a rubber septum. The cell is placed in a custom-made cuvette holder (OSU Physics and Chemistry Instrument shop, Stillwater, OK) with internal channels designed to circulate water from a constant-temperature water source. The cell holder is placed on a stir plate to maintain constant stirring in the cell throughout the experiment. The cuvette holder is equipped with fiber optic couplings harboring quartz $f/2$ collimating lenses, which couple via SMA-terminated optical fibers to the UV-VIS S2000 fiber optic spectrophotometer (Ocean Optics, Dunedin, FL).

iv). Coupled Oxidation Assays

The coupled oxidation reactions were carried out in the cell described above at 25° C with solutions containing 3.5 mL of the appropriate cytochrome b_5 mutant (14 μ M) in 3.5 mL of 50.0 mM phosphate buffer, pH 7 (H63V), and pH 9 (H39V). All reactions were initiated with the addition of hydrazine (1.5 μ L, 0.2 mM) as the source of reducing equivalents. When appropriate catalase (0.4 mM) was added just prior to the addition of hydrazine. The reaction was monitored with the aid of a UV-Vis spectrophotometer until the intensity of the Soret band was almost indiscernible in the electronic absorption spectrum. The product of the coupled oxidation reaction obtained with solutions of the H63V mutant was extracted with a solution of pyridine in chloroform, as described previously [31] and the organic phase was analyzed by UV-Vis spectroscopy and electrospray mass spectrometry. To extract the product of the coupled oxidation obtained

with the H39V variant, glacial acetic acid (1.5mL) and 5 M hydrochloric acid (8mL) were added to the solution after the coupled oxidation reaction was completed. The resultant solution was extracted with ethyl ether (2 x 5 mL) in order to remove unreacted heme. The aqueous layer was subsequently extracted with chloroform (1 x 10 mL) in order to extract the biliverdin. Electrospray mass spectrometric analysis of the organic layer was performed on a Quattro II triple quadrupole mass spectrometer (Micromass, Inc. Beverly, MA).

v). *Resonance Raman Spectroscopy*

Resonance Raman spectra, obtained by Dr. Pierre Möenne Loccoz, were taken at the Department of Biochemistry and Molecular Biology at Oregon Graduate Institute of Science and Technology in Beaverton Oregon.

vi). *Autooxidation of the Oxyferrous Complexes*

The autoxidation reactions of the H39V variant were carried out with solutions containing approximately 14 μM of the protein in 3.5 mL of phosphate buffer pH 9.0 at 17 °C. The anaerobic solution of the ferric protein was stoichiometrically reduced by adding small aliquots of an anaerobic solution of sodium dithionite with the aid of a gas-tight Hamilton syringe. When the ferric protein was completely reduced to the ferrous oxidation state, the solution was exposed to air, which resulted in the immediate formation of the oxyferrous complex ($\text{Fe}^{\text{II}}\text{-H39V-O}_2$). Electronic absorption spectra

were obtained at 30 s after exposure to air and every minute thereafter in order to monitor the oxidation of the Fe^{II}-H39V-O₂ complex to Fe^{III}-H39V. The rate constant for the autoxidation of the oxyferrous complex was obtained by fitting the time-dependent decay of the peak at 577 nm to a single exponential function.

vii). *HPLC Analysis of the Product of the Coupled Oxidation Reaction.*

The regioselectivity of the reaction products of the H63V and H39V mutants was assessed by analysis of the corresponding biliverdin dimethyl ester derivatives with the aid of a Beckman System HPLC chromatograph equipped with a diode array UV-Vis detector. Verdoheme obtained from the coupled oxidation of H63V was converted to biliverdin as described by Torpey and Ortiz de Montellano [32]. In brief, the green reaction mixture was extracted into CH₂Cl₂ and H₂O. The organic phase was washed with H₂O and concentrated under vacuum. One volume of MeOH was added and the solution was immediately purged with argon. While under argon, a saturated solution of KOH in MeOH was added and allowed to stand for 5 minutes before pouring it into a solution of aqueous HCl (25%). The resultant blue solution was stirred for 10 minutes and extracted with CH₂Cl₂, washed with H₂O, and concentrated under vacuum.

The synthesis of the dimethyl esters of biliverdin was carried out in a manner similar to that described by O'Carra and Colleran [33]. Solid biliverdin was dissolved in 1mL of ice-cold 4% H₂SO₄ in MeOH and stirred at 4° C for 12 hours. The mixtures were then diluted with 4 volumes of water and extracted with chloroform. The chloroform extracts were washed with distilled water until the washings were no longer

acidic. The chloroform solutions were then evaporated to dryness under a stream of argon and the solid residue was dissolved in methanol for reverse phase HPLC analysis. The samples were injected into a Waters μ Bondapak C18 (3.9 X 300 mm) column fitted with a Waters Spherisorb ODS-1 guard column and separated by isocratic elution with a methanol:water mixture 85:15 and a flow rate of 0.8 ml/min. The eluant was monitored at 380 nm and the retention times of the biliverdin isomers obtained from the coupled oxidation of the H39V and H63V mutants were compared to those obtained from samples of authentic α -biliverdin (Porphyrin Products, Utah), and from samples obtained from the coupled oxidation of the pyridine hemochrome. The retention times were also comparable to those obtained by Wilks and Moenne-Loccoz [34, 35].

viii). *Evaluating the Reactivity of Ferrous Protein with Hydrogen Peroxide*

The cell in Figure 1 was utilized to evaluate the effect of adding hydrogen peroxide to anaerobic solutions containing ferrous protein. Typical experiments were carried out with 3.5 mL of phosphate buffer pH 7.0 containing approximately 14 μ M of the protein at 25° C. The anaerobic solution of the ferric protein was stoichiometrically reduced by adding small aliquots of an anaerobic solution of sodium dithionite with the aid of a gas-tight Hamilton syringe. When the ferric protein was completely reduced to the ferrous oxidation state, one equivalent of hydrogen peroxide was added. The electronic absorption spectra were monitored until there were no more changes in the *soret*. This procedure was then repeated 3 to 5 cycles. Once the *meso*-hydroxyheme complex of H63V was formed it was titrated with one equivalent of sodium dithionite in

order to obtain the corresponding ferrous complex. Carbon monoxide was then bubbled through the resultant solution, while maintaining anaerobicity, thus forming a carbomonoxy adduct. To confirm the presence of a hydroxyheme-carbomonoxy complex, air was bubbled through the solution.

Results and Discussion

i). Characterization of H63V and H39V OM Cytochrome b_5 Mutants

The electronic absorption spectra of H63V and H39V heme complexes display a Soret band maximum at 404 nm and a characteristic high-spin (HS) marker characteristic of ferric hemoproteins possessing a proximal His ligand at 628 nm (Figure 2, solid line). Addition of sodium dithionite to an anaerobic solution containing the ferric variants produces species displaying electronic absorption spectra characteristic of high spin ferrous heme (dotted line in Fig. 2a and b). When carbon monoxide is bubbled through the solutions containing the ferrous proteins and the electronic absorption spectrum of the resultant solution is recorded, the spectra shown by dashed lines in Fig. 2a and b are obtained. These spectra are very similar to that obtained from the CO-complex of myoglobin, hence indicating that His 39 is the proximal ligand in the H63V mutant and that His 63 is the proximal ligand in the H39V protein.

The high frequency region of the Resonance Raman (RR) spectra of ferric the H63V and H39V mutants [36] indicated that the heme iron is in hexacoordinate high-spin/low-spin (6cHS/6cLS) equilibrium. This is consistent with a His-aqua axial coordination, as is observed in mammalian and bacterial HO [37]. The UV-Vis and RR

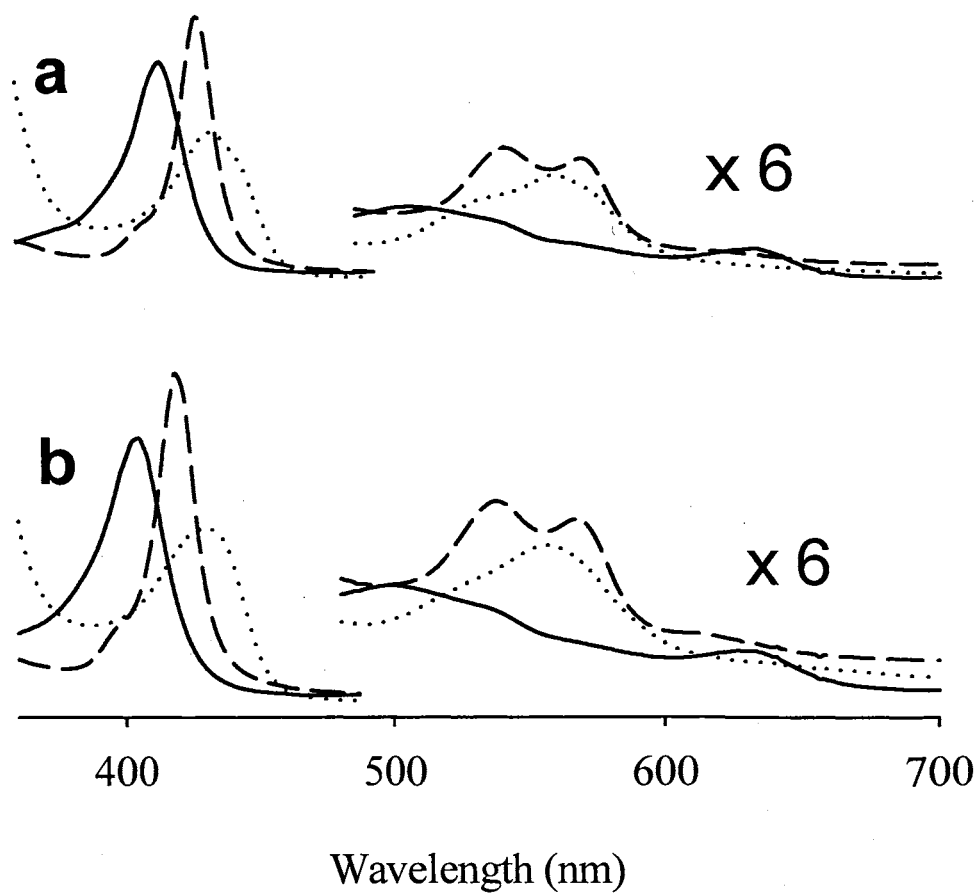


Figure 2. Electronic spectra of (a) H63V and (b) H39V OM cyt b_5 . (—) Fe (III), (···) Fe (II), (- - -) Fe (II)-CO

spectra of ferrous H63V and H39V [36] are characteristic of HS ferrous heme, and coordination to a proximal His ligand was confirmed by the observation of a $\nu(\text{Fe-His})$ at $\sim 220 \text{ cm}^{-1}$ [38].

ii). *Coupled Oxidation of the Heme in H63V and H39V Mutant Proteins*

The coupled oxidation of the heme in the H63V mutant was carried out utilizing hydrazine as a source of reducing equivalents and monitored by electronic absorption spectroscopy (Figure 3, top). The increase in the absorption at 660 nm is indicative of the formation of verdoheme. This product was confirmed by the electronic absorption spectrum obtained after the product of coupled oxidation was extracted into a chloroform-pyridine solution, which was identical to that of verdohemochrome[39].

By comparison, the coupled oxidation of the heme in the H39V mutant (Figure 3, bottom) results in bleaching of the Soret band and is not accompanied by an increase in absorption at $\sim 660 \text{ nm}$. These findings suggest that verdoheme does not accumulate during the coupled oxidation and is not the final product of the reaction. The nature of the final product was examined by extraction of the product into chloroform, after removal of unreacted heme with ether under acidic conditions. The UV-Vis spectrum of the chloroform extract is identical to that obtained from authentic biliverdin, hence demonstrating that H39V catalyzes the coupled oxidation of heme to biliverdin.

During the coupled oxidation of the heme in the H39V mutant, a transient species with absorbances at 540 and 577 nm reaches a maximum concentration within the first 15 min of reaction, before it is gradually converted into product (Figure 3). The electronic

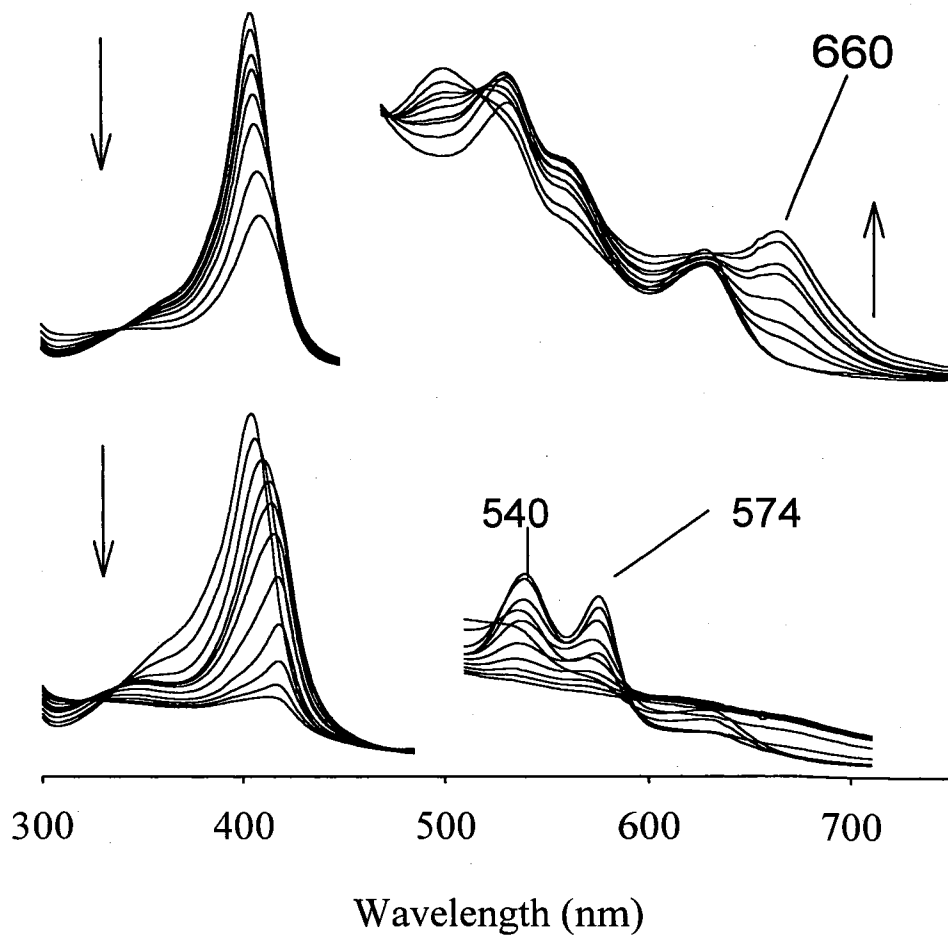


Figure 3. Electronic spectra of H63V (top) and H39V (bottom) OM cyt b₅ in the presence of hydrazine and O₂

absorption spectrum of this transient species, a metastable oxyheme complex, is reminiscent of the oxyheme complex in HO-1 [40]. The formation of a the oxyheme complex in H39V was corroborated by the observation of a $\nu(\text{Fe-O}_2)$ in its RR spectrum. Reduction of H39V by hydrazine in the presence of $^{18}\text{O}_2$ results in a 23 cm^{-1} downshift of a weak RR band located at 566 cm^{-1} , which was obtained in the presence of $^{16}\text{O}_2$ [36]. In the oxyheme complex of rat HO-1, a $\nu(\text{Fe-O}_2)$ was reported at the same frequency, within experimental error [41].

iii). Catalase Does Not Inhibit the Coupled Oxidation of the H39V Mutant of OM cyt b₅.

It has been recently reported that the coupled oxidation of myoglobin is inhibited by the presence of catalase [23], which suggests that the oxidant that hydroxylates the heme in myoglobin is non-coordinated H_2O_2 ; the latter is likely to originate from the reduction of non-coordinated O_2 by hydrazine (equation 1) [42]. It is therefore of interest to elucidate whether catalase has an inhibitory effect on the coupled oxidation of cytochrome b₅ axial ligand mutants.



When Fe^{III} -H39V is incubated with O_2 and hydrazine, the following observations are made whether catalase is present (Figure 4A) or absent (Figure 4B): During the initial stages of the reaction the oxyheme complex ($\text{Fe}^{\text{II}}\text{-O}_2\text{-H39V}$) is formed. This species reaches its maximum concentration within the first 15 min of reaction in the absence of catalase, as is evident by the fact that the bands at 540 and 577 nm (Figure 4), which are diagnostic of $\text{Fe}^{\text{II}}\text{-O}_2\text{-H39V}$. Thereafter, the intensity of these bands decreases

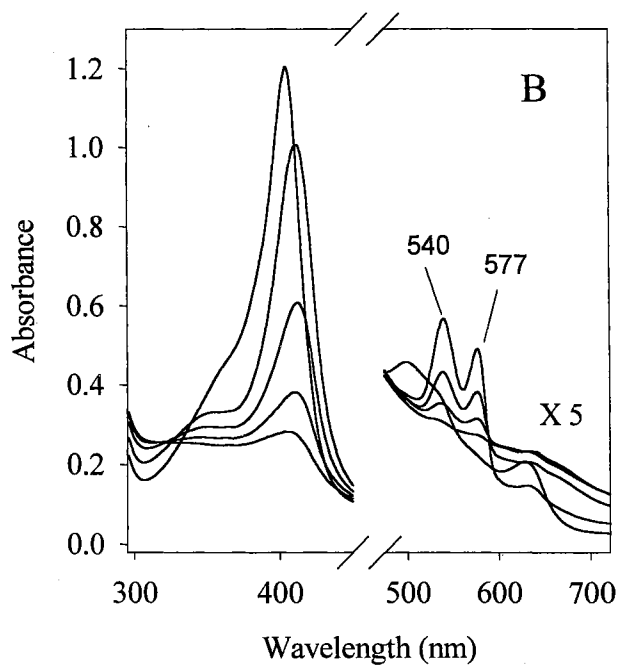
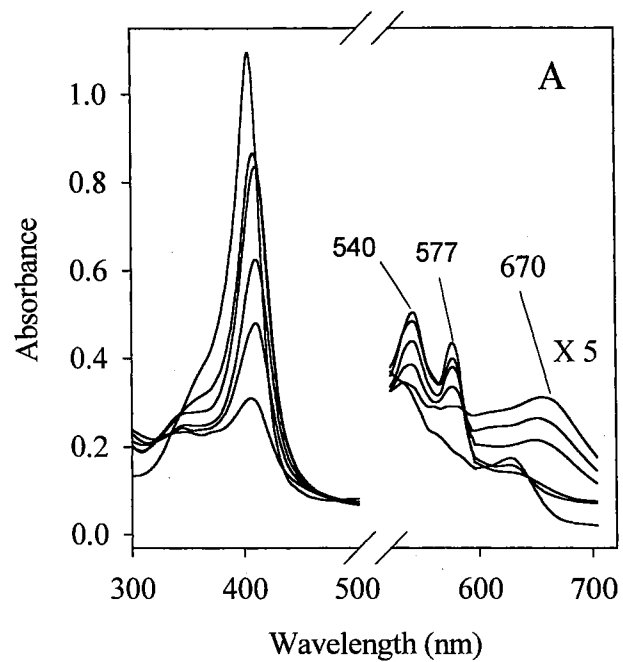


Figure 4. Electronic spectra obtained during the coupled oxidation of the H39V mutant in the presence of hydrazine and O_2 with (A) and without $0.4 \mu\text{M}$ catalase (B). Spectra were taken every 10 min over a period of 2 h.

with the simultaneous appearance and growth of a broad band centered at 670 nm, which suggests that the product of the coupled oxidation of the heme-H39V complex is Fe^{III}-biliverdin. The nature of this product was investigated by extracting it into chloroform after unreacted heme had been removed by extraction with ethyl ether under acidic conditions. The electronic absorption spectrum of the product of the coupled oxidation reaction dissolved in chloroform is identical to the spectrum obtained from authentic biliverdin (Figure 5) thus corroborating that the latter is formed whether catalase is present or absent. It is also interesting to note that the yield of biliverdin is higher when the coupled oxidation is carried out in the presence of catalase, as can be seen graphically in Figure 6-B and spectroscopically from the relative intensity of the 670 nm bands in Figure 4-A (+ catalase) and 4-B (- catalase). Accordingly, the rate of formation for the oxyheme complex in the presence of catalase is twice as long than in the absence of catalase as seen in Figure 6-A. The higher yield of biliverdin is likely to originate from the protective role that catalase exerts by scavenging non-coordinated H₂O₂. In fact, if hydrogen peroxide is mixed with Fe^{III}-H39V, or with the oxyheme complex of H39V, the Soret band decreases in intensity but neither verdoheme nor biliverdin are formed at detectable levels.

The fact that catalase does not inhibit the coupled oxidation of the heme-H39V complex, together with the observation that the oxyheme complex of H39V is accumulated in the initial stages of the reaction suggest that the coupled oxidation of the heme-H39V complex is brought about by coordinated H₂O₂ (Fe^{III}-OOH), which is formed by the reduction of coordinated O₂ (Fe^{II}-O₂). Additional evidence suggesting that

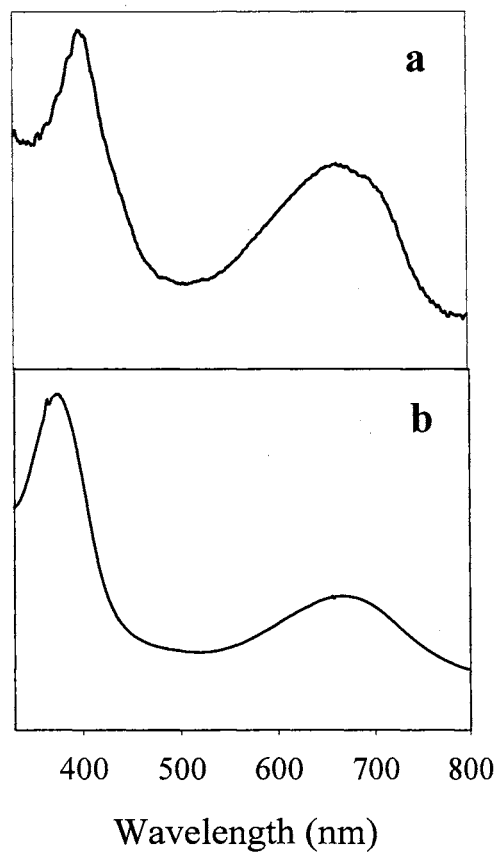


Figure 5. Electronic spectrum of (a) biliverdin obtained from the coupled oxidation of the heme in the H39V mutant, (b) authentic biliverdin.

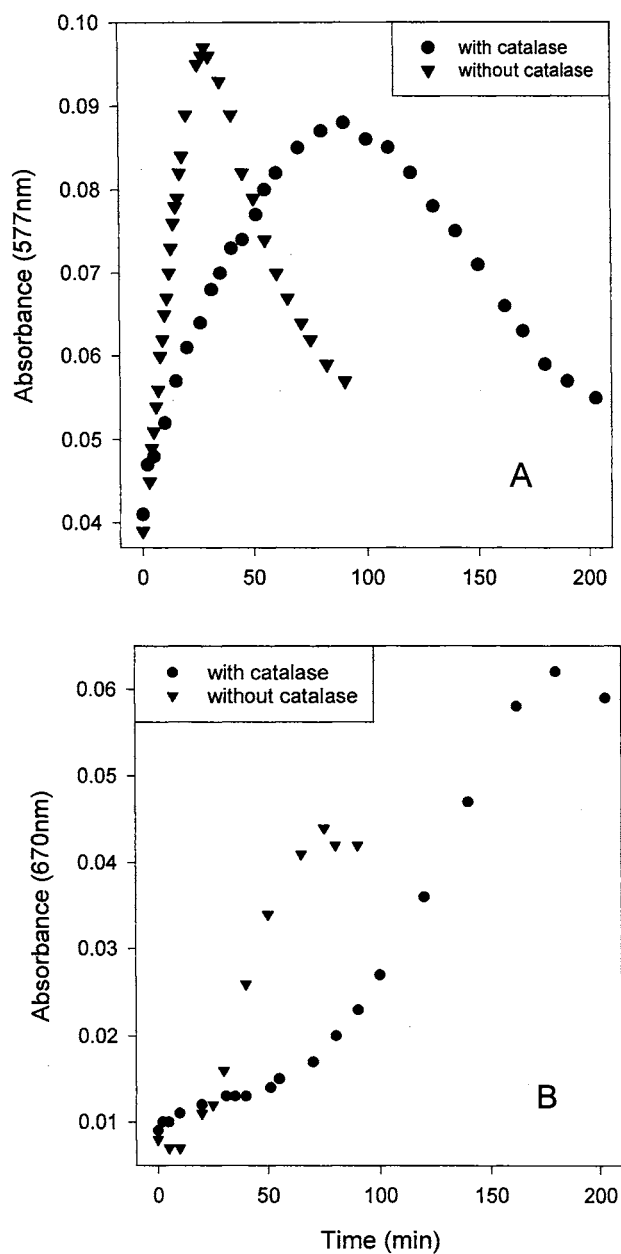


Figure 6. (A) The rate of formation for the oxyheme complex of the H39V mutant during the coupled oxidation in the presence and in the absence of catalase. (B) Amount of biliverdin formation for the H39V mutant during the coupled oxidation in the presence and in the absence of catalase.

the heme-H39V complex is indeed oxidized by coordinated hydrogen peroxide was obtained by reacting the oxyferrous complex of H39V with hydrazine in the presence of catalase. To this end, Fe^{III}-H39V was reduced with one equivalent of sodium dithionite under anaerobic conditions. The anaerobic solution containing Fe^{II}-H39V was bubbled with air, which resulted in the immediate formation of the Fe^{II}-O₂-H39V complex, as is evident from the characteristic bands at 544 and 577 nm in the electronic absorption spectrum shown in Figure 7. If the solution containing Fe^{II}-O₂-H39V is allowed to stand in air, the oxyheme complex is autoxidized to Fe^{III}-H39V with a half-life of approximately 1 h (Figure 7 top). It is apparent that the autoxidation of the Fe^{II}-O₂-H39V complex cleanly restores Fe^{III}-H39V, without significantly decreasing the intensity of the Soret band, thus indicating that the process of autoxidation does not cause heme destruction. On the other hand, if catalase and hydrazine are added immediately after the oxyferrous complex has been formed, the latter is transformed into biliverdin, as is apparent from the decrease in intensity of the bands located at 544 and 577 nm and from the concomitant emergence and growth of a broad band at 640 nm (Figure 7 bottom). The presence of catalase ensures that non-coordinated hydrogen peroxide is scavenged, hence, the fact that the oxyferrous complex is oxidized to biliverdin upon addition of the sacrificial electron donor in the presence of catalase strongly suggests that the oxidation of the oxyheme complex is likely to be initiated by the reduction of coordinated dioxygen (Fe^{II}-O₂) to coordinated peroxide (Fe^{III}-OOH). The latter presumably attacks the heme to form *meso*-hydroxyheme, which in turn, is converted to verdoheme and then biliverdin in the presence of O₂ and hydrazine.

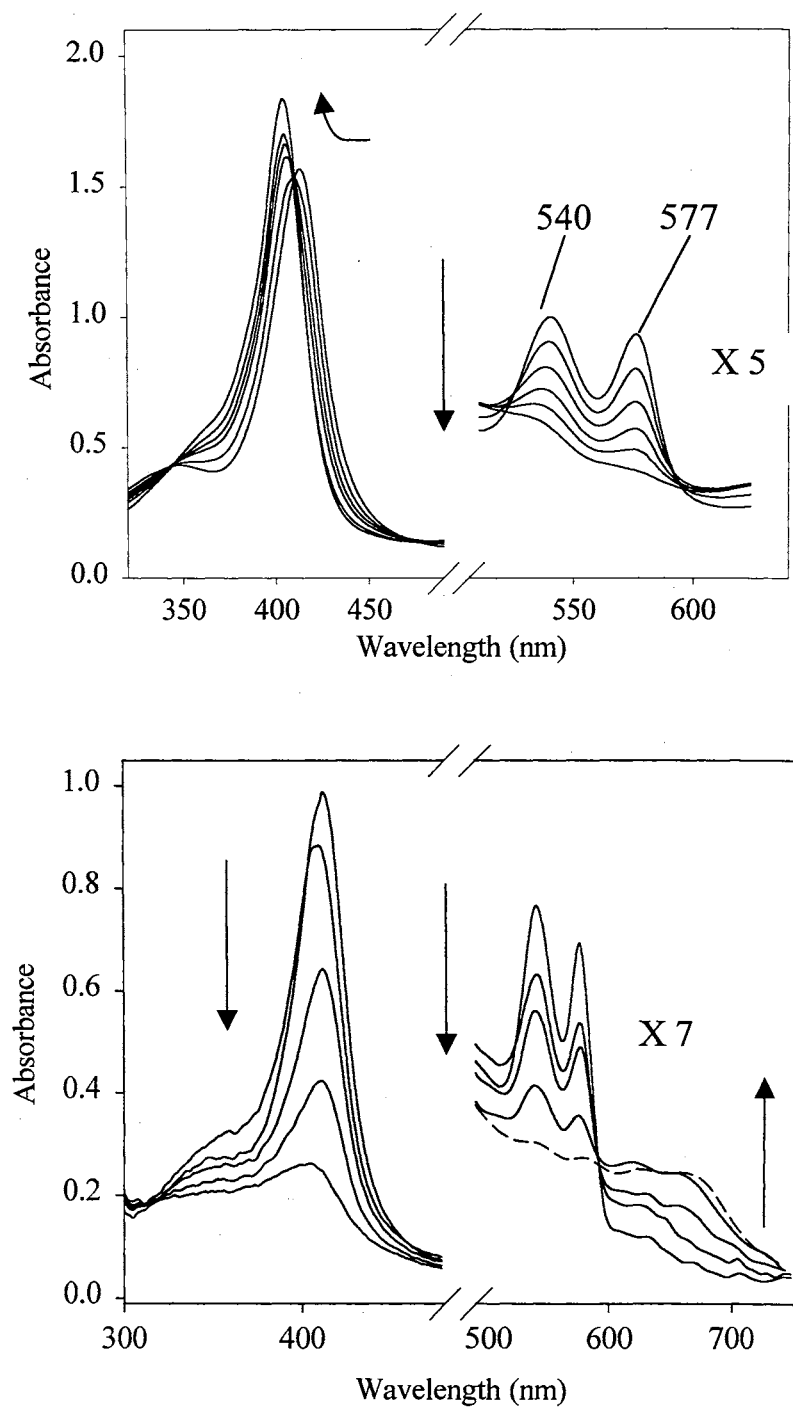


Figure 7. Top: Electronic spectra obtained during the autoxidation of the H39V-O₂ complex prepared by the addition of sodium dithionite to an anaerobic solution of H39V, followed by exposure to air. Bottom: Electronic spectra obtained approximately 30 seconds after the oxy ferrous complex was formed and immediately adding catalase and hydrazine.

iv). HPLC Results

The dimethyl ester (DME) derivatives of biliverdin, originating from the product of coupled oxidation of the heme, were analyzed via HPLC. The regiospecificity results are shown in Figure 8. The retention time of the different biliverdin isomers was determined to be α , β , δ , and γ , on the basis of previously reported analysis [35, 43]. The pyridine hemochrome shows all four meso positions are attacked by oxygen to produce a random mixture of isomeric biliverdins. The chromatogram shows 4 peaks eluted with retention times in the order α (12.3 min), β (13.7 min), δ (15.12 min), and γ (18.1 min) (Figure 8-a). These results are in agreement with values reported previously for the pyridine hemochrome [43, 44]. The α - biliverdin standard eluted one peak with the retention time of 12.3 minutes (α) see Fig. 8-b. This also corresponds to the α peak from the pyridine hemochrome. It is evident from the results obtained that the coupled oxidation of the heme in the H39V mutant produced >90% of γ and 10% of the δ isomer (Fig. 8-d). In contrast, analysis of the products obtained from the H63V mutant showed >80% γ , <15% δ , and <5% β (Figure 8-c). Unlike the H39V mutant, the H63V mutant indicated random changes in the regioselectivity of its coupled oxidation reactions. HPLC results of other reactions carried out in our lab for the H63V mutant showed approximately 60% γ , 40% δ , and 20% α for one reaction, and 60% α and 40% γ for another. These results suggest that the H63V mutant has a non-coordinated hydrogen peroxide that converts the heme-H63V complex to its verdoheme complex causing the random attack.

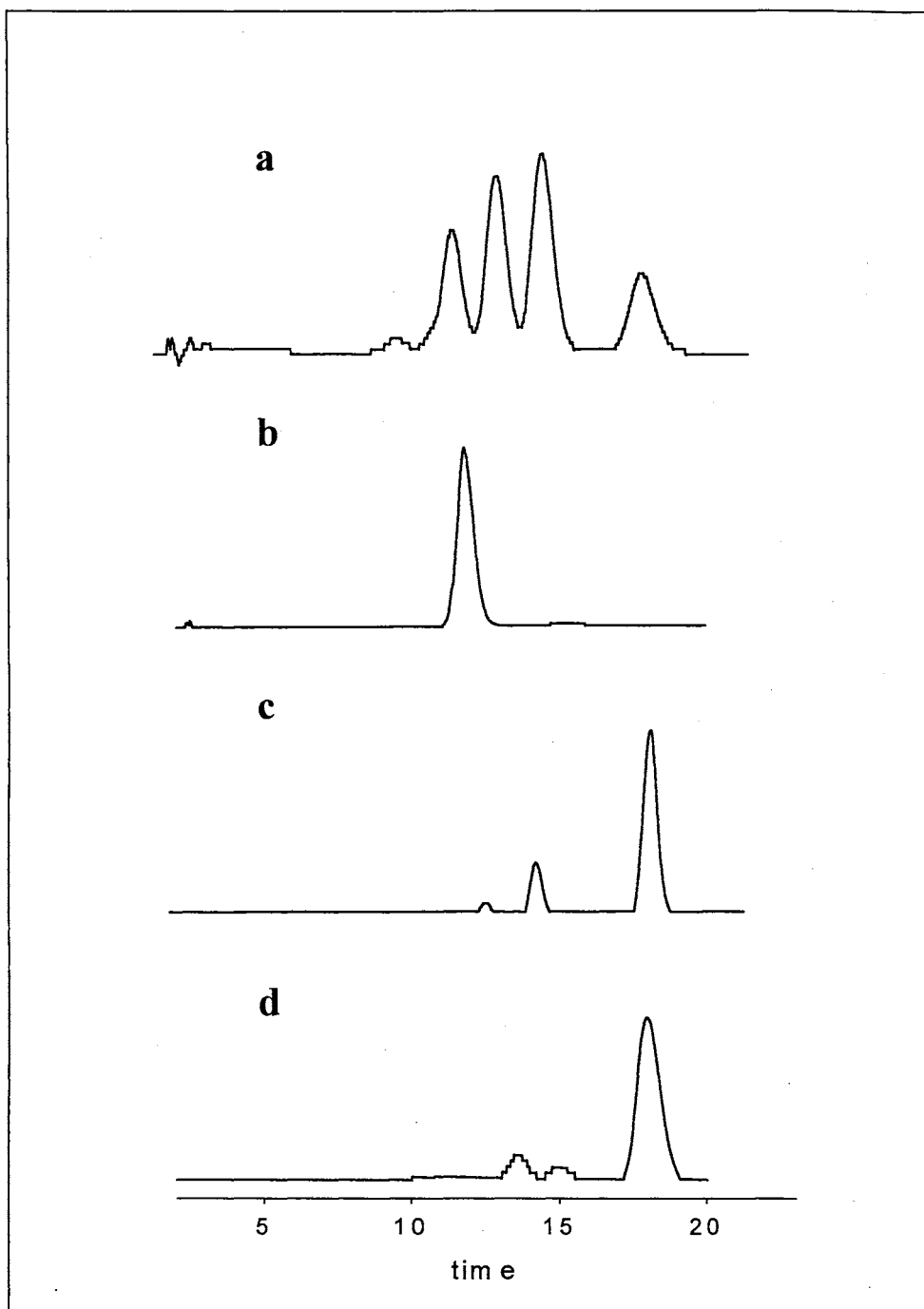


Figure 8. Regiospecificity obtained from the HPLC analysis of samples containing DME derivatives of biliverdin originating from the product of the coupled oxidation of (a) pyridine verdohemeochrome, α (12.3 min), β (13.7 min), δ (15.12 min) γ (18.1 min); (b) α -biliverdin standard, α (12.3 min); (c) H63V coupled oxidation product, γ (18.0 min) and δ (13.7 min) (d) H39V coupled oxidation product, γ (18.0 min) and β (13.7 min).

v). *Relative Stability of the Oxyferrous Complex of the H63V and H39V Mutants*

The relative stability of the oxyferrous complex of the H63V and H39V mutants was further assessed by measuring its rate of autoxidation. The ferrous oxyheme complex of H39V was prepared by stoichiometric addition of sodium dithionite to an anaerobic solution of ferric H39V, followed by exposure to O₂. The UV- vis spectrum of the resultant solution also displays the peaks at 540 and 577 nm (Figure 9). By comparison, when ferrous H63V is exposed to air, the ferric species is formed within a few seconds without detectable accumulation of a ferrous oxyheme complex. An apparent autoxidation rate constant ($k_{ox} = 1.4 \pm 0.2 \text{ h}^{-1}$) was measured for the ferrous oxyheme complex of H39V by following the time-dependent decay of the peak at 577 nm [45]. The relatively low value of k_{ox} and the transient accumulation of the oxyheme complex during the coupled oxidation reaction indicate that the distal environment in H39V stabilizes the oxyheme complex. To understand which residue was responsible for the stability of the mutants, a molecular model of the H39V and H63V mutants were built from the X-ray coordinates of OM cyt b₅. The H39V model indicates that the NH group in Gly 41 may stabilize the corresponding Fe-O₂ complex via the formation of a hydrogen bond. By comparison, a model of the H63V mutant indicates that similar interactions between O₂ and the distal pocket are not possible in this mutant, consistent with the rapid autoxidation of the H63V-O₂ complex.

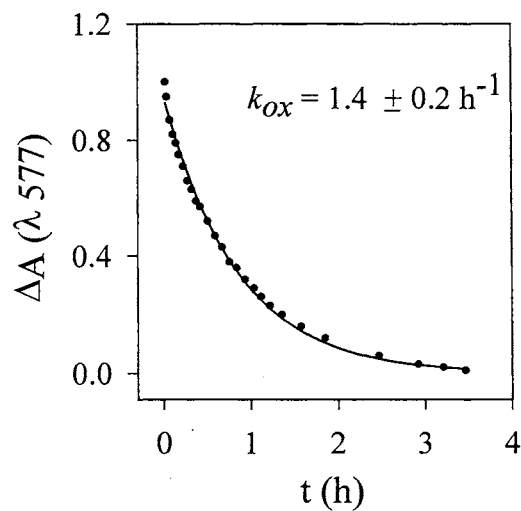
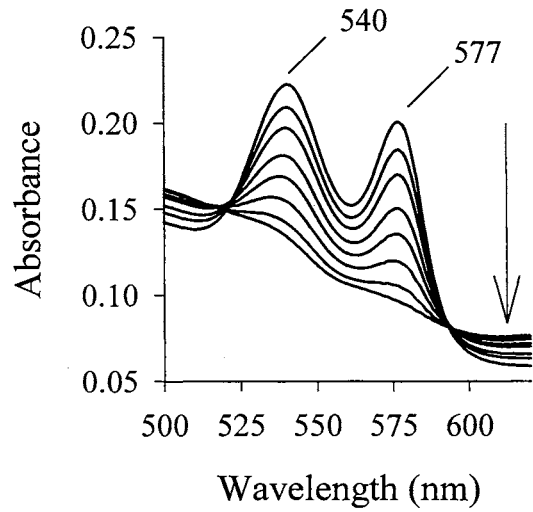


Figure 9. Top: Electronic spectra obtained during the autoxidation of the H39V-O₂ complex prepared by the addition of sodium dithionite to an anaerobic solution of H39V. Bottom: The rate constant for the autoxidation of the H39V-O₂ complex was measured by fitting the time-dependent decay of the peak at 577nm to a single exponential function.

vi). *The Distal Helix Flexibility and Heme Oxygenase Activity.*

The X-ray crystal structures of human HO (hHO-1)[7] and *N. meningitidis* (nm-HO)[8] demonstrated that although the proximal sites of these two enzymes provide the histidine ligand and are very similar to one another, the corresponding distal sites have very few structural features in common. However, there are two important common structural motifs that are interesting to consider: (a) Unlike peroxidases or myoglobin, heme oxygenases do not have a distal histidine or other polar amino acid that is positioned to stabilize ligands coordinated to the sixth position of the heme iron. (b) The only polar residues that are conserved in the distal pocket of these two heme oxygenases and that are sufficiently close to form a hydrogen bond with distal ligands (H_2O_2 or O_2) are the carbonyl oxygen and amide nitrogen of Gly-139 and Gly-143 in hHO-1 [8], and Gly-116 and Gly-120 in nm-HO [8]. It has been proposed that the role of these conserved Gly residues is to impart flexibility to the distal helix, allow close contact of the helix backbone with the heme, and interact with distal heme ligands [8]. A similar conclusion was reached from the X-ray crystal structure of rat HO-1[46], where Gly-139 and Gly-143 are also located in close proximity to the heme iron, and therefore can form hydrogen bonds with distal heme ligands. A detailed comparison of the distal helix structures of human and rat HO-1 suggested that Gly-139 and Gly-143 are indeed likely to facilitate flexibility in the distal helix of HO (Figure 10). The notion that distal helix flexibility might be important in facilitating heme oxygenation activity is supported by the fact that replacement of Gly-139 or Gly-143 in HO-1 for bulkier amino acids suppresses heme oxygenase activity, and in some cases the mutants acquire peroxidase

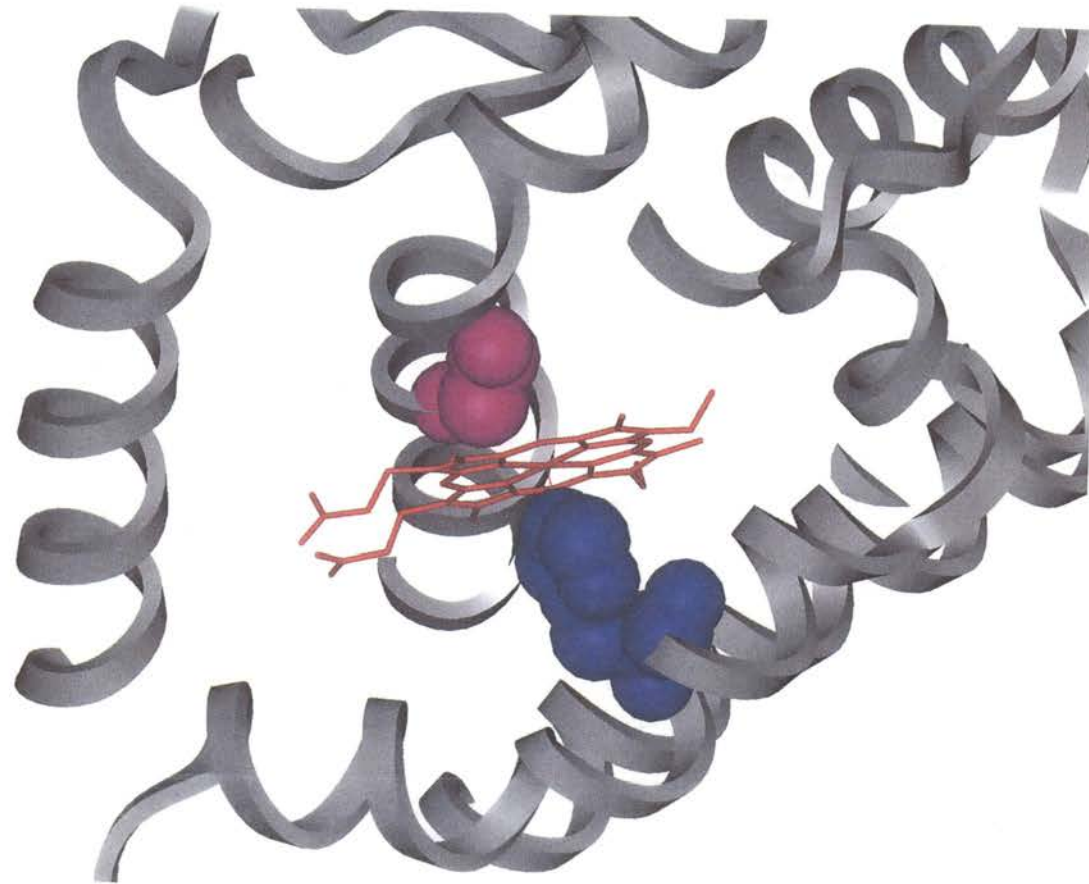


Figure 10. *Molecular Model of HO-1.* Gly 139 (CPK rendering in pink) and 143 are directly contacting the heme (stick rendering in red).

activity [47]. In this context, it is interesting to point out that the distal pocket of the H39V mutant of OM cytochrome b₅ possesses two glycine residues, Gly-41 and Gly-42, see Figure 11. The amide hydrogen of Gly-41 is located 4.7 Å and the carbonyl oxygen of Gly-42 is located at 6.4 Å from the heme iron, respectively, thus suggesting that these residues might play a role in stabilizing a distal ligand by forming a hydrogen bond. It is also interesting to hypothesize that Gly-41 and Gly-42 in the distal pocket of the H39V mutant function in a role reminiscent of Gly-139 and Gly-143 in h-HO-1 and rat-HO-1, and Gly-116 and Gly-120 in nm-HO, in that these residues, by providing distal pocket flexibility facilitate the activation of O₂ that results in heme oxygenation of the heme-H39V complex to biliverdin. Consequently, Gly-41 and Gly-42 were replaced for Ala (H39V/G41A and H39V/G42A), thus introducing the minimum perturbation that would allow us to test whether flexibility of the distal helix is an important structural element for heme oxygenation activity.

When the ferric H39V/G41A double mutant is incubated with hydrazine in the presence of air, the spectrum of the resultant solution changes from that displaying a characteristic Soret $\lambda_{\text{max}} = 405$ nm and relatively featureless visible region to a spectrum with Soret $\lambda_{\text{max}} = 418$ nm and bands at 542 nm and 580 nm in the visible region, which is characteristic of an oxyferrous species. This was corroborated by the fact that an identical spectrum is obtained if a cuvette containing an anaerobic solution Fe^{II}-H63V is bubbled with air. In contrast to the observations made with the oxyferrous complex of the H39V mutant, which is converted into biliverdin upon incubating it with hydrazine and O₂, the heme in the oxyferrous complex of the H39V/G41A double mutant is

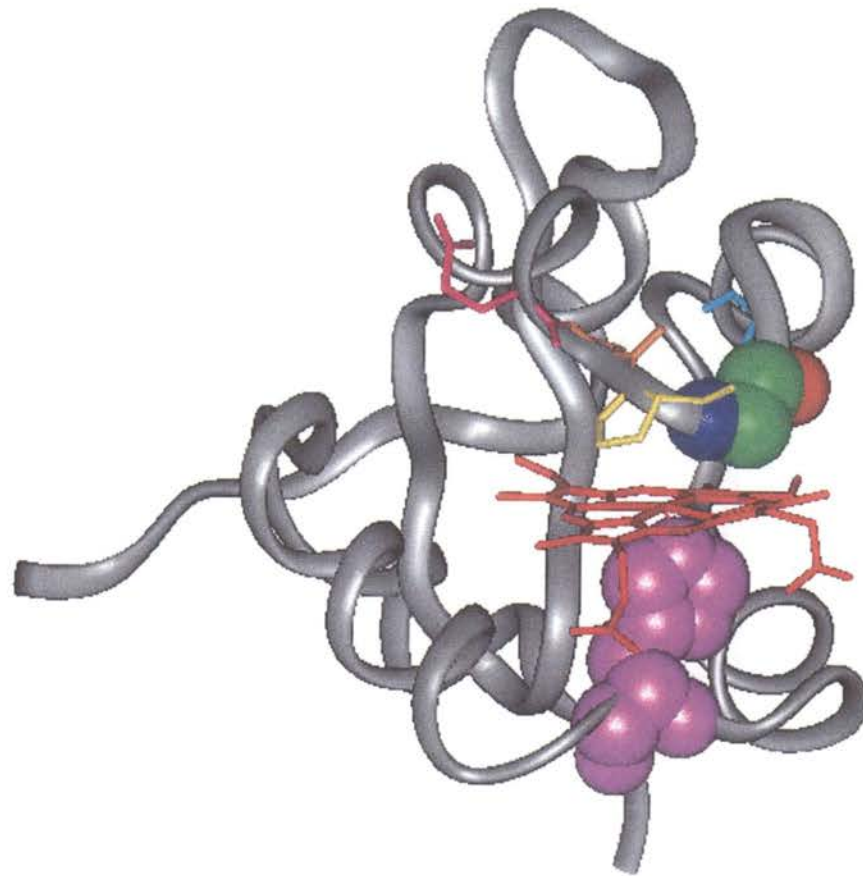


Figure 11. (A) *Molecular Model of the H39V Mutant of OM Cytochrome b₅*. The sequence Glu³⁸-Val³⁹-Pro⁴⁰-Gly⁴¹-Gly⁴², located on top of the heme, is shown with stick rendering. Gly41 in this sequence is shown in CPK rendering to illustrate that its nitrogen atom (blue) is located near the heme iron. Consequently, it is likely that the stability of the Fe²⁺-O₂ complex of this mutant originates from the formation of a hydrogen bond between Gly41 N-H and the terminal oxygen in the Fe²⁺-O₂ complex.

destroyed over a period of approximately 4 hours, without producing either verdoheme or biliverdin (Figure 12). Similar observations were made when $\text{Fe}^{\text{II}}\text{-O}_2\text{-H39V/G41A}$ was prepared by bubbling air into an anaerobic solution containing $\text{Fe}^{\text{II}}\text{-H39V}$, followed by the addition of hydrazine, thus corroborating that the $\text{Fe}^{\text{II}}\text{-O}_2$ complex of the double mutant is not readily converted into the $\text{Fe}^{\text{III}}\text{-OOH}$ species required for heme oxidation. The role played by Gly-42 was probed in a similar manner with the aid of the H39V/G42A double mutant. When this protein is incubated with hydrazine and O_2 the Soret band shifts to the red, and the visible region indicates a slight accumulation of the oxyferrous complex; however, in the course of approximately 4 hours the heme is completely destroyed, without forming verdoheme or biliverdin (Figure 13). These findings are therefore in agreement with the hypothesis that Gly-41 and Gly-42, by imparting flexibility to the distal helix, contribute to the heme oxygenating activity exhibited by the H39V mutant.

vii). Catalase Inhibits the Coupled Oxidation of the H63V Mutant

When $\text{Fe}^{\text{III}}\text{-H63V}$ is incubated with O_2 and hydrazine as a sacrificial electron donor a gradual decrease in the intensity of the Soret band is accompanied by the appearance and growth of a band centered at 660 nm (Figure 14-A). It has been previously demonstrated that the emergence and growth of a band at 665 nm during the coupled oxidation process is diagnostic of the formation verdoheme [24, 26]; this was corroborated by the electronic absorption spectrum of the reaction product extracted into a chloroform-pyridine solution, which is identical to that previously reported for

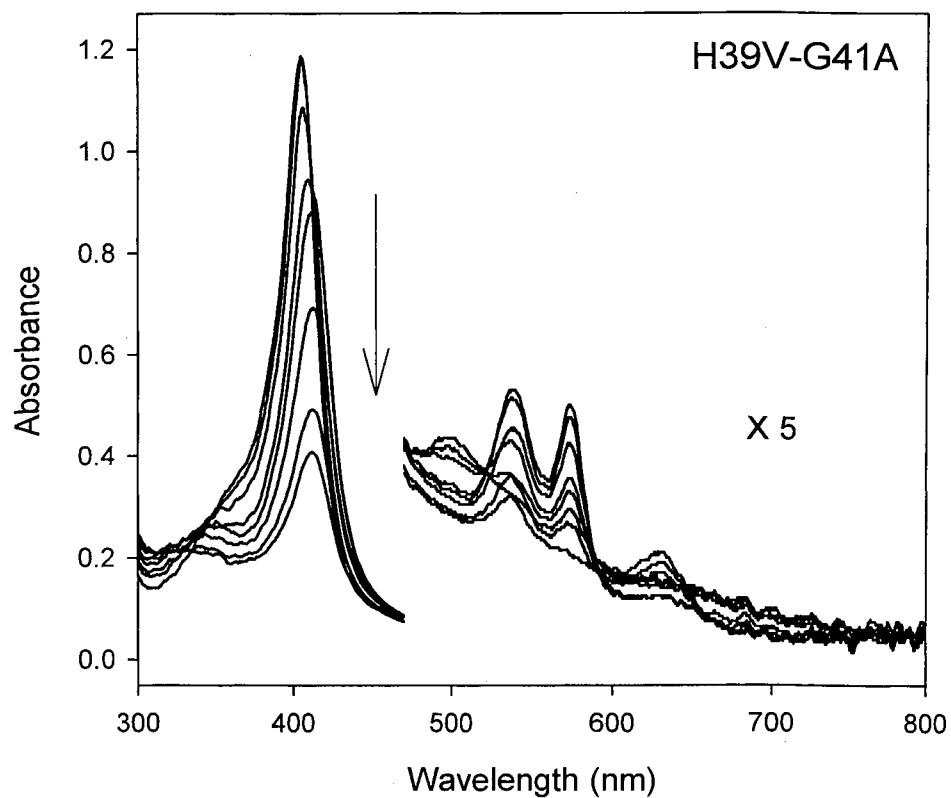


Figure 12. Electronic spectra obtained during the coupled oxidation of the H39V-G41A mutant in the presence of hydrazine and O_2 . Spectra were taken over a period of 12 h.

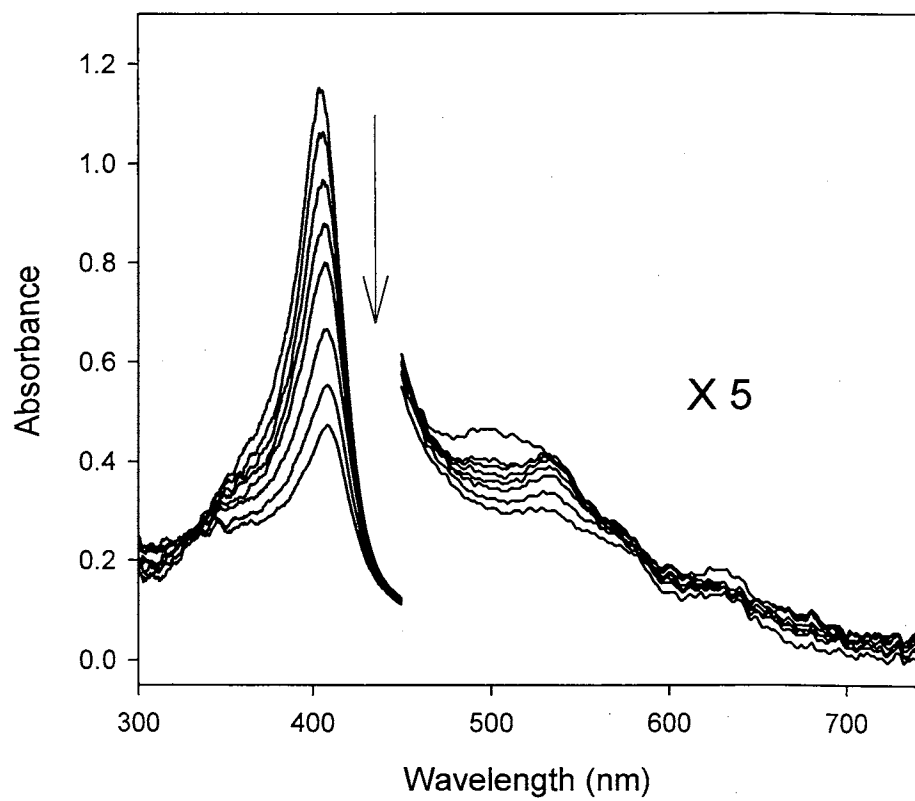


Figure 13. Electronic spectra obtained during the coupled oxidation of the H39V-G42A mutant in the presence of hydrazine and O₂. Spectra were taken over a period of 4 h.

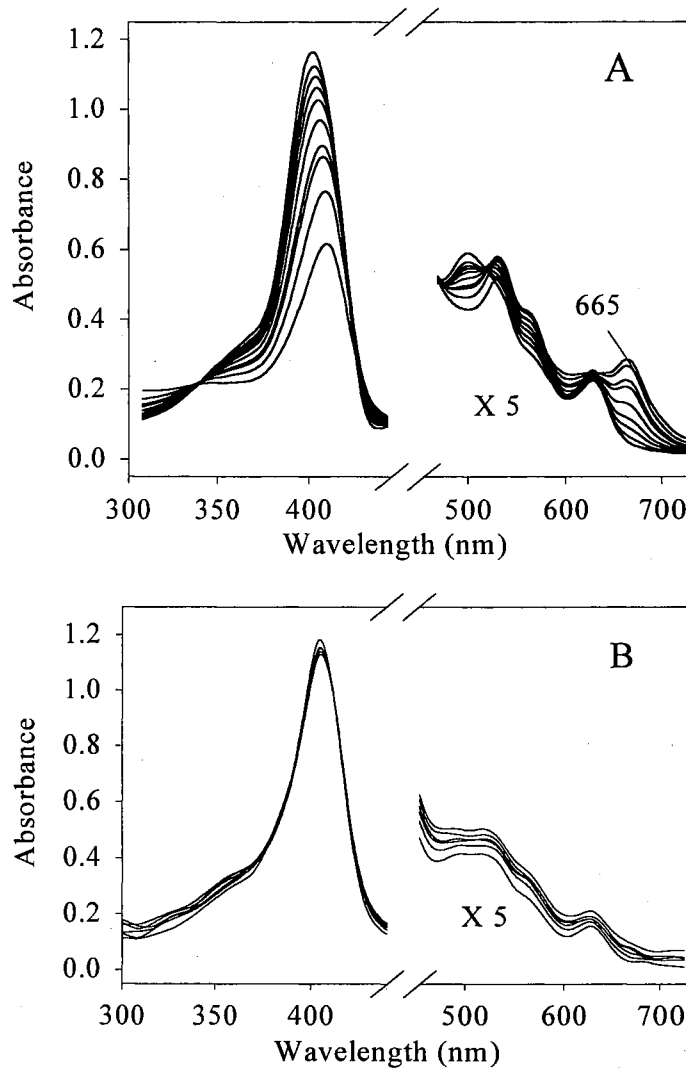


Figure 14. Electronic spectra obtained without (A) and with $0.4 \mu\text{M}$ catalase (B) during the coupled oxidation of the H63V in the presence of hydrazine and O_2 . Spectra were taken at 10 minute intervals for 2.5 hours.

authentic verdohemochrome [39, 48, 49]. In plain contrast, when Fe^{III}-H63V is incubated with O₂ and hydrazine in the presence of catalase, the only spectral change that is observed corresponds to a slight decrease (~ 5%) in the intensity of the Soret band (Figure 14-B). It is therefore apparent that the presence of catalase inhibits the coupled oxidation of the heme in H63V, presumably by scavenging non-coordinated H₂O₂, which is generated in the reaction mixture via the reduction of non-coordinated O₂ by hydrazine (equation 1) [42]. Consequently, it is conceivable that H₂O₂, generated in solution from non-coordinated O₂, reacts with Fe^{III}-H63V to form the Fe^{III}-OOH hydroxylating species, in a manner similar to that described for HO. This possibility was probed by incubating Fe^{III}-H63V with 2 equivalents of H₂O₂ in the presence of air. These experiments demonstrated that addition of H₂O₂ to Fe^{III}-H63V causes a small red shift of the Soret band at 409 nm and the appearance of α and β bands at 530 nm and 562 nm respectively, without an increase in absorbance around 660 nm, indicating that neither verdoheme or biliverdin is formed (Figure 15). These results suggest that the 409 nm species is a ferryl species similar to that shown for the reaction of h-HO-1 mutants with H₂O₂ [50].

The gradual decrease in the intensity of the Soret band in the presence of H₂O₂ must result from non-specific destruction of the heme by hydrogen peroxide. Consequently, although non-coordinated hydrogen peroxide is the oxidant that converts the heme-H63V complex to the corresponding verdoheme complex, this oxidative process cannot be brought about by reacting Fe^{III}-H63V with H₂O₂. An alternative path consistent with the finding that catalase inhibits the coupled oxidation of the heme-H63V complex would entail a reaction between Fe^{II}-H63V and H₂O₂. Insights gained from testing this alternative hypothesis are described below.

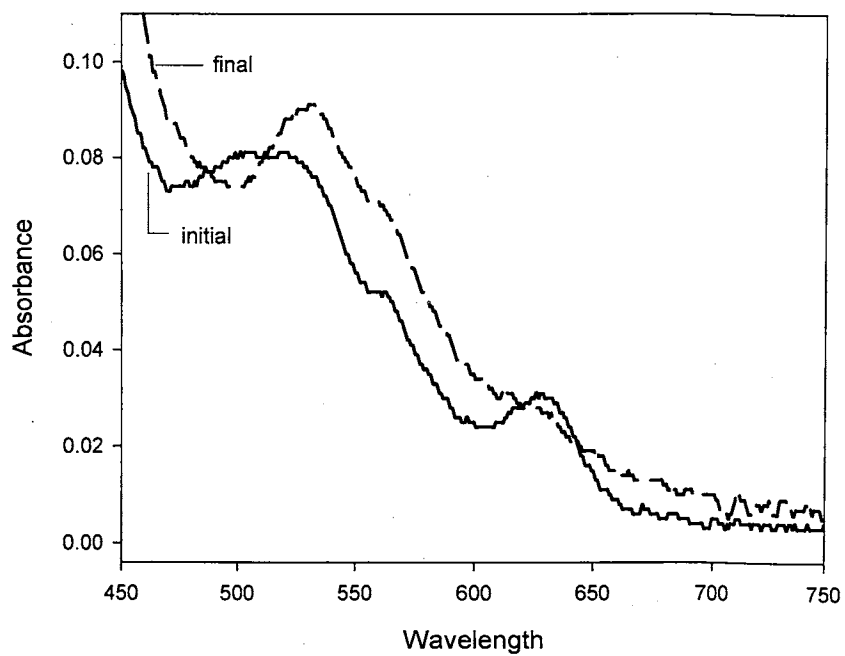
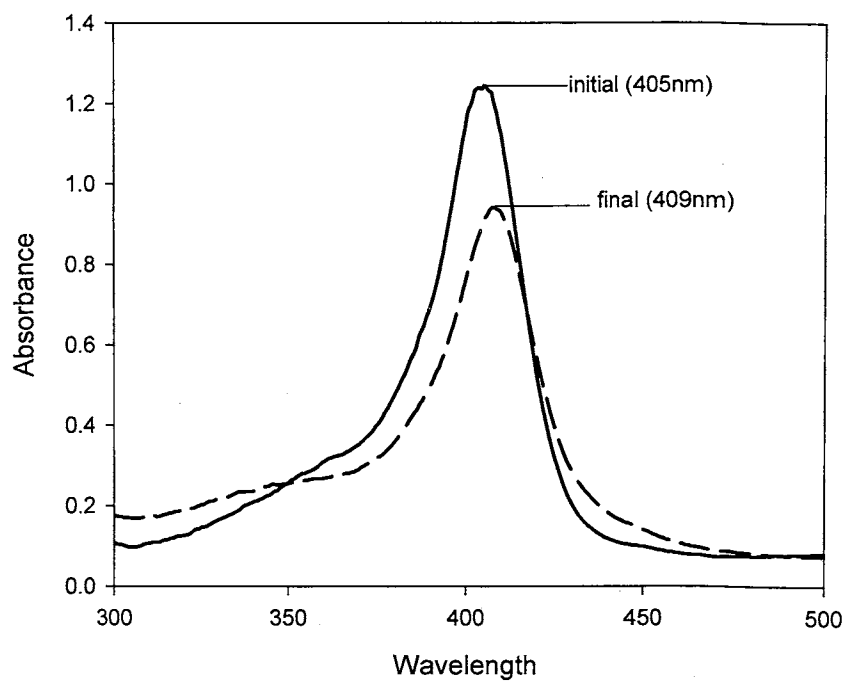


Figure 15. Fe^{III}-H63V mutant + H₂O₂. initial H63V (—), 35 min after 2 equivalents of H₂O₂ (- - -).

When an anaerobic solution of Fe^{III}-H63V is treated with one equivalent of sodium dithionite, the electronic absorption spectrum of the ferric species, which displays a Soret band at 405 nm, is replaced by a spectrum characteristic of Fe^{II}-H63V, exhibiting a Soret band at 423 nm. Subsequent addition of two equivalents of an anaerobic solution of H₂O₂ to Fe^{II}-H63V induces time-dependent spectral changes. After approximately 30 minutes the electronic absorption spectrum does not change any further and displays a Soret band at 407 nm (Figure 16-a), and relatively featureless visible region (Figure 16-a'). However, exposing the contents of the cuvette to air results in the formation of verdoheme, as can be seen from the decrease in the intensity of the Soret band (Figure 16-b) and the growth of a band at 667 nm (Figure 16-b'). Moreover, if the solution is then bubbled with CO, the band at 667 nm decreases in intensity with the concomitant appearance and growth of a band at 626 nm (Figure 16-c); the latter is characteristic of verdoheme axially coordinated by a proximal histidine and a distal CO [12, 14, 24, 51], and therefore provides corroborating evidence that verdoheme is formed upon mixing anaerobic solutions of Fe^{II}-H63V and H₂O₂, followed by exposure to O₂. The relative intensity of the Soret to 667 nm band (Figures 16-b and b', respectively) indicates that the conversion of Fe^{II}-H63V to verdoheme-H63V is not quantitative, rather, it suggests that less than 30% of the heme is converted to verdoheme. Nevertheless, these results clearly indicate that hydrazine sets the stage for the coupled oxidation process to occur by participating in two independent reactions: (a) the reduction of Fe^{III}-H63V to Fe^{II}-H63V and (b) the reduction of non-coordinated O₂ to produce non-coordinated H₂O₂. In turn, non-coordinated H₂O₂ and Fe^{II}-H63V react to produce verdoheme, presumably via a *meso*-hydroxyheme intermediate.

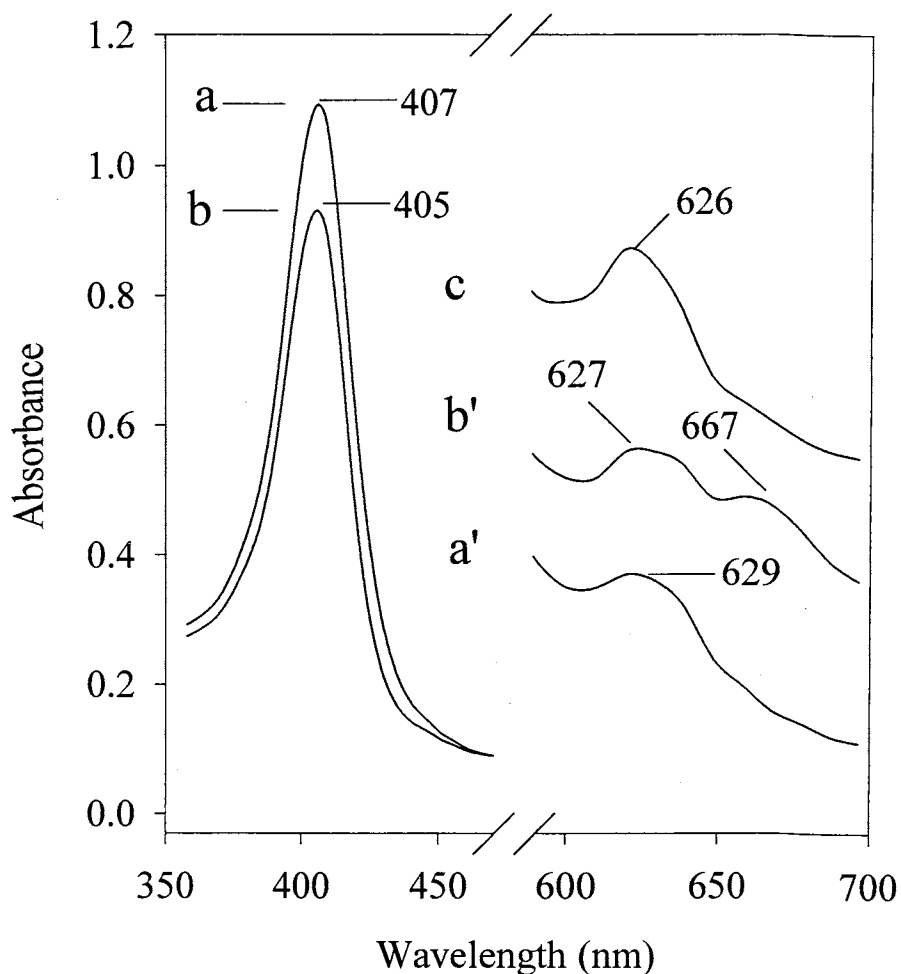


Figure 16. Electronic spectra of an anaerobic solution of Fe^{III} -H63V treated with one equivalent of sodium dithionite and subsequent additions of two equivalents of an anaerobic solution of H_2O_2 to Fe^{II} -H63V. Electronic absorption spectra were taken every 10 minutes until there was no further change. The final resulting spectrum (a) has the soret band at 407 nm and (a') a featureless visible region. The formation of verdoheme can be seen with (b) a decrease in the intensity of the soret band and (b') the growth of the 667 nm peak. Upon addition of CO to verdoheme, CO-verdoheme peaks are formed (c).

When an anaerobic solution of Fe^{III}-H63V, displaying a Soret band at 405 nm (Figure 17-1), is reduced with one equivalent of sodium dithionite, the spectrum of the resultant solution displays a Soret band at 423 nm (Figure 17-1'). Subsequent addition of one equivalent of anaerobic H₂O₂ results in a gradual (~30 min) blue shift of the Soret band, which results in a spectrum that exhibits a Soret band at 406 nm (Figure 17-2). If this solution is titrated again with one equivalent of sodium dithionite, while maintaining strict anaerobic conditions, the resultant solution exhibits a spectrum with a Soret band at 422 nm (Figure 17-2'). When this solution is treated with one equivalent of an anaerobic solution of H₂O₂ the Soret band shifts to 409 nm (Figure 17-3), over a period of ~ 30 min. This cycle was repeated two more times, resulting in the spectra shown by Figures 17-3' and 17-4 upon the third reduction with dithionite followed by the addition of one equivalent of H₂O₂, and spectra 17-4' and 17-5 upon reducing with dithionite, followed by addition of hydrogen peroxide for a fourth time. It is evident from Figure 17 that upon subjecting the H63V mutant to repetitive cycles in which the protein is first reduced with dithionite and then oxidized with H₂O₂, the Soret band, which is initially located at 405 nm, gradually shifts to 417 nm as the number of cycles is increased, whereas the Soret band corresponding to reduced Fe^{II}-H63V gradually shifts from 423 to 420 nm. These observations suggest that with each cycle, the reaction between Fe^{II}-H63V and H₂O₂ leads to the gradual accumulation of a species that is stable under anaerobic conditions. It is possible to hypothesize that this species might be *meso*-hydroxyheme because when air is bubbled through the solution displaying the spectrum shown in Figure 17-5, with the corresponding visible region shown in trace a of the inset in Figure 17, verdoheme is formed. The formation of verdoheme is apparent from the emergence and growth of a

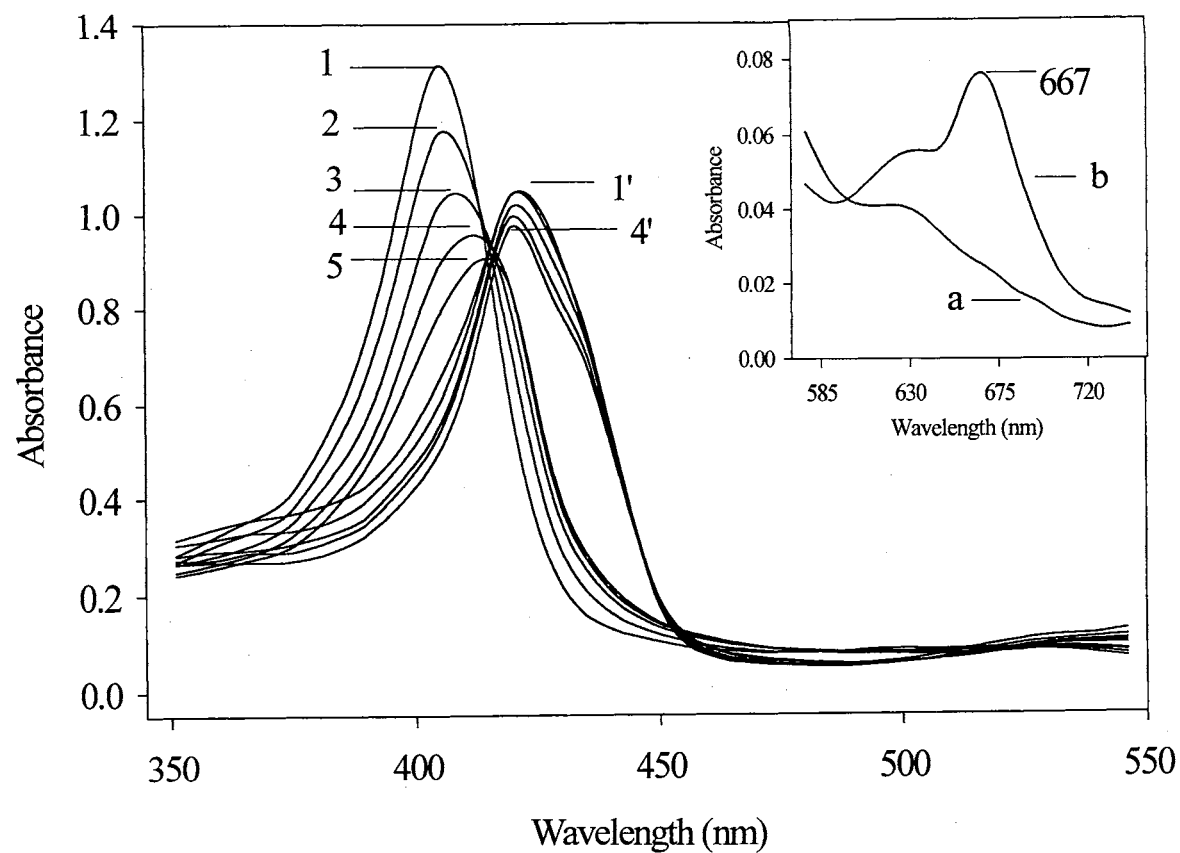


Figure 17. Resulting electronic spectra of the titration of Fe^{III}- H63V (1) using one equivalent of sodium dithionite and subsequent addition of one equivalent of anaerobic H₂O₂. (1'-4') are the resulting spectra after the addition of sodium dithionite and (2-4) are the spectra after the subsequent addition of H₂O₂. Spectrum (5) is the final spectrum before the addition of air. Inset: (a) the final addition of H₂O₂ corresponding to spectrum 4. (b) Verdoheme accumulation after exposure to air.

band at 667 nm, which is shown in trace b in the inset of Figure 17. Additional evidence suggesting that the intermediate accumulated by the repetitive reactions between Fe^{II} -H63V and H_2O_2 is the *meso*-hydroxyheme-H63V complex is described below.

It is well established that the *meso*-hydroxyheme complexes of heme oxygenase [52, 53] and myoglobin [19] react with O_2 to produce the corresponding verdoheme complexes. It has been suggested that ferric *meso*-hydroxyheme is converted to ferric verdoheme by simple exposure to O_2 without the need for a reducing equivalent [53]. An alternative mechanism invoking the need of a reducing equivalent to form ferrous *meso*-hydroxyheme, which subsequently reacts with O_2 to form ferrous verdoheme has also been proposed [52, 54]. More recently it has been suggested that under physiological conditions both reaction pathways might be possible and their relative importance is likely to depend on the concentrations of NADPH, cytochrome P450 reductase and O_2 in the cell [55]. It is important to point out, however, that there is complete agreement on the fact that *in vitro* the CO complex of ferrous *meso*-hydroxyheme is converted to the CO complex of ferrous verdoheme when the latter is allowed to react with dioxygen [52-54]. In fact, this is a chemical property unique to *meso*-hydroxyheme. Therefore, if the reaction between Fe^{II} -H63V and H_2O_2 does indeed produce *meso*-hydroxyheme, the corresponding CO complex should be converted into the carbomonoxy adduct of the H63V-verdoheme complex upon exposure to air. This hypothesis was tested by performing an experiment in which the putative *meso*-hydroxyheme-H63V complex was first accumulated by means of anaerobically reducing a solution of Fe^{III} -H63V with one equivalent of sodium dithionite, followed by the addition of one equivalent of an

anaerobic solution of hydrogen peroxide, and repeating this cycle four times, as described above. After the last equivalent of an anaerobic solution of H_2O_2 was added, the resultant solution exhibited a spectrum (Figure 18-a) with a Soret band at 417 nm. This solution, presumably containing mainly the ferric *meso*-hydroxyheme complex of H63V, was titrated with one equivalent of sodium dithionite in order to obtain the corresponding ferrous complex, which exhibits a Soret band at 420 nm (Figure 18-b). When carbon monoxide was bubbled through the resultant solution, while still maintaining strict anaerobic conditions, the electronic absorption spectrum changes from that shown in Figure 18-b to the spectrum shown in Figure 18-c, which exhibits an intense Soret band at 420 nm and bands at 540 and 567 nm in the visible region. This spectrum is typical of ferrous low-spin hemes axially coordinated by a carbomonoxy ligand and distinct from that exhibited by the CO complex of Fe^{II} -H63V, thus indicating that the intermediate accumulated by the repetitive cycles in which Fe^{II} -H63V is reacted with H_2O_2 is capable of forming a carbomonoxy adduct. When the anaerobic solution containing the carbomonoxy adduct of the accumulated intermediate was bubbled with air, the resultant electronic absorption spectra showed the emergence and rapid growth of a band at 626 nm (trace 1 in the inset of Figure 18), which is diagnostic of the presence of a verdoheme-carbomonoxy complex axially coordinated by a histidine and a carbomonoxy ligands. Upon continued bubbling of air through the solution, the band at 626 nm decreases and disappears, with the concomitant emergence and growth of a band at 667 nm (trace 2 in the inset of Figure 18), which is typical of the H63V-verdoheme complex. On the basis of this observations it is possible to conclude that the intermediate species accumulated during the cycles in which Fe^{II} -H63V is allowed to react with H_2O_2 under

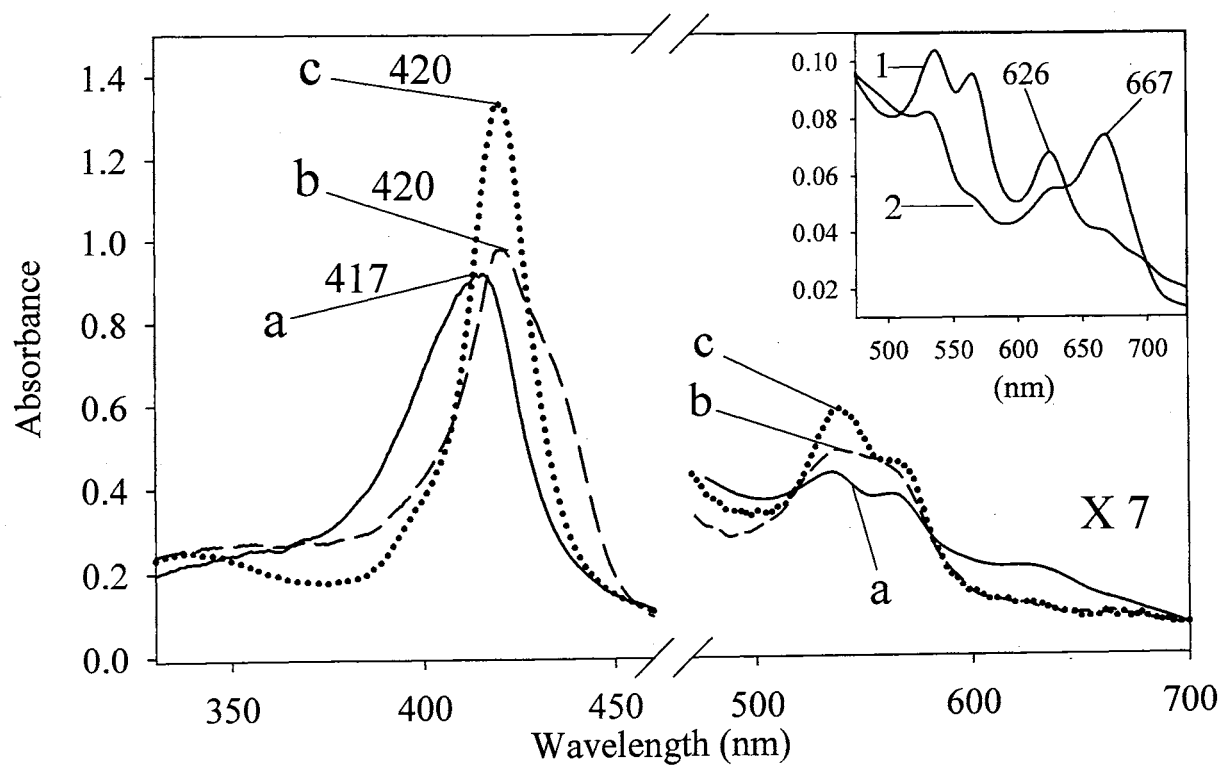


Figure 18. (a) Electronic spectrum of the ferric *meso*-hydroxyheme complex of H63V. (b) Electronic spectra of the ferrous complex obtained by titrating the ferric *meso*-hydroxyheme complex of H63V with one equivalent of sodium dithionite. (c) the carbomonoxy adduct formed after anaerobically bubbling CO.

Inset: (1) verdoheme-carbomonoxy complex (2) H63V-verdoheme complex formed upon continued bubbling of air.

strict anaerobic conditions is very likely the *meso*-hydroxyheme complex of H63V, thus indicating that the coupled oxidation of the heme complex of H63V is brought about by non-coordinated H_2O_2 , and it proceeds via the formation of a *meso*-hydroxyheme intermediate.

Conclusions

The significance of these findings resides in the fact that the coupled oxidation of hemoproteins has been used as a model to study heme catabolism [15, 19, 20, 22, 24, 56, 57] because it was assumed that it is brought about by coordinated O_2 , which in the presence of a reducing agent, typically ascorbate or hydrazine, is converted to the Fe^{III} -OOH oxidizing species. However, the results reported herein demonstrate the coupled oxidation of the H63V mutant of OM cyt b_5 differs from the process of heme oxygenation carried by heme oxygenase in the nature by which the oxidant, H_2O_2 , is generated. In the coupled oxidation process, non-coordinated O_2 is reduced by hydrazine in order to form non-coordinated H_2O_2 ; the latter, in turn, oxidizes ferrous heme to *meso*-hydroxyheme, which in the presence of excess O_2 is rapidly converted into verdoheme. In contrast, O_2 in the heme oxygenation process is first coordinated to the heme iron ($\text{Fe}^{\text{II}}\text{-O}_2$) before a second reducing equivalent converts it into the ferric hydroperoxide ($\text{Fe}^{\text{III}}\text{-OOH}$) oxidizing species known to hydroxylate heme, thus forming *meso*-hydroxyheme (Scheme I). Consequently, the first clear mechanistic distinction between the coupled oxidation and heme oxygenation processes resides in the path followed to generate the oxidant.

It is of interest to compare the findings described herein with insights gained from studying the coupled oxidation of iron porphyrins, a process that has been extensively studied by Balch and coworkers [49, 58-63]. These investigators monitored the degradation of pyridine containing solutions of iron (II) octaethylporphyrin, $(py)_2Fe^{II}(OEP)$, by O_2 , utilizing hydrazine as a sacrificial electron donor, and concluded that in the first stage of heme oxidation the conversion of a ferrous porphyrin to a *meso*-oxygenated complex involves H_2O_2 and not O_2 as an oxidant [61]. More recently the same group demonstrated that treatment of anaerobic pyridine solutions of $(py)_2Fe^{II}(OEP)$ with hydrogen peroxide at $-30\text{ }^\circ\text{C}$ results in the formation of *meso*-oxygenated porphyrin complexes [62, 63]. Thus, the evidence described in this report, which demonstrate that the coupled oxidation of the heme-H63V complex is brought about by the oxidation of Fe^{II} -H63V by non-coordinated H_2O_2 , is in good agreement with insights gained from studying the coupled oxidation of iron-porphyrin model complexes. Hence, the observations made with iron porphyrins and with the H63V mutant of OM cytochrome b_5 , together with the fact that the coupled oxidation of myoglobin has been shown to be inhibited by catalase [23], suggest that the coupled oxidation of those hemoproteins not involved in heme catabolism is likely to be mediated by non-coordinated H_2O_2 . It is important to point out, however, that although the coupled oxidation of H63V appears to be representative of a common process by which hemoproteins are oxidized, the coupled oxidation of the H39V mutant of OM cytochrome b_5 proceeds in a manner akin to that displayed by heme oxygenase, i.e. via the reduction of a coordinated O_2 molecule ($Fe^{II}-O_2$).

REFERENCES

1. Ponka, P., *Cell Biology of Heme*. Am. J. Med. Sci., 1999. **318**: p. 241-256.
2. Maines, M.D., *The Heme Oxygenase System: A Regulator of Second Messenger Gases*. Annu. Rev. Pharmacol. Toxicol., 1997. **37**: p. 517-554.
3. Ortiz de Montellano, P.R., *Heme Oxygenase Mechanism: Evidence for an Electrophilic, Ferric Peroxide Species*. Acc. Chem. Res., 1998. **31**: p. 543-549.
4. Sun, J., A. Wilks, P.R. Ortiz de Montellano, and T.M. Loehr, *Resonance Raman and EPR spectroscopic studies on heme-heme oxygenase complexes*, in *Biochemistry*. 1993. p. 14151-7.
5. Sun, J., T.M. Loehr, A. Wilks, and P.R. Ortiz de Montellano, *Identification of Histidine 25 as the Heme Ligand in Human Liver Heme Oxygenase*, in *Biochemistry*. 1994. p. 13734-40.
6. Ito-Maki, M., I. Kazunobu, K.M. Matera, M. Sato, M. Ikeda-Saito, and T. Yoshida, *Demonstration that Histidine 25, but Not 132, is the Axial Heme Ligand in Rat Heme Oxygenase-1*. Arch. Biochem. Biophys., 1995. **317**: p. 253-258.
7. Schuller, D.J., A. Wilks, P.R. Ortiz de Montellano, and T.L. Poulos, *Crystal Structure of Human Heme Oxygenase-1*. Nature Struct. Biol., 1999. **6**: p. 860-867.
8. Schuller, D.J., W. Zhu, I. Stojiljkovic, A. Wilks, and T.L. Poulos, *Crystal Structure of Heme Oxygenase from the Gram-Negative Pathogen Neisseria meningitidis and a Comparison with Mammalian Heme Oxygenase*. Biochemistry, 2001. **40**: p. 11552-11558.

9. Springer, B.A., S. Sligar, G., J. Olson, S., and G. Phillips Jr., N., *Mechanisms of Ligand Recognition in Myoglobin*. Chem. Rev., 1994. **94**: p. 699-714.
10. Yoshida, T., M. Noguchi, and G. Kikuchi, *Oxygenated Form of Heme-Heme Oxygenase Complex and Requirement for Second Electron to Initiate Heme Degradation from the Oxygenated Complex*. J. Biol. Chem., 1980. **255**: p. 4418-4420.
11. Yoshida, T. and G. Kikuchi, *Features of the Reaction of Heme Degradation Catalyzed by the Reconstituted Microsomal Heme Oxygenase System*. J. Biol. Chem., 1978. **253**: p. 4230-4236.
12. Yoshida, T., M. Noguchi, and G. Kikuchi, *A New Intermediate of Heme Degradation Catalyzed by the Heme Oxygenase System*. J. Biochem., 1980. **88**: p. 557-563.
13. Ishikawa, K., M. Sato, M. Ito, and T. Yoshida, *Importance of Histidine 25 of Rat Heme Oxygenase for its Catalytic Activity*. Biochem. Biophys. Res. Commun., 1992. **182**: p. 981-986.
14. Wilks, A. and P.R. Ortiz de Montellano, *Rat Liver Heme Oxygenase*. J. Biol. Chem., 1993. **268**: p. 22357-22362.
15. Brown, S.B., *Stereospecific Haem Cleavage*. Biochem. J., 1976. **159**: p. 23-27.
16. Brown, S.B. and R.F.G. King, *The Mechanism of Haem Catabolism*. Biochem. J., 1978. **170**: p. 297-311.
17. Brown, S.B. and R.F.G.J. King, *¹⁸O Studies of Haem Catabolism*. Biochem. Soc. Trans., 1976. **4**: p. 197-201.

18. Lemberg, R., *Chemical Mechanism of Bile Pigment Formation*. Rev. Pure Appl. Chem., 1956. **6**: p. 1-23.
19. Sano, S., T. Sano, I. Morishima, Y. Shiro, and Y. Maeda, *On the Mechanism of the Chemical and Enzymatic Oxygenations of α -Oxyprotohemin IX to Fe-biliverdin IX α* . Proc. Natl. Acad. Sci. USA, 1986. **83**: p. 531-535.
20. O'Carra, P. and E. Colleran, *Haem Catabolism and Coupled Oxidation of Haemproteins*. FEBS Lett., 1969. **5**: p. 295-298.
21. Sakamoto, H., Y. Omata, G. Palmer, and M. Noguchi, *Ferric α -Hydroxyheme Bound to Heme Oxygenase Can Be Converted to Verdoheme by Dioxygen in the Absence of Added Reducing Equivalents*. J. Biol. Chem, 1999. **274**: p. 18196-18200.
22. Murakami, T., I. Morishima, M. Toshitaka, S.-i. Ozaki, I. Hara, H.-J. Yang, and Y. Watanabe, *Effects of the Arrangement of a Distal Catalytic Residue on Regioselectivity and Reactivity in the Coupled Oxidation of Sperm Whale Myoglobin Mutants*. J. Am. Chem. Soc., 1999. **121**: p. 2007-2011.
23. Sigman, J.A., X. Wang, and Y. Lu, *Coupled Oxidation of Heme by Myoglobin is Mediated by Exogenous Peroxide*. J. Am. Chem. Soc., 2001. **123**: p. 6945-6946.
24. Rodriguez, J.C. and M. Rivera, *Conversion of Mitochondrial Cytochrome b_5 into a Species Capable of Performing the Efficient Coupled Oxidation of Heme*. Biochemistry, 1998. **37**: p. 13082-13090.
25. Rodriguez, J.C., T. Desilva, and M. Rivera, *Efficient Coupled Oxidation of Heme Performed by the H63M Variant of Outer Mitochondrial Membrane Cytochrome b_5* . Chem. Lett., 1998: p. 353-354.

26. Avila, L., H.-w. Huang, J.C. Rodríguez, P. Moënné-Loccoz, and M. Rivera, *Oxygen Activation by Axial Ligand Mutants of Mitochondrial Cytochrome b₅: Oxidation of Heme to Verdoheme and Biliverdin*. *J. Am. Chem. Soc.*, 2000. **122**: p. 7618-7619.
27. Rice, J.K., I.M. Fearnley, and P.D. Barker, *Coupled Oxidation of Heme Covalently Attached to Cytochrome b₅₆₂ Yields a Novel Biliprotein*. *Biochemistry*, 1999(38): p. 16847-16856.
28. Rivera, M.B.-M., C.; Christensen, K.A.; Little, J.; Wells, M.A.; Walker, F.A., *Biochemistry*, 1992. **31**: p. 12233-12240.
29. Rivera, M.S., R.; Girdhar, D.; Wirtz, M. Ass.; Zhang, X.; Wang, X.; White, S., *Biochemistry*, 1998. **37**: p. 1485-1494.
30. Rodríguez, J.C., T. Desilva, and M. Rivera, *Efficient coupled oxidation of heme performed by the H63M variant of outer mitochondrial membrane cytochrome b₅*, in *Chemistry Letters*. 1998. p. 353-354.
31. Rodríguez, J.C.R., M., *Biochemistry*, 1998. **37**: p. 13082.
32. Torpey, J. and P.R. Ortiz de Montellano, *Oxidation of the meso-methylmesoheme regioisomers by heme oxygenase. Electronic control of the reaction regioselectivity*, in *J. Biol. Chem.* 1996. p. 26067-26073.
33. O'Carra, P. and E. Colleran, *Separation and identification of biliverdin isomers and isomer analysis of phycobilins and bilirubin*, in *J. Chromatogr.* 1970. p. 458-68.
34. Wilks, A. and P. Moënné-Loccoz, *Identification of the proximal ligand His-20 in heme oxygenase (Hmu O) from Corynebacterium diphtheriae. Oxidative cleavage*

- of the heme macrocycle does not require the proximal histidine*, in *Journal of Biological Chemistry*. 2000. p. 11686-11692.
35. Sakamoto, H., Y. Omata, Y. Adachi, G. Palmer, and M. Noguchi, *Separation and identification of the regioisomers of verdoheme by reversed-phase ion-pair high-performance liquid chromatography, and characterization of their complexes with heme oxygenase*, in *Journal of Inorganic Biochemistry*. 2000. p. 113-121.
36. Avila, L.H., H. ; Rodriguez, J.C.; Moenne-Loccoz, P. ; Rivera, M., *J. Am. Chem. Soc.*, 2002. **122**: p. 7618-7619.
37. Sun, J., et al. . , *Resonance Raman and EPR Spectroscopic Studies on Heme-Heme Oxygenase Complexes*. , *Biochemistry*, 1993. **32**: p. 14151-14157.
38. Kitagawa, T., in *Biological applications of Raman Spectroscopy*, T.G. Spiro, Editor. 1988, Wiley: New York. p. 197-131.
39. Lagarias, J.C., *The Structure of Verdohemochrome and its Implications for the Mechanism of Heme Catabolism*. *Biochim. Biophys. Acta*, 1982. **717**: p. 12-19.
40. Yoshida, T., M. Noguchi, and G. Kikuchi, *Oxygenated Form of Heme-Heme Oxygenase Complex and Requirement for Second Electron to Initiate Heme Degradation from the Oxygenated Complex*. *J. Biol. Chem.*, 1980. **255**: p. 4418-4420.
41. Takahashi, S.I., K.; Takeuchi, N.; Ikeda-Saito, M.; Yoshida, T.; Rousseau, D. L., *J. Am. Chem. Soc.*, 1995. **117**: p. 6002.
42. Audrieth, L.F. and B.A. Ogg, *The Chemistry of Hydrazine*. 1951, New York: Wiley.

43. Zhu, W., A. Wilks, and I. Stojiljkovic, *Degradation of heme in gram-negative bacteria: the product of the hemO gene of Neisseriae is a heme oxygenase*, in *Journal of Bacteriology*. 2000. p. 6783-6790.
44. Wilks, A. and P. Moenne-Loccoz, *J of Biol. Chem.*, 2000. **275**(16): p. 11686-11686.
45. Brantley, R.E., Jr., S.J. Smerdon, A.J. Wilkinson, E.W. Singleton, and J.S. Olson, *The mechanism of autooxidation of myoglobin*, in *J. Biol. Chem.* 1993. p. 6995-7010.
46. Masakazu, S., Y. Omata, Y. Kakuta, H. Sakamoto, M. Noguchi, and K. Fukuyama, *Crystal Structure of Rat Heme Oxygenase-1 in Complex with Heme*. *FEBS Lett.*, 2000. **471**: p. 61-66.
47. Liu, Y., L.K. Lightning, H. Huang, P. Moenne-Loccoz, D.J. Schuller, T.L. Poulos, T.M. Loehr, and P.R. Ortiz de Montellano, *Replacement of the Distal Glycine 139 Transforms Human Heme Oxygenase-1 into a Peroxidase*. *J. Biol. Chem.*, 2000. **275**: p. 34501-34507.
48. Balch, A.L., R. Koerner, and M.M. Olmstead, *Crystallographic Characterization of Octaethylverdohaem*. *J. Chem. Soc. Chem. Commun.*, 1995: p. 873-874.
49. Balch, A.L., B.C. Noll, and N. Safari, *Structural Characterization of Low-Spin Iron(III) Complexes of Octaethylxoporphyrin*. *Inorg. Chem.*, 1993. **32**: p. 2901-2905.
50. Liu, Y., L.K. Lightning, H.-w. Huang, P. Moenne-Loccoz, D.J. Schuller, T.L. Poulos, T.M. Loehr, and P.R.O.d. Montellano, *Journal of Biological Chemistry*, 2000. **275**(44): p. 34501-34507.

51. Yoshida, T. and M. Noguchi, *Features of Intermediary Steps around the 688-nm Substance in the Heme Oxygenase Reaction*. J. Biochem., 1984. **96**: p. 563-570.
52. Matera, K.M., S. Takahashi, H. Fujii, H. Zhou, K. Ishikawa, T. Yoshimura, D.L. Rousseau, T. Yoshida, and M. Ikeda-Saito, *Oxygen and one reducing equivalent are both required for the conversion of .alpha.-hydroxyhemin to verdoheme in heme oxygenase*, in *J. Biol. Chem.* 1996. p. 6618-24.
53. Liu, Y., P. Moënne-Loccoz, T.M. Loehr, and P.R. Ortiz de Montellano, *Heme Oxygenase-1, Intermediates in Verdoheme Formation and the Requirement for Reduction Equivalents*. J. Biol. Chem., 1997. **272**: p. 6909-6917.
54. Migita, C.T., H. Fujii, K.M. Matera, S. Takahashi, H. Zhou, and T. Yoshida, *Molecular Oxygen Oxidizes the Porphyrin Ring of the Ferric α -Hydroxyheme in Heme Oxygenase in the Absence of Reducing Equivalent*. Biochim. Biophys. Acta, 1999. **1432**: p. 203-213.
55. Ortiz de Montellano, P.R. and A. Wilks, *Heme Oxygenase Structure and Mechanism*. Adv. Inorg. Chem., 2000. **51**: p. 359-407.
56. Saito, S. and H.A. Itano, *Verdohemochrome IX α : Preparation and oxidoreductive cleavage to biliverdin IX α* . Proc. Natl. Acad. Sci. USA, 1982. **79**: p. 1393-1397.
57. Hildebrand, D.P., H.-L. Tang, Y. Luo, C.L. Hunter, M.S. Hunter, G.D. Brayer, and A.G. Mauk, *Efficient Coupled Oxidation of Heme by an Active Site Variant of Horse Heart Myoglobin*. J. Am. Chem. Soc., 1996. **118**: p. 12909-12915.
58. Balch, A.L., L. Latos-Gra y ki, B.C. Noll, M.M. Olmstead, S. Ludimila, and N. Safari, *Structural Characterization of Verdoheme Analogs. Iron Complexes of Octaethyoxoporphyrin*. J. Am. Chem. Soc., 1993. **115**: p. 1422-1429.

59. Balch, A.L., L. Latos-Gra y ki, B.C. Noll, M.M. Olmstead, and N. Safari, *Isolation and Characterization of an Iron Biliverdin-Type Complex That is Formed Along with Verdohemochrome During the Coupled Oxidation of Iron(II) Octaethylporphyrin*. J. Am. Chem. Soc., 1993. **115**: p. 9056-9061.
60. Balch, A.L., R. Koerner, L. Latos-Gra y ki, J.E. Lewis, T.N. St. Claire, and E.P. Zovinka, *Coupled Oxidation of Heme without Pyridine. Formation of Cyano Complexes of Iron Oxophlorin and 5-Oxaporphyrin (Verdoheme) from Octaethylheme*. Inorg. Chem., 1997. **36**: p. 3892-3897.
61. St. Claire, T.N. and A.L. Balch, *In Situ Monitoring of the Degradation of Iron Porphyrins by Dioxygen with Hydrazine as Sacrificial Reductant. Detection of Paramagnetic Intermediates in the Coupled Oxidation Process by ¹H NMR Spectroscopy*. Inorg. Chem., 1999. **38**: p. 684-691.
62. Kalish, H.R. and L. Latos-Grazynki, *Heme/Hydrogen Peroxide Reactivity: Formation of Paramagnetic Iron Oxophlorin Isomers by Treatment of Iron Porphyrins with Hydrogen Peroxide*. J. Am. Chem. Soc., 2000. **122**: p. 12478-12486.
63. Kalish, H., J.E. Camp, M. Stepien, L. Latos-Grazynski, and A.L. Balch, *Reactivity of Mono-Meso-Substituted Iron(II) Octaethylporphyrin Complexes with Hydrogen Peroxide in the Absence of Dioxygen. Evidence for Nucleophilic Attack on the Heme*. J. Am. Chem. Soc., 2001. **123**: p. 11719-11727.

CHAPTER 4

A COMPARISON OF ANAEROBIC SPECTROELECTROCHEMICAL CELLS FOR DETERMINING THE REDUCTION POTENTIAL OF ENZYMES

Introduction

Spectroelectrochemistry, SEC, gathers information about electrochemical systems that could not be collected in purely electrochemical experiments. SEC combines electrochemistry and nonelectrochemical techniques such as spectroscopy (i.e. UV-Vis Spectroscopy). In a specially designed electrochemical cell, a redox active compound is oxidized or reduced. The products of the redox transformations are then monitored in situ by spectrophotometric techniques [1]. SEC is a particularly useful system for indirect electrochemical measurements that typically have to be applied to biological macromolecules, like enzymes, which sometimes will not undergo direct charge exchange with an electrode, due to steric or electrostatic reasons [1]. Instead, one uses smaller molecules, called mediators, to exchange charge heterogeneously with the electrode, and homogeneously with the macromolecules [1-3]. Mediators provide a mechanism for enforcing and maintaining electrochemical equilibrium with the macromolecules; hence they are useful for characterizing standard potential for redox centers in these species [4]. For an "ideal mediator" the following properties should be considered: (1) well-defined electron stoichiometry; (2) known formal reduction potential; (3) fast heterogeneous and homogeneous electron transfer; (4) readily soluble

in aqueous media at or near pH =7; (5) stable in both oxidized and reduced forms; (6) no optical interference where optical monitoring of the biocomponent is used; (7) no interaction with the biocomponent in a manner which alters the reduction potential of the enzyme [5, 6]. The reduction potential of a compound is another important consideration in the choice of mediator. The reduction potential of the mediator should be within ± 118 mV of the biocomponent being studied to mediate the electron transfer [6]. A list of the mediators commonly used in our lab is shown in Table 1.

Spectroelectrochemical methods have been routinely used to determine the reduction potential of a variety of electron transfer enzymes. However, for enzymes that use oxygen as a substrate, such as heme oxygenase, it is imperative that the spectroelectrochemical cell be specifically designed to accommodate these types of enzymes. The main difficulty in designing spectroelectrochemical cells for this use is the maintenance of an oxygen-free system over extended periods of time, usually 1-4 hours [3]. Other considerations are the complexity of construction, being able to maintain good stirring, and using minimal volume of solution for the experiment. Using the cell models described in Stankovich's, and Kuwana's papers [3, 7], two spectroelectrochemical cells, described later in this chapter, have been designed and optimized for the electrochemical studies of oxygen activating enzymes. The primary improvements made on previous designs are: (a) a smaller working volume, (b) simpler design, (c) ease of use, and (d) modular construction. Due to the more simple design of the cuvette and the use of a fiber optic diode array spectrometer, overall increased flexibility in the apparatus is achieved. These SEC cell systems will be tested and compared by determining the reduction potentials of several species of the bacterial enzyme heme oxygenase, HO:

Corynebacterium diphtheriae (HmuO), *Neisseria meningitidis* (HemO), and *Pseudomonas aeruginosa* (PigA).

HO is a membrane bound enzyme that catalyzes the first step in the oxidative degradation of heme. As briefly mentioned in chapter 3, the products of the reaction, Fe, biliverdin and CO, have important physiological roles. Iron released by HO activity is known to regulate genes including that of NO synthase. Enzymatic reduction of biliverdin yields the potent antioxidant bilirubin. Furthermore, CO is thought to play a similar role to that of NO in signal transduction and communication.

Even though the heme environment in HO is similar to that of myoglobin in that its heme is coordinated by a proximal histidine (His) (non-ionized non hydrogen bonded) and a distal water ligand, their reduction potentials are very different. The reduction potential for hHO-1 was reported to be -65 mV vs. SHE [8] compared to the potential of myoglobin (55.9 mV) [9]. Accordingly, since the evolutionary relationship between the mammalian and bacterial heme oxygenase enzymes are not fully understood, it is necessary to compare the factors that control the reduction potentials of the bacterial HO enzymes vs the mammalian HO enzymes.

Theory

i.) *Potentiometric titration with sodium dithionite*

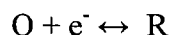
The most commonly used method for quantitatively reducing enzymes is by means of a potentiometric titration with sodium dithionite [3]. Dithionite is used because it has a relatively negative potential and is colorless in the visible region of the

electromagnetic spectrum. Unfortunately, dithionite has several disadvantages: (1) its redox potential changes with pH, (2) it is very reactive with oxygen, so it must be prepared anaerobically, (3) it is unstable at low pH values, thus cannot be used in redox titrations below pH 6.5, and (4) its oxidation product, bisulfite, forms complexes with flavoproteins oxidases and potentially other enzymes [3, 10]. These limitations make it suspect that dithionite is not fully reliable as an exogenous mediator of electrons to spectroelectrochemical experiments.

In order to carry out potentiometric titrations with dithionite as a reductant, a voltmeter is connected to a reference and indicating electrode. The potential measured by the voltmeter is given by the equation below

$$E_{\text{volt}} = E_{\text{ind}} - E_{\text{ref}} \quad \text{Eq. 1}$$

E_{ind} is the potential of the indicating electrode (Pt or gold wire) and the E_{ref} is the potential of the reference electrode, Ag / AgCl saturated with KCl, whose potential is 197 mV versus SHE. For a redox couple in solution such as



the potential experienced at the indicating electrode is given by the Nernst equation. (Eq. 2).

$$E_{\text{ind}} = E^{\circ} + 2.303 \frac{RT}{nF} \log \frac{[\text{ox}]}{[\text{red}]} \quad \text{Eq. 2}$$

Where E_{ind} is the potential at the indicating electrode, E° is the formal reduction potential of the redox couple, $2.303 RT/F$ are fundamental constants having a combined numerical value of 59.2 mV, and n is the number of electrons transferred for the redox couple.

When $[Ox] = [Red]$ the potential of the indicating electrode is equal to the formal reduction potential of the redox couple. In the potentiometric experiment, the redox state, hence the potential sensed, E_{ind} , is changed by the addition of a reducing (sodium dithionite) or oxidizing (potassium ferricyanide) agent. For heme proteins and other enzymes harboring appropriate chromophores, due to the intense absorption in the UV-Vis region, the ratio of oxidized protein to reduce is monitored spectroscopically.

Table 1. List of Mediators

MEDIATORS	Red Pot (V)	(V)	Used in Enzyme soup for:
Compound	(vs. SHE)	Ag / AgCl	*A-E
N,N,N', N'-Tetramethyl-p-phenylenediamine	0.27	0.073	
1,2-Napthoquinone-4-sulfonic acid	0.21	0.020	
2,5-Dimethyl-p-benzoquinone	0.18	-0.017	
1,2-Napthoquinone	0.15	-0.040	A,C,D,E
Toluylene blue	0.11	-0.082	A,C,D,E
Phenazine methosulfate	0.08	-0.117	A,C,D,E
Hexaamineruthenium (III) chloride	0.05	-0.147	A,B,C,D,E
Duroquinone	0.00	-0.192	A,B,C,D,E
Pentaaminechlororuthenium (III) di-chloride	-0.04	-0.237	A,B,C,D,E
Potassium indigo-tetrasulfonate	-0.04	-0.243	
5,8-Dihydroxy-1,4-napthoquinone 95%	-0.05	-0.247	A,B,C,D,E
2,5- dihydroxy-p-benzoquinone	-0.06	-0.257	A,B,C,D,E
Indigo Carmine	-0.12	-0.322	B,C,D,E
2-hydroxy-p-napthoquinone	-0.13	-0.334	
2-Hydroxy-1,4-napthoquinone	-0.13	-0.334	A,B,C,D,E
Anthraquinone-1,5-disulfonic acid	-0.17	-0.372	B,C,D,E
Anthraquinone-2,6-disulfonic acid	-0.18	-0.381	
Phenosafrafin	-0.25	-0.449	
Anthraquinone-2 sulfonic acid	-0.25	-0.452	
Safranine O	-0.28	-0.486	
Benzyl viologen dichloride	-0.35	-0.555	A,B,C,D,E
Methylviologen	-0.44	-0.646	A,B,C,D,E

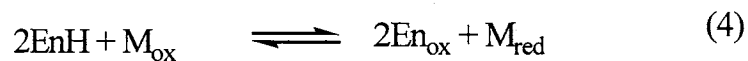
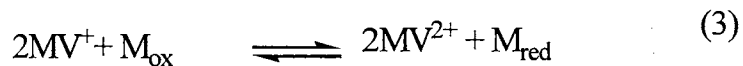
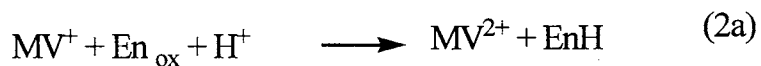
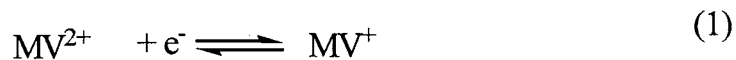
* A=HmuO; B=H20A; C=HemO; D=H23A; E=PigA

ii.) Potentiometric titration with a potentiostat and an electron transfer mediator, MV

An alternative potentiometric titration, without the use of dithionite, can be conducted using potentiometry facilitated by a potentiostat and appropriately selected mediators. One of the advantages of using this type of spectroelectrochemical technique is that the oxidized and reduced forms of the analyte adsorbed on the electrode and in the bulk solution can be quickly adjusted to an equilibrium state when the appropriate potential is applied to the cell [2]. This requires the experiment be performed in the presence of two kinds of mediators, an electron transfer mediator such as methyl viologen (MV) and a mixture of three or more redox mediators [2, 3, 11]. Methyl viologen is used because it has a very negative redox potential ($E^\circ = -0.450$ V vs SHE) and fast rate of electron transfer [3]. This very negative potential allows the MV to transfer the electrons homogeneously to the analyte with relative ease.

This process is best illustrated by following the first electron transfer to an enzyme (En). Initially, electrons are collected from the electrode by MV at very negative potentials, Eq. 1. Then MV^{+0} transfers electrons to both the enzyme (Eq. 2a and 2b) and the redox mediator (Eq. 3). As the concentration of the one-electron-reduced form of the enzyme (EnH^0) increases, it equilibrates with the redox mediator, M (Eq. 4). At each point in the titration the system is allowed to equilibrate. The potential E_{ind} at equilibrium is the overall reduction potential perceived by the enzyme. At each equilibrium step the potential of the system and the spectrum monitoring the ratio of oxidized protein to reduced are recorded, see Results section.

Spectroelectrochemistry using this method requires a more rigorous adherence to the maintenance of the anaerobicity of the cell.



Experimental

i.) Enzyme Preparation

The HO enzymes were provided by Angela Wilks from the University of Maryland, Baltimore, Maryland. Their expression and purification are outlined in publications by Wilks et al. [12, 13].

ii.) Potentiometric titrations with sodium dithionite.

The spectroelectrochemical setup used for the potentiometric titrations with sodium dithionite consisted of a custom-made cell, Figure 1. The cell was constructed from a quartz cuvette (1.0 cm path-length) fused to a custom made set of ports through a gradient coupling (OSU Glass Shop, Stillwater, OK). The cell was outfitted with a platinum working electrode, an Ag / AgCl reference electrode and a magnetic stirrer. It was also equipped with a Rotaflow stopcock that serves as an inlet for argon needed to establish a positive pressure of argon throughout the experiment. A small port was also placed into the glass to degas the solutions with argon and to introduce the protein samples and mediators with aid of Hamilton gas tight syringes. This port was then fitted with a rubber septum. The cell was placed in a cuvette holder (OSU Physics and Chemistry Instrument shop, Stillwater, OK) with internal channels designed to accept a constant temperature water source with the aid of a refrigerating circulator (VWR). The holder was then placed on a stir plate to maintain constant stirring in the cell throughout the experiment. The cuvette holder was equipped with fiber optic couplings with quartz $f/2$ collimating lenses, which couple via SMA-terminated optical fibers to the UV-VIS S2000 fiber optic spectrophotometer (Ocean Optic, Dunedin, FL). The voltmeter was connected to the reference and indicating electrodes to measure the potential. The spectrochemical titrations were carried out by adding appropriate volumes of a 100 mM solution of sodium dithionite to a solution consisting of the enzyme and the redox mediators (25 μ M) chosen for the enzyme. The mediators used (Table 1) were carefully chosen for each enzyme based on the properties for “ideal mediators” listed in the introduction. Benzyl viologen and methyl viologen were not used for the dithionite titrations. The potentiometric titration was monitored by following the intensity of the

absorbance of the oxidized Soret band of the enzymes being measured and the equilibrium potential resulting from each addition of dithionite. A Nernst plot was plotted showing the potential vs. the $\log [\text{Ox}] / [\text{Red}]$.

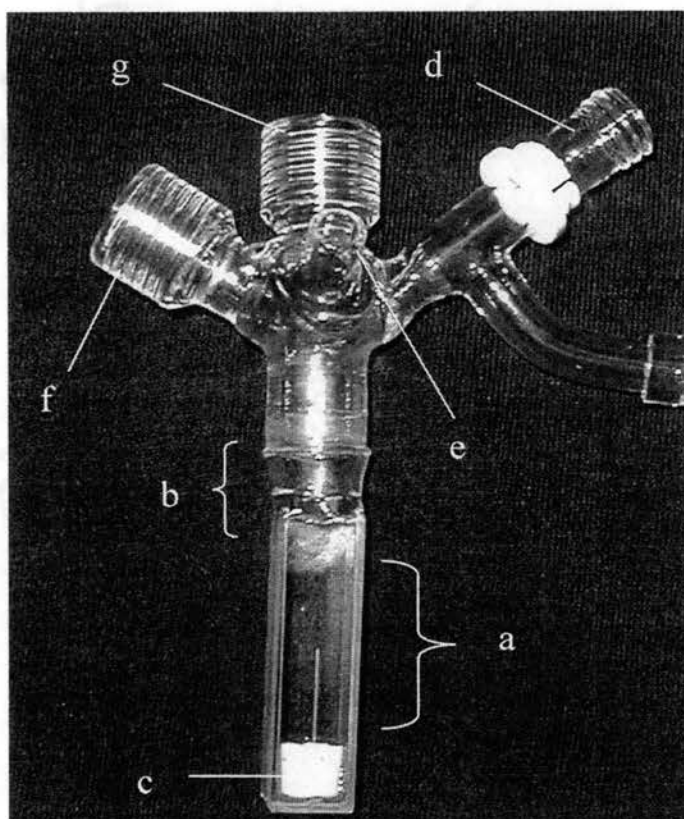


Figure 1. SEC cell used for dithionite titrations. The cell body is outfitted with (a) a 10 mm pathlength quartz cuvette connected to glass outlets via a gradient seal (b). A Teflon[®] coated magnetic cell stirrer (c) was sealed into the cell used for continuous stirring. A Rotaflow stopcock serves as an inlet for argon (d) and a small glass port (e) is used for reagent delivery and as an argon outlet. This port can be sealed with a rubber septum. A platinum wire is used as the working electrode and placed in port (f) and port (g) is used for the Ag / AgCl electrodes that serves as the reference electrode.

ii.) Potentiometric titration with a potentiostat and an electron transfer mediator, MV

The spectroelectrochemical setup used for measuring the redox potentials of the enzymes with this method consisted of a spectrophotometer, refrigerating circulator (VWR), voltmeter, potentiostat and a custom-made spectroelectrochemical cell. The cell is shown in figure (2). The cell was constructed using a standard quartz cuvette (1.0 cm path-length) shortened by cutting it so that the total volume of the cell would be approximately 2.5 mL. Three outlets were also placed on the cell for the following electrodes: a reference electrode (Ag / AgCl, custom-made PEEK electrode from Cypress Systems, Lawrence KS), an indicating electrode (0.02" gold wire, 99.9%, Refining Systems, Inc., Henderson, Nevada), and a counter electrode (Ag / AgCl, custom-made PEEK electrode from Cypress Systems, Lawrence KS). It was also equipped with a Rotaflow stopcock connected to a Schlenk line. The Schlenk line was used to keep a positive pressure of argon throughout the experiments and to pump and purge the cell free of oxygen before the start of each experiment. A small port was also placed into the glass to introduce the protein samples and mediators with the aid of Hamilton gas tight syringes. This port was fitted with a rubber septum prior to the pump and purge cycles.

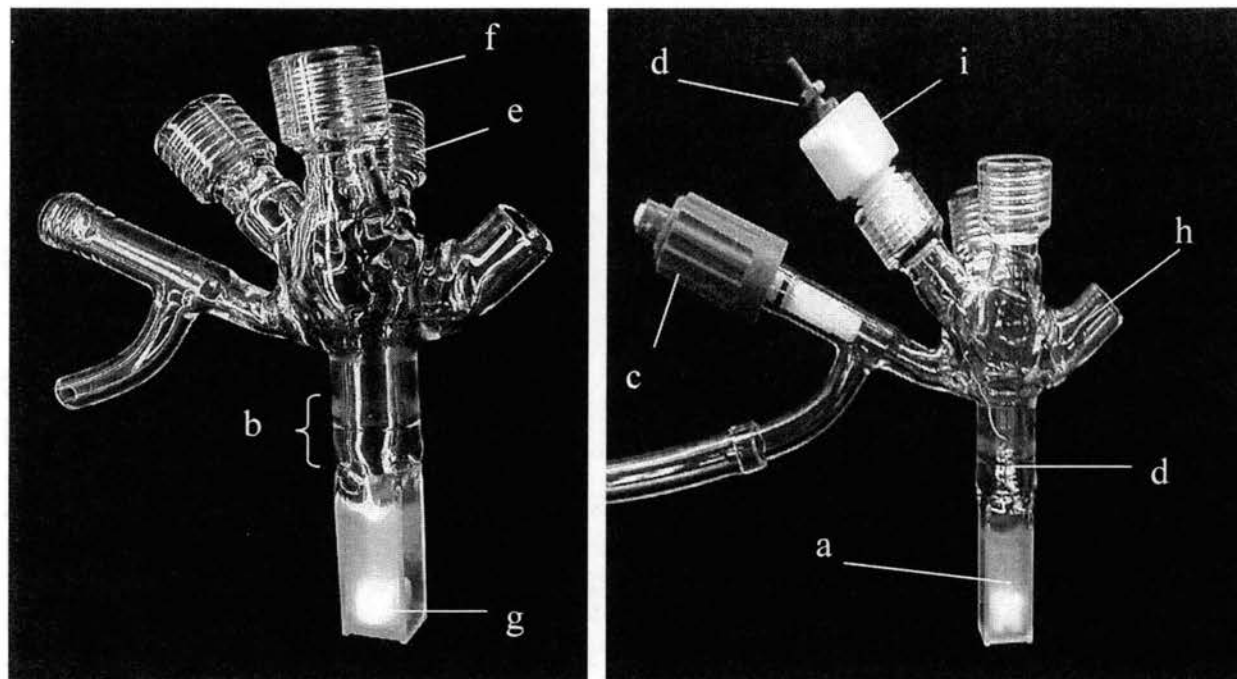


Figure 2. Two different views of the cell used for spectroelectrochemical measurements. The cell body is outfitted with (a) a 10 mm pathlength quartz cuvette connected to glass outlets via a gradient seal (b). A Teflon[®] coated magnetic cell stirrer (g) was placed into the cell. A Rotaflow stopcock serves as an inlet for argon (c) and a small glass port (h) is used for reagent delivery and as an argon outlet. This port can be sealed with a rubber septum. A gold wire (d) is used as the working electrode and ports (e) and (f) are used for the Ag / AgCl electrodes that serve as the reference and counter electrodes respectively. All electrodes were fitted into Ace Teflon[®] plugs (i) for anaerobicity (The cell was constructed at the OSU Glass Shop, Stillwater, OK).

The cell was placed in a cuvette holder with internal channels designed to accept a constant temperature water source (OSU Physics and Chemistry Instrument Shop, Stillwater, OK) from a refrigerating circulator. The holder was then placed on a stir plate to maintain constant stirring in the cell throughout the experiment. The cuvette holder was equipped with fiber optic couplings with quartz $f/2$ collimating lenses, which couple via SMA-terminated optical fibers to the UV-VIS S2000 fiber optic spectrophotometer (Ocean Optics, Dunedin, FL). The potentiostat used was a BAS-CV 50W (Bioanalytical Systems, West Lafayette, IN).

The spectroelectrochemical titrations were carried out using a mediator soup appropriately chosen for each enzyme being used following the guidelines outlined in the introduction. A list of the mediators used with their corresponding reduction potentials are in Table 1. Measurements were performed at temperatures ranging from 10°C - 19°C due to the instability of the enzyme at higher temperatures. Lower temperatures were problematic due to optical problems associated with condensation of water from the atmosphere onto the electrochemical cell. A solution (2.5 mL) containing the MV, mediators, and buffer was placed in the cell and degassed for an hour. The cell was then closed and the enzyme was added with a gas tight syringe. The system was subjected to four cycles of evacuation and argon equilibration. The electrodes were then placed in the cell under positive argon pressure.

The potential was first set at a value sufficiently negative to cause the enzyme to reduce and was maintained at this value throughout the titration. The potential was applied to the anaerobic system while being stirred to increase the rate of transport to and from the working electrode. This process, represented by Eq. (4), was allowed to come to

equilibrium at open circuit after a fixed applied potential for 1 or 2 minutes. The equilibration time ranged from 2 to 15 minutes as determined by the stability of the potential reading. The potential was then measured at the indicator electrode and the absorption of the wavelength being monitored was recorded electronically. This process was then repeated until the enzyme was completely reduced. The amount of time that the reducing potential was applied depended on the potential measured after equilibration. The recommended cell potential interval is approximately 20 mV between points.

iv.) *Determination of the formal reduction potential*

In the determination of the formal reduction potential of a redox protein using potentiometric titrations, the concentration of the reduced and oxidized states of the redox protein are determined from the optical absorption of the electronic absorption spectrum of the solution in the cell. This information is supplemented by the simultaneously observed reduction potential of the cell. These two pieces of information can be interpreted through the Nernst equation, Eq. 5.

The derived equations used to determine the reduction potentials were Eq. 5-9. Figure 2 shows a collection of spectra obtained from the experiments and can be used to demonstrate the calculation equation derivations. Point (a) is the absorbance of the fully reduced enzyme being monitored at a certain wavelength; point (b) is the absorbance of the fully oxidized species being measured at the same wavelength and; point (c) is the change in absorbance of the species being reduced at any given time, Figure 2.

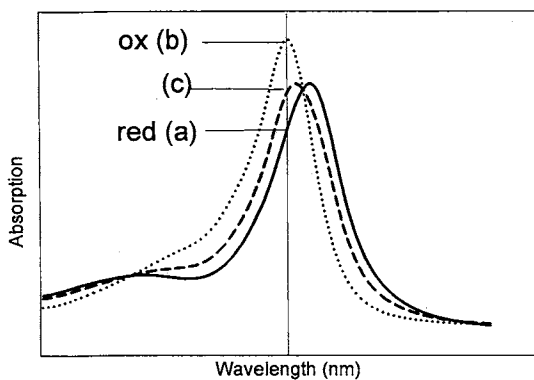


Figure 3. Spectral features used for calculation equation derivations. The absorbance is read at the monitored wavelength.

The ratio of $[ox] / [red]$ at the electrode surface is determined by

$$E(mV) = E^{\circ} + 59 \log \frac{[ox]}{[red]} \quad \text{Eq. 5}$$

As defined in Figure 2, the fully reduced absorbance monitored at the Soret's maximum wavelength = $(b-a)$ and the partially reduced absorbance at any point within the titration = $(b-c)$.

$$f_{red} = \frac{[red]}{[tot.conc.]} = f_{red} = \frac{(b-c)}{(b-a)} \quad (\text{as defined on Figure 2}) \quad \text{Eq. 6}$$

$$f_{ox} = \frac{[ox]}{[tot.conc.]} = 1 - f_{red} \quad \therefore 1 - f_{ox} = f_{red} \quad \text{Eq. 7}$$

Substituting $\frac{f_{ox}}{f_{red}}$ for $\frac{[ox]}{[red]}$ into Eq. 5 gives,

$$E = E^{\circ} + 59 \log \frac{f_{ox}}{f_{red}} \quad \text{which can be rearranged and substituted to give}$$

$$\frac{E - E^\circ}{59} = \log \frac{[ox]}{[red]} = \log \frac{\left(\frac{[red]}{[tot.conc.]} \right)}{\left(\frac{[ox]}{[tot.conc.]} \right)} = \log \left(\frac{f_{ox}}{f_{red}} \right) \quad \text{Eq. 8}$$

By plotting the potential exhibited by the indicating electrode (E_{ind}) vs. the $\log (f_{ox} / f_{red})$, one obtains a straight line with slope equal to 59 mV and with the y-intercept equal to the midpoint potential of the redox couple in solution. A plot of potential vs. the log of the ratio of oxidized to reduced is called a Nernst plot.

In order to determine if the mediators are covering the potential range needed, f_{ox} (calculated) vs E were also plotted, see Figure 4. To calculate f_{ox} (calc), the following equations were used:

Using Equations 7 and 8,

rearranging

$$\frac{E - E^\circ}{59} = \log \frac{[f_{ox}]}{1 - f_{ox}} \Rightarrow 10^{\frac{E - E^\circ}{59}} = \frac{[f_{ox}]}{1 - f_{ox}} \Rightarrow (1 - f_{ox}) 10^{\frac{E - E^\circ}{59}} = f_{ox}$$

distributing

$$10^{\frac{E - E^\circ}{59}} - f_{ox} * 10^{\frac{E - E^\circ}{59}} = f_{ox}$$

adding to both sides and dividing to isolate f_{ox}

$$10^{\frac{E - E^\circ}{59}} = f_{ox} + f_{ox} * 10^{\frac{E - E^\circ}{59}} \Rightarrow 10^{\frac{E - E^\circ}{59}}$$

$$= f_{ox} \left(1 + 10^{\frac{E - E^\circ}{59}} \right) \quad \text{Finally, simplifying to solve for}$$

f_{ox} will give Eq. 9.

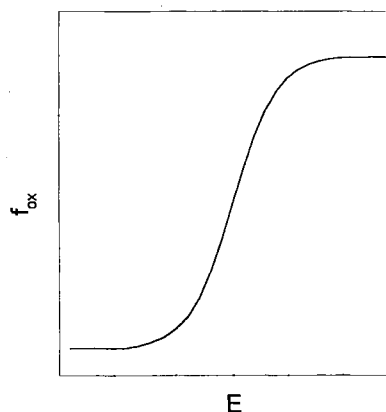


Figure 4. Sigmoidal graph fitting f_{ox} vs. E

$$f_{ox} = \frac{10^{\frac{E-E^{\circ}}{59}}}{1 + 10^{\frac{E-E^{\circ}}{59}}} \quad \text{Eq. 9}$$

Using the midpoint potential from the Nernst plot and substituting into Eq. 9. one can plot f_{ox} vs E as shown in Figure 4. The sigmoidal curve relates the fraction of the oxidized mediators to the reduction cell controlled at the indicated potentials, hence mediators are needed to cover the potential at all points with non-zero slopes.

Results and discussion

The reduction potential of bacterial strains of heme oxygenase, *Corynebacterium diphtheriae* (HmuO), *Neisseria meningitidis* (HemO), and *Pseudomonas aeruginosa* (PigA) have been measured using the anaerobic spectroelectrochemical cells designed for two different potentiometric techniques (Table 2). The spectra of the potentiometric titration using sodium dithionite of these enzymes are shown in Figure 5. For HemO, Figure 5A, the reduction of ferric to ferrous red shifts the Soret band from 405 nm to 420 nm. The midpoint reduction potential determined from Nernst plots based on the absorbance at 405 nm was 93.5 mV, with a slope of 70 ± 5 mV. The Soret band of the ferrous is also less than 50% intense than the ferric, hence the heme is being lost. On the contrary, the enzyme PigA reacts very differently. The reduction of ferric to ferrous red shifts the Soret band from 406 nm to 434 nm, with a slope of 54 mV. Comparing both values to that of wild-type hHO-1, as reported by Yi Liu, et.al.[9], the values obtained were found to be significantly higher.

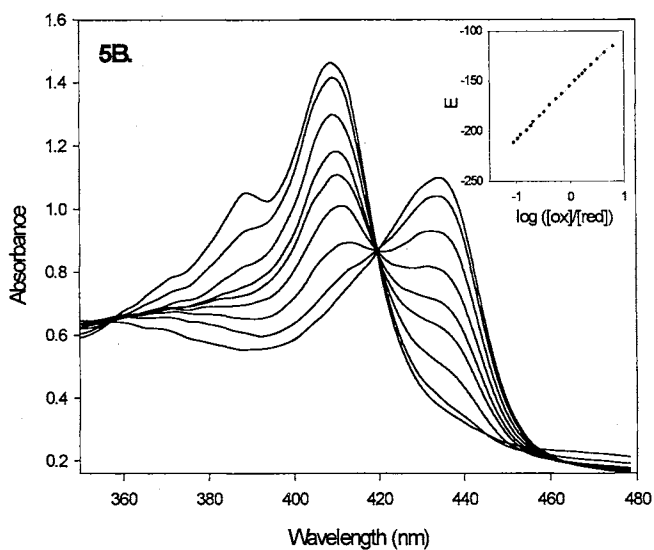
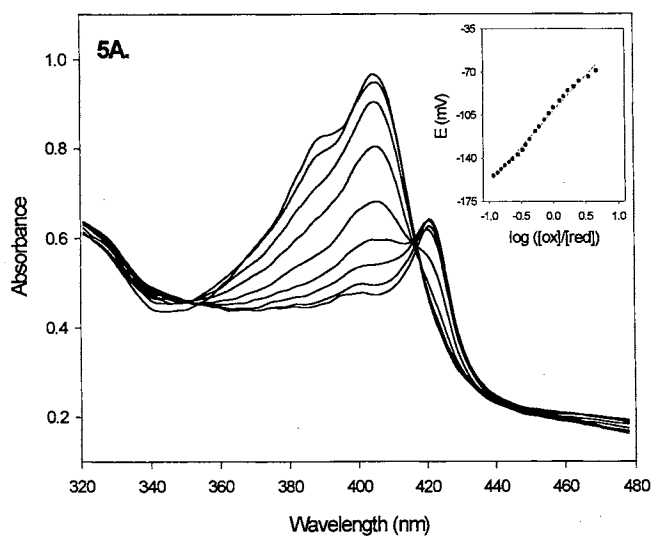


Figure 5. Spectroelectrochemical titration using sodium dithionite of **(A)** HemO ($\sim 90 \mu\text{M}$ protein in 50 mM potassium phosphate buffer pH=7.0, 18°C). The inset is a Nernst plot derived from the change in absorbance at 404.94 nm. The average reduction potential was found to be $93.5 \pm 1.4 \text{ mV}$ vs. SHE. **(B)** PigA ($\sim 90 \mu\text{M}$ protein in 50 mM potassium phosphate buffer pH=7.0, 23°C). The inset is a Nernst plot derived from the change in absorbance at 433.81 nm. The average reduction potential was found to be $41.4 \pm 0.94 \text{ mV}$ vs. SHE.

Enzyme	Potential (mV vs SHE) Dithionite titration	Slope (mV)	Potential (mV vs SHE) Potentiostat and MV	Slope (mV)	Temp in °C
<i>hHO-1</i> *			-65 ± 1	63 ± 1	25
HmuO	NA	NA	-71.5 ± 7.5	79.0 ± 0	19
HemO	93.5 ± 1.4	70 ± 5	24.5 ± 7.5	74.3 ± 9.3	18-20
PigA	41.4 ± 0.94	54 ± 2	55.0 ± 6.0	109.5 ± 6.5	19

Table 2- Results of potentiometric titrations for HO

* *hHO-1* is the published value for human heme oxygenase-1 at 25°C [9].

HmuO, HemO, and PigA were then titrated using a potentiostat, MV and mediators, see Figure 6. For HmuO, Figure 6A, the reduction of ferric to ferrous red shifts the Soret band from 404 nm to 420 nm. The midpoint reduction potential determined from Nernst plots based on the absorbance at 404 nm was -71.5 mV, with a slope of 79 ± 0 mV. For HemO, Figure 6B, the reduction of ferric to ferrous red shifts the Soret band from 405 nm to 422 nm. The midpoint reduction potential determined from Nernst plots based on the absorbance at 405 nm was 24.5 mV, with a slope of 74 ± 9 mV. Finally, for PigA, Figure 6C, the reduction of ferric to ferrous red shifts the Soret band from 405.6 nm to 422 nm. The midpoint reduction potential determined from Nernst plots based on the absorbance at 405.6 nm was 93.5 mV, with a slope of 55 ± 6 mV. In comparing the spectra and reduction potentials for the enzymes using both techniques, there are some discrepancies that were noted.

For the dithionite titration, the reduction potentials determined for HemO were more positive than the values obtained with the potentiostat and MV technique. HemO

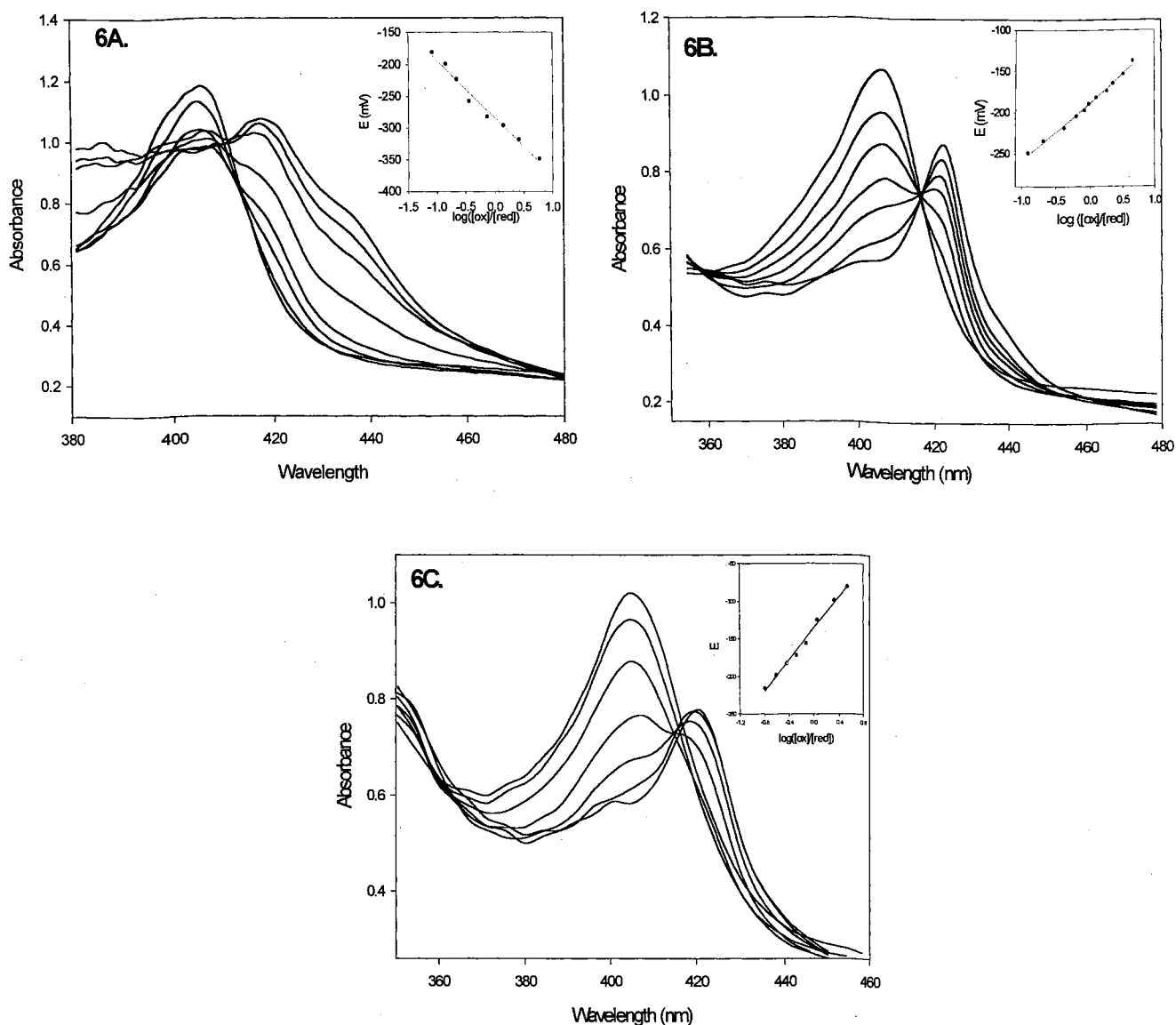


Figure 6. SEC titration using a potentiostat and MV and mediators of (A) HmuO ($\sim 90 \mu\text{M}$ protein in 50 mM potassium phosphate buffer pH=7.0, 19°C). The inset is a Nernst plot derived from the change in absorbance at 404.25 nm. The average reduction potential was found to be $-71.5.0 \pm 7.5$ mV vs. SHE (B) HemO ($\sim 90 \mu\text{M}$ protein in 50 mM potassium phosphate buffer pH=7.0, 19°C). The inset is a Nernst plot derived from the change in absorbance at 404.94 nm. The average reduction potential was found to be 24.5 ± 7.5 mV vs. SHE. (C) PigA ($\sim 90 \mu\text{M}$ protein in 50 mM potassium phosphate buffer pH=7.0, 19°C). The inset is a Nernst plot derived from the change in absorbance at 406.32 nm. The average reduction potential was found to be 55.0 ± 6.0 mV vs. SHE.

had a reduction potential of 93.5 mV with the dithionite titration and a more negative value of 24.5 mV for the titration via the potentiostat and MV. HemO's reduction potentials calculated from the changes at 404.94 nm differed by 69 mV. For PigA, on the other hand, the reduction potential calculated by both the dithionite titration and the potentiostat with MV experiment only differed by 13 mV. Even though the reduction potentials were closer in value for PigA, the sodium dithionite titration differed from the potentiostat titration. The reduction of ferric to ferrous for the PigA enzyme red shifts the Soret band from 406 nm to 433 nm, (Figure 5C) for the dithionite titration. On the contrary, the reduction of ferric to ferrous for the electrochemical titration using the potentiostat and MV results in a red shift of the Soret band from 406 nm to approximately 420 nm (Figure 6C).

The positive shift in potential seen for HemO via the dithionite titration might be due to the use of sodium dithionite. Sodium dithionite, if contaminated with small amounts of (bi) sulfite, will cause the redox potential of the solution to become more positive as the dithionite is increased [14]. The reasons for the differences in Soret changes are unknown, but they could be caused by sodium dithionite by-products complexing with HO. This effect should be studied in greater detail by comparing the HO Soret shifts and studying the enzyme's effects with different reducing agents such as hydrazine or ascorbate.

Conclusions

Both spectroelectrochemical techniques are good techniques for determining the reduction potential of enzymes, however they may not be suited for all types of enzymes.

Unfortunately, the shortcomings and aberrations of the PigA and HemO spectra clearly demonstrated the downfalls of dithionite as a reductant, hence the use of the potentiostat, MV, and mediators was found to be more reliable. The SEC cell designed for this technique excelled at maintaining anaerobicity and reproducible results. To further test the SEC cell using the potentiostat and MV with mediators, titrations with OM Cytochrome b₅ were also done. The calculated reduction potential was found to be -91 mV (vs SHE), see Figure 7. This value is in accordance to the reduction potential value previously calculated for b₅ in our lab [15]. Given that the potentiometric titration using a potentiostat, MV, and mediators does not destroy the heme in Cytochrome b₅, the spectra gave tight isosbestic points, and the Nernst plot had a slope of 62 mV, it can be concluded that this technique is a relatively good technique that can replace the dithionite titrations for most enzymes including delicate enzymes such as HO.

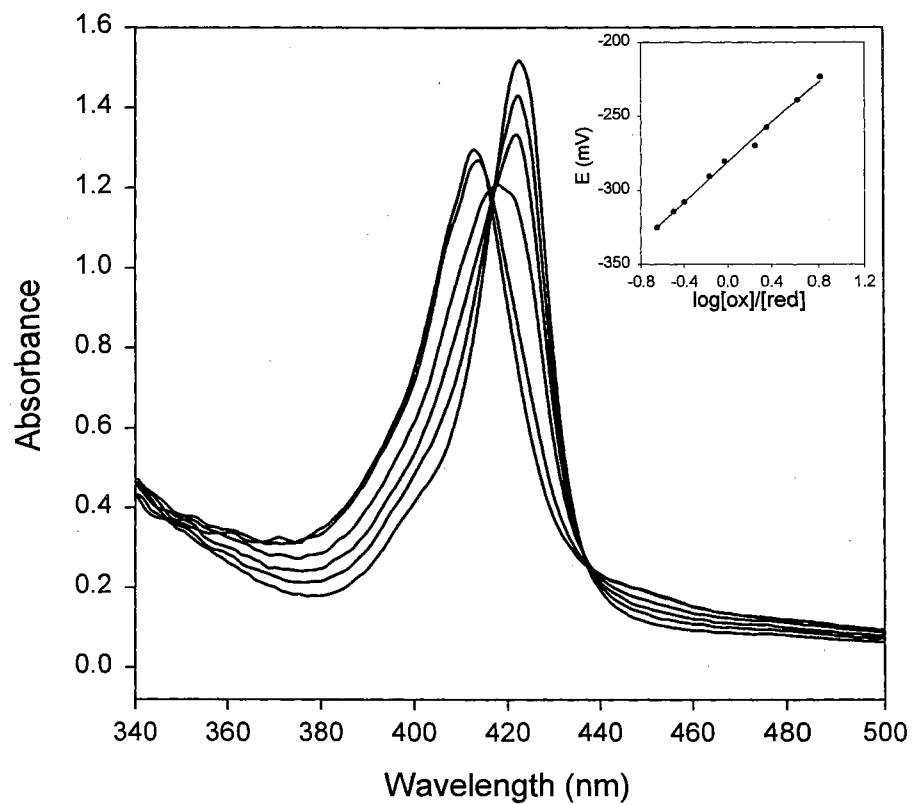


Figure 7. SEC titration using a potentiostat and MV and mediators of (A) OM Cytochrome b5 (wild type) ($\sim 90 \mu\text{M}$ protein in 50 mM potassium phosphate buffer pH=7.0, 19°C). The inset is a Nernst plot derived from the change in absorbance at 557.5 nm. The average reduction potential was found to be -90.0 mV vs. SHE. The slope was 62 mV .

References

1. Bard, A. and L.R. Faulkner, *Electrochemical Methods Fundamentals and Applications*. 2nd ed. 2001, New York: Wiley and Sons.
2. Dong, S., J. Niu, and T.M. Cotton, *Ultraviolet/Visible Spectroelectrochemistry of Redox Proteins*. *Methods in Enzymology*, 1995. **246**: p. 701-732.
3. Stankovich, M.T., *An anaerobic spectroelectrochemical cell for studying the spectral and redox properties of flavoproteins*, in *Anal. Biochem.* 1980. p. 295-308.
4. Burgess, J.D. and F.M. Hawkrigde, *Direct Electrochemistry of Proteins and Enzymes at Electrodes*. *Electroanalytical Methods for Biological Materials*, ed. A. Brajter-Toth and J.Q. Chambers. 2002, New York: Marcel Dekker, Inc. 109-113.
5. Niki, K., O. Vrana, and V. Brabec, *Spectroelectrochemistry*, in *Experimental Techniques in Bioelectrochemistry*, V. Brabec, D. Waltz, and G. Milazzo, Editors. 1996, Birkhauser Verlag: Boston. p. 251-286.
6. Fultz, M.L. and R.A. Durst, *Mediator compounds for the electrochemical study of biological redox systems: a compilation*, in *Anal. Chim. Acta.* 1982. p. 1-18.
7. Szentrimay, R., P. Yeh, and T. Kuwana, eds. *Electrochemical Studies of Biological Systems*. ACS Symposium, ed. D.T. Sawyer. Vol. 38. 1977, American Chemical Society: Washington. 142-169.

8. Varadarajan, R., T.E. Zewert, H.B. Gray, and S.G. Boxer, *Effects of buried ionizable amino acids on the reduction potential of recombinant myoglobin*, in *Science (Washington, D. C., 1883-)*. 1989. p. 69-72.
9. Liu, Y., P. Moenne-Loccoz, D.P. Hildebrand, A. Wilks, T.M. Loehr, A.G. Mauk, and P.R. Ortiz de Montellano, *Replacement of the Proximal Histidine Iron Ligand by a Cysteine or Tyrosine Converts Heme Oxygenase to an Oxidase*, in *Biochemistry*. 1999. p. 3733-3743.
10. Clark, W.M., *Oxidation-Reduction Potentials of Organic Systems*. 1960, Baltimore: The Williams and Wilkens Company.
11. Watt, G.D., *An Electrochemical Method for Measuring the Redox Potentials of Low Potential Proteins by Microcoulometry at Controlled Potentials*. *Analytical Biochemistry*, 1979. **99**: p. 399-407.
12. Wilks, A. and P. Moenne-Loccoz, *Identification of the proximal ligand His-20 in heme oxygenase (Hmu O) from Corynebacterium diphtheriae. Oxidative cleavage of the heme macrocycle does not require the proximal histidine*, in *Journal of Biological Chemistry*. 2000. p. 11686-11692.
13. Wilks, A. and M.P. Schmitt, *Expression and characterization of a heme oxygenase (Hmu O) from Corynebacterium diphtheriae. Iron acquisition requires oxidative cleavage of the heme macrocycle*, in *Journal of Biological Chemistry*. 1998: United States. p. 837-41.
14. Mayhew, S.G., *The Redox Potential of Dithionite and SO₂- from Equilibrium Reactions with Flavodoxins, Methyl Viologen and Hydrogen plus Hydrogenase*. *Eur. J. Biochem*, 1978. **85**: p. 535-547.

15. Rivera, M., R. Seetharaman, D. Girdhar, M. Wirtz, X. Zhang, X. Wang, and S. White, *The Reduction Potential of Cytochrome b5 Is Modulated by Its Exposed Heme Edge*, in *Biochemistry*. 1998. p. 1485-1494.

VITA

Ludivina Avila Z

Candidate for the Degree of

Doctor of Philosophy

Thesis: ELECTROCHEMICAL AND SPECTROSCOPIC STUDIES OF
METALLOPROTEINS AND OXYGEN ACTIVATING HEMOPROTEINS

Major Field: Chemistry

Biographical:

Personal Data: Born in Weslaco, Texas, on March 27, 1971, the daughter of Homero and Leonor Avila.

Education: Graduated from Donna High School, Donna, Texas in May 1989; received Bachelor of Science degree in Chemistry from St. Edward's University, Austin, Texas in May 1993; received Master of Science degree with a major in Chemistry from Texas A & M University-Kingsville, Kingsville, Texas in 1998. Completed the requirements for the Doctor of Philosophy degree with a major in Chemistry at Oklahoma State University in August, 2002.

Experience: Employed at SACHEM, Inc., Austin Texas as a chemist from 1993-1995; employed at Texas A & M University-Kingsville, Kingsville, Texas as the Laboratory Coordinator for the Department of Chemistry 1995-1997; employed as a graduate teaching assistant, 1997, and as a graduate research assistant at Oklahoma State University, Department of Chemistry, 1998-present.

Professional Memberships: American Chemical Society, American Association for the Advancement of Science.